Zurich University
of Applied Sciences

School of
Engineering

ZAV Center for Aviation

Emission Characteristics Variability of Commercial Turbofan Engines: A 10-Year Study

A public report of the project AGEAIR II

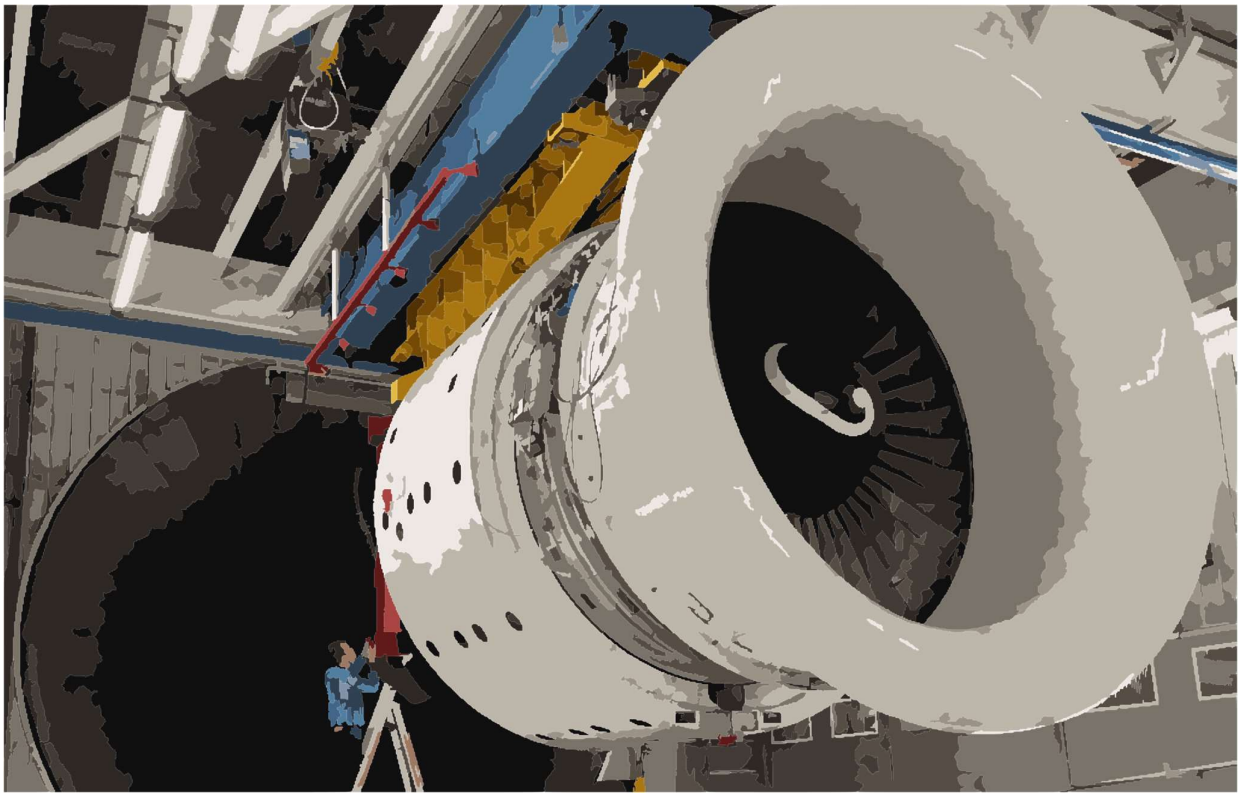

Dr. Lukas Durdina
Dr. Jacinta Edebeli
Curdin Spirig

December 2023

Title page graphics: PW4000-94 engine in an engine test cell with the exhaust sampling probe extended and undergoing inspection by L.D. Vectorized. With permission of SR Technics Switzerland AG.

Table of content

1. Executive summary

Background
This report, compiled over a decade of research, investigates the emission characteristics of commercial turbofan engines. It highlights the need for updated emission data, critical for environmental regulations and technological advancements in aviation.

Objectives
The primary goal was to understand the variability in emission characteristics of in-service commercial jet engines CFM56-7B, CFM56-5B, CFM56-5C, Pratt & Whitney PW4000-94 and PW4000-100 focusing on regulated emissions like NOx, CO, hydrocarbons, visible smoke (smoke number, SN), and non-volatile particulate matter (nvPM).

Methodology
The study involves emissions testing in an engine test cell, using standardized sampling and measurement systems compliant with ICAO emissions certification standards. The focus is on engines undergoing pass-off tests after repair or overhaul, providing insights into real-world operational emissions.

Key Findings
Variability in Emissions: The research identifies significant variability in emissions due to factors like engine type, operating conditions, ambient conditions, and maintenance history. For the regulatory landing and take-off (LTO) cycle used for emissions certification, the mean NOx emissions of all engine types tested agreed with the certified emissions in the ICAO emissions databank within 25%. A similarly good agreement was found for CO emissions. In contrast, the HC emissions were more scattered and were on average higher than certification data. The smoke number and nvPM emissions varied significantly. The emission indices (EI, amount of pollutant / kg fuel burned) of nvPM mass of a given engine type varied by up to an order of magnitude at high thrust (take-off and climb). The nvPM mass emissions and SN were on average higher than certification data in the ICAO emissions databank for all engine types. The measured nvPM EI number agreed poorly with estimates calculated from SN of certified newly manufactured engines. Depending on the method, the predicted EI numbers were up to an order of magnitude lower or higher than mean EIs determined from our measurements.

Impact of Maintenance and Operation on nvPM emissions: Maintenance workscopes (repair, overhaul, performance restoration) may substantially impact nvPM emissions, highlighting the importance of regular maintenance for optimal engine performance and reduced emissions. Analysis done on the most comprehensive dataset for the CFM56-7B engine demonstrates that overhaul led to significant reductions in nvPM emissions.

Impact of ambient conditions on nvPM emissions: Ambient temperature and relative humidity measurably affected nvPM emissions. The temperature effect was most pronounced at low thrust; this was also the case for relative humidity. The nvPM emissions at low thrust (idle, taxiing) increased significantly with decreasing ambient temperatures. This finding is crucial for local air quality as low ambient temperatures are associated with limited atmospheric dilution.

Implications
For Policy and Regulation: These findings underline the need for revising current emission models and regulatory practices to better reflect real-world engine performance and emissions.

Operational Recommendations: The report suggests that airlines and maintenance facilities can reduce non-CO2 emissions, especially nvPM, through proactive engine maintenance and operational strategies.

Conclusion
This comprehensive study on turbofan engine emissions provides valuable insights into factors affecting engine emissions. It contributes significantly to the aviation industry's understanding of emissions, aiding in the development of more accurate models for environmental impact assessment and informing policy and technological advancements.

2. Acknowledgements

The emissions measurement data in this report were collected in the framework of projects funded by the Swiss Federal Office of Civil Aviation (FOCA) running from 2012 to 2023 (A-PRIDE and EMPAIREX run by Empa, and AGEAIR and AGEAIR II run by ZHAW Centre for Aviation). The data analysis was performed in the framework of the AGEAIR II project.

The authors are grateful to all current and former research collaborators contributing to the data used in this report, namely former Empa colleagues Dr. Benjamin Brem, Dr. Miriam Elser and Mr. David Schönenberger and former ZHAW colleagues Mr. Manuel Roth, and Dr. Julien Anet.

Mrs. Alice Suri and Mr. Theo Rindlisbacher from Swiss FOCA have guided this work from the very beginning and helped with data merging and reduction.

This work would not have been possible without the enduring support of SR Technics Switzerland AG, who accommodated all our research and technical needs. Namely, Mr. Frithjof “Ziggy” Siegerist often went to great lengths to make the seemingly impossible happen and has been a linchpin of the entire operation. The test cell mechanics and shift leaders often had to endure our questions and requests and they never hesitated with their help. The leadership and presence of Michael “Mike” Weiner in the engine testing operations was inspirational and he is sorely missed.

3. Introduction

Aviation's expanding role in global transport brings both economic and social benefits and significant environmental challenges. Despite advancements in aviation technology leading to more efficient, cleaner, and quieter engines, these improvements are overshadowed by the increasing volume of air traffic, contributing to climate change and local air pollution. Aviation remains one of the most challenging sectors to decarbonize.

This technical challenge is compounded by the difficulty in accurately quantifying aviation emissions. Both CO2 and non-CO2 emissions are critical, but there is a lack of reliable data, leading to high uncertainties in models and predictions. The primary resource for estimating regulated emissions, including NOx, CO, hydrocarbons, visible smoke and non-volatile particulate matter (nvPM), is the International Civil Aviation Organization's (ICAO) Engine Emissions Databank (EEDB). However, the EEDB, which relies on the standardized Landing and Takeoff (LTO) cycle developed in the 1970s, is not representative of real-world operations. The LTO cycle, while useful for comparing engine types, is limited in scope and does not reflect the emissions of engines in service. Additionally, the testing of emissions is typically done on newly manufactured engines, not accounting for performance variations due to long-term usage.

Jet engine performance deteriorates with accumulated flight hours and flight cycles. The main reasons for engine removal from service are deteriorated exhaust gas temperature (EGT) margin, i.e., the engine is running too hot with a risk of permanent damage, and deteriorated fuel consumption. Figure 1 shows examples of these characteristics that are closely tracked by the operators. Engine maintenance and overhaul recover the lost EGT margin and performance. However, the performance never returns to the state of a new engine.

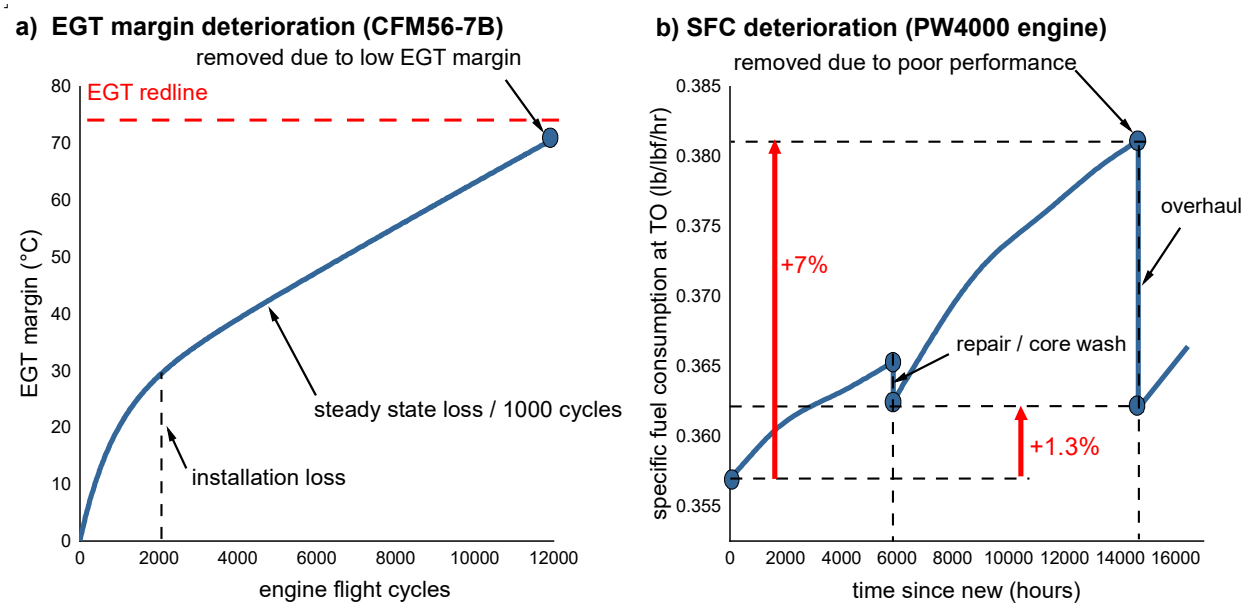

Figure 1 Examples of engine performance deterioration over time. Exhaust gas temperature (EGT) margin decrease with increasing flight cycles (a) and the increase of specific fuel consumption with engine hours. The graphs are adapted from Ackert, 2015; Valenta, 2010.

No such characteristics have been known for regulated emissions. The emissions of NOx and nvPM mass (and visible smoke) have been observed to increase with increasing number of cycles[1], but no measurements of engine emissions are mandatory at any point during the engine's service life.

Our study addresses this significant gap. We aim to investigate the variability in emission characteristics of in-service commercial jet engines, a subject scarcely explored in public research. Emission

[1] Proprietary work done by engine manufacturers and reported to the ICAO's Committee on Aviation Environmental Protection (CAEP).

measurements were performed in an engine test cell at SR Technics, Zurich airport, during pass-off tests following a repair or overhaul using a standardized sampling and measurement system compliant with the ICAO emissions certification standards. By focusing on emissions of in-service engines, this study seeks to provide a more accurate understanding of aviation's environmental impact, contributing valuable insights for future emissions regulation and technological development in aviation.

4. Methodology

4.1. Engine test cell and exhaust sampling

Engine emission tests were performed on engines undergoing pass-off tests in an indoor test cell at SR Technics, Zurich Airport, Switzerland. The U-shaped test cell is shown schematically in Figure 2. The inlet air duct is vertical, and the air is turned 90° by a set of vanes. Downstream of the engine, the exhaust gases mixed with ambient air pass through an exhaust silencer, after which the flow is turned 90° upwards into a stack. The test cell is correlated for five turbofan engine types with rated thrust up to 310 kN (70k lbf). The unique feature of this test cell is a permanently installed traversable exhaust sampling probe that can sample within 0.8-1.7 m downstream of the exhaust nozzles of the engines tested. All data in this study were collected at the engine exit plane using this single-hole traversable probe.

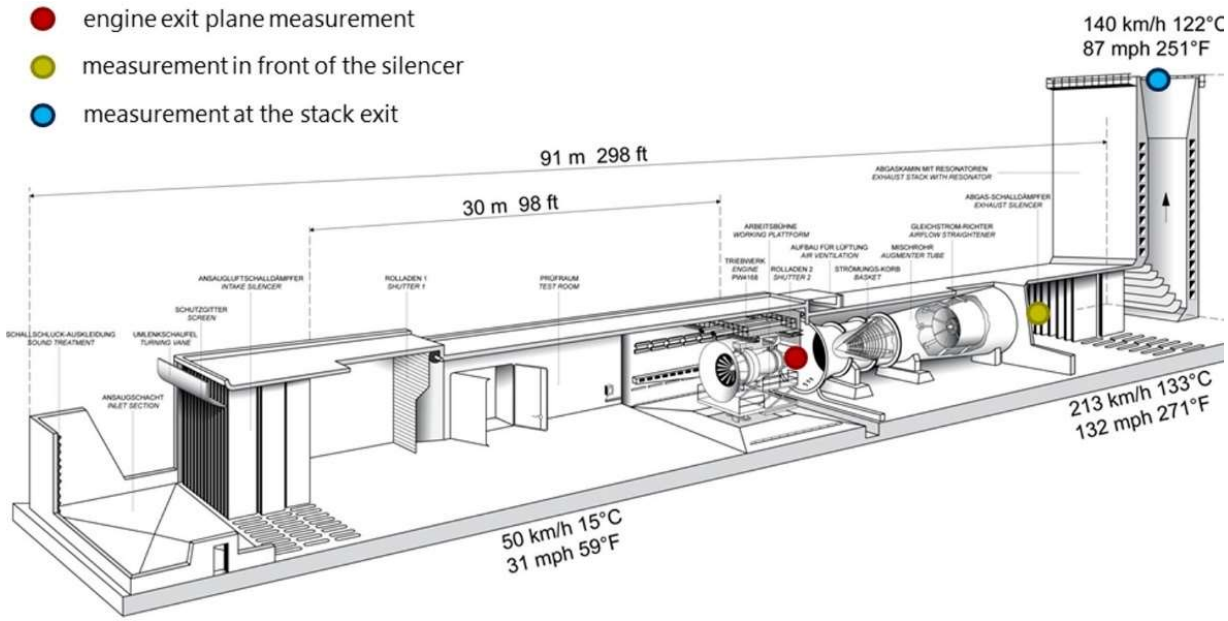

Figure 2 Schematic of the SR Technics test cell 01. Exhaust samples in this study were extracted at the engine exit plane (red circle). Original figure courtesy of SR Technics.

4.2. Engine tests

An overview of the engine types tested is shown in Table 1. Prior to the engine test, the engines underwent various maintenance workscopes. Based on the extent of the workscope, the workscopes are classified by SR Technics into repair (a least significant amount of work done), overhaul and performance restoration. The latter two workscopes include overhauled main modules. We are using this classification in our analysis below. The engine tests were done according to the procedures in the engine shop manuals. The test cycle started with a mechanical checkout test, which includes a sequence for breaking in new or overhauled components. The break-in cycle includes several thrust steps from idle to take-off. The emission tests were carried out mostly during the break-in cycle. Some emission tests only included a subset of test points at low thrust.

Table 1 Overview of the engines tested.

Engine type	Application	Combustor variants tested	Rated thrust / No. of ratings	No. of engines tested overall	No. of complete tests with high thrust
CFM56-7B	Boeing 737NG family (100% share)	Original single annular combustor and Tech Insertion (low NOx)	18-27k lbf / 6 ratings	34	25
CFM56-5B	Airbus A320ceo (~50% share)	Original single annular combustor and Tech Insertion (low NOx)	21.5-32k lbf / 9 ratings	22	13
CFM56-5C	Airbus A340-200/300 (100% share)	Single annular combustor	32-34k lbf / 3 ratings	8	7
Pratt & Whitney PW4000-94	Boeing 767, Boeing 747, MD-11, Airbus A300, Airbus A310	Reduced smoke and Phase III	52-62k lbf / 5 ratings	16	11
Pratt & Whitney PW4000-100	Airbus A330 (~25% share)	Floatwall, Talon II and Talon IIB (low NOx)	64-70k lbf/ 3 ratings	21	11

4.3. Fuel properties

The engines were fueled with a conventional Jet A-1 fuel delivered to the test cell from the Zurich Airport fuel supply. Fuel samples were taken off the fuel line downstream of the test cell fuel pump. The fuel samples were taken mostly during major test campaigns and detailed fuel properties are not available for each engine test. Figure 1 shows trends in selected fuel parameters in the samples taken at the facility between late 2012 and late 2022. Over the decade, the fuel became cleaner, with decreasing trends in total aromatics and polycyclic aromatics (naphthalenes). In turn, the fuel density decreased, and the fuel hydrogen content likely increased slightly. Fuel hydrogen analysis was carried out using an inaccurate method (ASTM D5291) and the data are not reliable (data not shown). The fuel sulfur content seems to have decreased slightly. The observed variability in fuel composition had no measurable effect on the regulatory gaseous emissions. It may have affected the variability of nvPM emissions, especially at low thrust (Brem et al., 2015). Given the large uncertainties in the fuel composition effect predictions and the lack of reliable fuel hydrogen content data in this study, we did not perform any fuel composition corrections and assumed a fuel H/C ratio of 1.95 in emissions indices (EI) calculations.

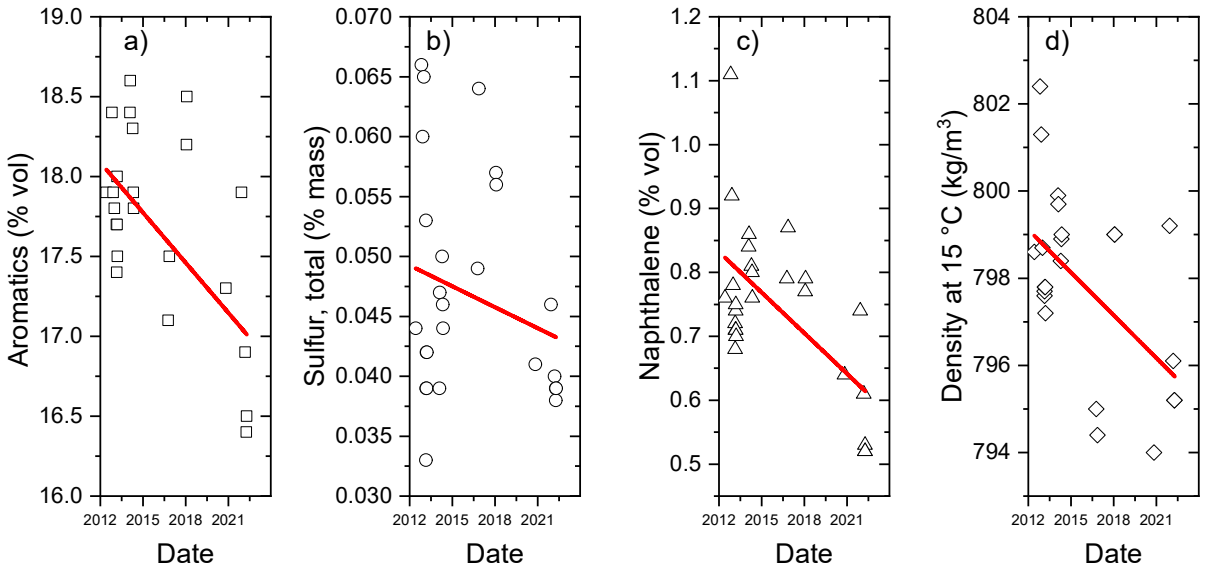

Figure 3 Fuel composition tracking over time: total aromatics - ASTM D6379 (a), sulfur - ASTM D5453 (b), naphthalene - ASTM D1840 (c), and density - EN ISO 12185 (d).

4.4. Sampling and measurement system

4.4.1. Section 1 (Exhaust sampling probe and heated sample line)

The traversable single orifice (8 mm ID) exhaust sampling probe is shown in Figure 4. The first version of the probe installed until 2014 only traversed vertically. The second version used for emission tests between 2014 and 2022 can traverse both vertically and horizontally. Several versions of the sampling head made of Inconel alloy were used, maintaining the same sampling orifice diameter and distance from the engine exit plane. A detailed description of the probe can be found in the literature. (Brem et al., 2016; Durdina et al., 2017, 2021) The sampling location for each engine type was determined empirically to optimize carbon balance (agreement between the engine air-fuel ratio (AFR) and the exhaust AFR, see section 8.1) and was kept the same for each engine test of a given engine.

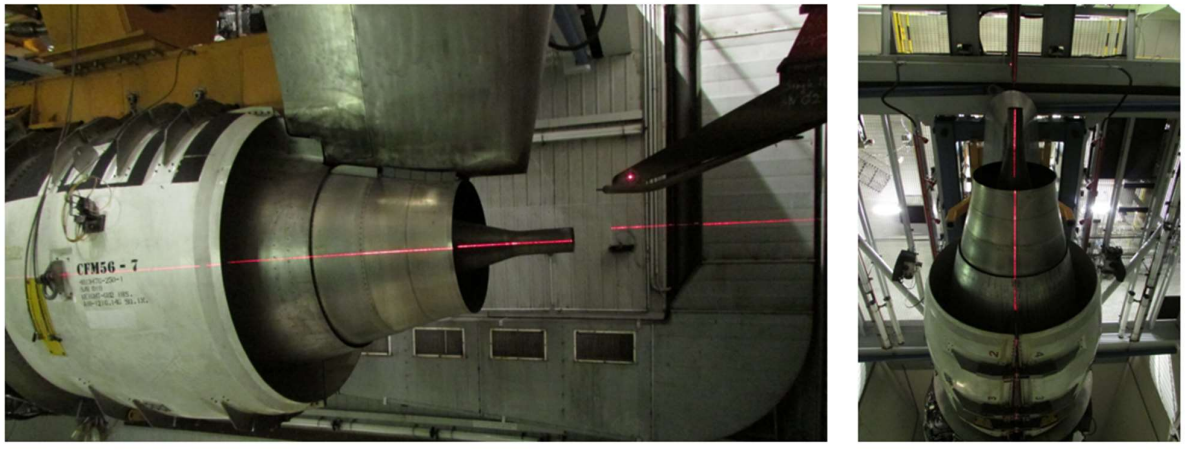

Figure 4: Exhaust sampling probe in the SR Technics test cell deployed behind a CFM56-7B engine. Photo courtesy of SR Technics.

The sampling and measurement system downstream of the probe, now known as the Swiss Mobile Aircraft Engine Emissions System (SMARTEMIS), is an ICAO Annex 16 vol. II compliant system. SMARTEMIS was used for the first-ever nvPM certification-like emission test (Durdina et al., 2017) and

subsequently, it was used for nvPM certification tests of various engine types in various facilities. The basic system configuration has remained the same since the first intercomparison tests done with the system prototype (Lobo et al., 2015). The following detailed description applies to the latest version of the system.

The arrangement of the ICAO Annex 16, Volume II, Appendix 7 standardized sampling system is shown in Figure 5. Since 2017, a Scanning Mobility Particle Sizer (SMPS) has been operated in parallel with the nvPM mass and number measurement.

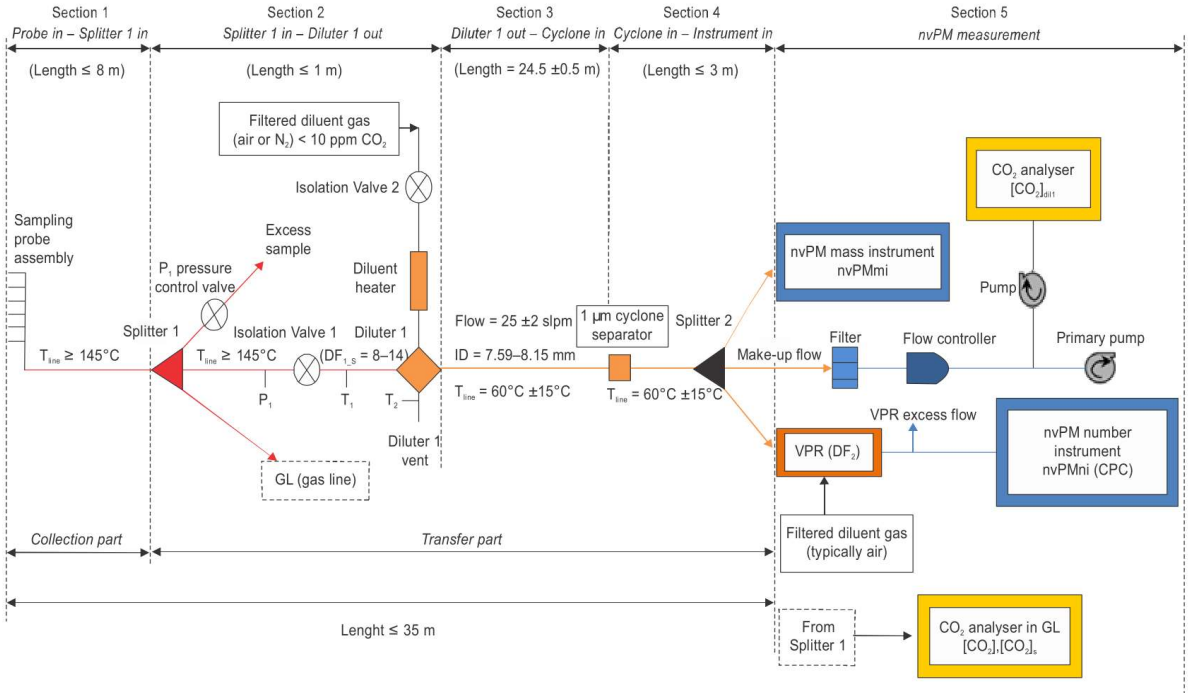

Figure 5: Standardized nvPM sampling system (adapted from Figure A7-1 in ICAO Annex 16, Volume II, Appendix 7).

The connection from the probe outlet to the Splitter1 inlet consists of a 160°C heated, 5 m long, 7.95 mm inner diameter (ID) stainless steel (1.4571) line (Hillesheim, H300 DN08 VA).[2]

4.4.2. Section 2 (Splitter 1, Isolation Valve 1 and Diluter 1)

Section 2, commonly referred to as the "diluter box", contains the components described in the following sections. The total length of the unit from Splitter1 inlet to Diluter1 outlet is 0.85 m.

At the inlet to Section 2, the Splitter 1 assembly splits the sample into the transfer part line, the Gas Line (GL), and the excess sample line. The material of the custom-made splitter assembly is stainless steel. The splitter temperature was maintained at 160°C with a custom-made heating bag that also heated the Isolation Valve 1 and the connector to Diluter 1. No change from the ID or step-shoulders is present in the flow paths to the isolating valve and in the excess flow. Furthermore, the split angles relative to the incoming flow are 15° to both the excess flow path and the GL path. The ID of the GL is 6 mm. A pneumatically driven regulating valve (Bürkert) is used as the P1 control valve in the excess flow path. This valve is a full bore (8 mm ID).

A pneumatically driven ball valve (Swagelok) with PTFE seals is used as the Isolation Valve1 to isolate the flow path to Diluter1 from the splitter. The flow path through the valve is a full bore with a minimal step at the valve ball of less than 15% of the 8.0 mm valve inlet and outlet ID. The valve was heated to 160°C with the same heating bag that was used for heating the Splitter1 assembly. A type K thermocouple monitors the wall temperature (T1) of the Splitter1 body.

[2] A 6 m long line of the same model was used for a subset of the emissions tests.

An ejector diluter (DI-1000, Dekati Inc.) dilutes the sample flow. The unit has an inlet ID of 8.0 mm. HEPA-filtered synthetic air (< 1ppm CO_2) was used as diluent. The diluent pressure was maintained at 2.3 – 2.7 bars for the diluent flow specified by the manufacturer. A gas heater (DH-1723/1711, Dekati Inc.) conditions the diluent to reach a diluted gas temperature of 60°C and the commercially available heating jacket (DH-1523/1511, Dekati Inc.) keeps the diluter system at a temperature of 60°C.
The Diluter1 vent included a full-bore pneumatic isolation valve which was open to ambient.

4.4.3. Section 3 (Transfer Line)

Two segments of 7.95 mm ID, 12 m, 60°C trace heated line (H-300, Hillesheim Inc.) with a heated junction in between are used for Section 3. The temperature of each line segment is controlled by two sleeve-embedded temperature sensors and two heating regulators. The core material of the line is carbon-impregnated Teflon (PTFE EX, Bola Inc.) with a conductivity better than 1 kΩ/ m. The line is electrically grounded through the connectors on both ends. The flow rate through the line was maintained typically at 23-24 slpm, verified by a reference flow meter and differential pressure measurement.

4.4.4. Section 4 (Cyclone, Splitter 2 and Measurement System Interface)

A custom-made stainless-steel cyclone separator (BGI Inc. Model 3800) is installed at the nvPM rack inlet. This cyclone separator has a manufacturer-determined aerodynamic diameter cut point of 1 µm and a sharpness $(D_{16}/D_{84})^{0.5}$ of 1.225. The IDs of the cyclone connectors is 7.75 mm. A custom-made heating sleeve maintained the temperature of the cyclone at 60°C. This sleeve also contains the Splitter2 assembly.

After the cyclone, a custom-made 3-way stainless steel flow splitter with split angles of 30° is used to split the sample flow into three paths. This splitter was trace heated to 60°C. The IDs are the following: Inlet: 7.75 mm, Outlet to nvPM mass instrument (nvPMmi): 4.55 mm, Outlet to nvPM number instrument (nvPMni): 4 mm, and the Outlet to Make up Flow path: 7.75 mm.

The connection from the Splitter 2 to the nvPMmi consists of a 4.55 mm ID, 60°C trace heated stainless steel line. The total line length from Cyclone inlet to the nvPMmi is 1.4 m. The connection from the splitter to the nvPMni consists of a 4 mm ID, 60°C trace heated stainless steel line. The total line length from the Cyclone inlet to the nvPMni inlet is 1.5 m. The connection to the SMPS is unheated (carbon-impregnated silicone tube). The line length to the SMPS instrument was 1 m with a 4 mm ID.

4.4.5. nvPM system instruments

The nvPM mass concentration is determined with a Micro Soot Sensor (MSS, Model 483, AVL Inc.) based on the photoacoustic detection principle. The MSS was calibrated on annual basis by the manufacturer.

The commercially available APC instrument from AVL Inc. measures the nvPM number concentration of particles >10 nm (d_{50} = 10 nm). This instrument has a built-in Volatile Particle Remover (VPR) unit consisting of two dilution steps with a 350°C heated oxidation catalyst and a sulfur trap. After the second dilution, a condensation particle counter (CPC, TSI 3790E) counts the number of non-volatile particles. The VPR penetration efficiencies were determined during the annual instrument calibration. The APC instrument requires pressurized air. We utilized the same synthetic air (< 1 ppm CO_2) as for the dilution system with a separate pressure control regulated at ~2 bar.

A scanning mobility particle sizer (SMPS, Model 3938 consisting of a 443.69 mm long differential mobility analyzer Model 3081A, electrostatic classifier Model 3082, aerosol neutralizer Model 3077A and a condensation particle counter, Model 3776, TSI Inc.) is used to measure the particle size distributions. The instrument was factory-checked and calibrated every year.

The make-up flow in the measurement section consists of a sintered metal filter (HAM-LET, Z-600) a mass flow controller (Vögtlin, red-y series), a 2 L pulsation damping reservoir, and a dual-head membrane pump (KNF Inc.). The damping reservoir is necessary to minimize pressure fluctuations that are introduced during pump operation.

A non-dispersive infrared absorption (NDIR) CO_2 analyzer (Thermo Inc., Model 410i) measures the diluted CO_2 concentrations downstream in the pump exhaust. The analyzer is connected to the pump

exhaust with a T connector and a Teflon protection filter at the analyzer inlet protected the instrument from particle contamination. The instrument used is compliant with the specifications in Attachment B to Annex 16 Appendix 3.

4.4.6. Gas Line (GL) Instrumentation

A 25 m, 6 mm ID, 160°C heated PTFE line (Hillesheim, H-300) transports raw exhaust from the Splitter1 outlet to the raw gas instrumentation. A 160°C heated filter protects a 160°C heated membrane pump (KNF Inc., HN 035) from contamination. The flow rate varied between 10 slpm (gas analyzers only) and 20 slpm (gas analyzers and smoke number sampling). After the pump, the gas flow is split into five flow paths; one leading to the smoke meter (Chell CSM2000), one leading to the combined gas analyzer Horiba PG-250 measuring dry gas sample (CO_2, CO and NO_x), one leading to an additional NO/NO2 analyzer Ecophysics CLD844 (hot and wet sample measurement), one leading to the FID (HC, hot and wet sample measurement), and an excess flow path exhausted to ambient.

The PG-250 was operated until 2020 downstream of a portable gas conditioning unit (M&C Tech group Inc., PSS-5) to bring the dew point temperature of the raw gas to 5°C. In 2020, the gas conditioning unit was replaced with a Nafion dryer (Permapure, Inc.). An additional 19" rack (gas rack 2) with gas analyzers sampled downstream of the dryer, in parallel with the PG-250. The gas rack 2 includes the following analyzers: Thermo 410iQ (CO2), Thermo 48iQ (CO), Thermo 43i (SO2), and a multi-gas calibrator Thermo 146iQ.

All gas analyzers were calibrated using certified calibration gas mixtures. The zero and span calibrations were performed on an hourly basis. Multipoint calibration checks were performed several times during a test campaign.

4.5. Data reduction and analysis

The SMARTEMIS data were merged with selected engine performance data. The merged 1Hz data were averaged for 60 seconds during periods of stable engine thrust and emissions. The datasets were processed using an in-house Python-based tool. The gaseous and nvPM EIs were calculated according to the ICAO emissions certification standards (ICAO, 2017).

All gaseous EIs were corrected to ISA sea level (T_{ISA} = 288.15K, p_{ISA} = 101.325 kPa) and reference humidity of 6.34 g water / kg dry air according to Appendix 3 of the ICAO Annex 16, vol II. (ICAO, 2017). To do so, engine performance at ISA sea level needed to be determined. For each engine type, we determined correlations for combustor inlet pressure (p3), fuel flow and thrust as a function of combustor inlet temperature (T3). The standard day corrections, where needed, were performed using common formulas with nondimensional parameters, connected to the Mach numbers in the engine turbomachinery (Kurzke & Halliwell, 2018).

A general formula for the correction of a parameter (y) can be written as:

$$y_{corr} = \frac{y}{(X\theta)^a \delta^b}$$

In this formula, θ stands for the temperature ratio T/ T_{ISA} and δ for the pressure ratio p/p_{ISA}, and *X* stands for the humidity correction term ($R/R_{dry\ air}$, where $R_{dry\ air}$ =287.04 J/kg*K)

The corrections for thrust and fuel flow also include corrections for inlet air water condensation, aircraft installation (only for thrust), and test facility effects (facility modifiers). Facility modifiers are determined empirically from test cell correlations and the correction is on the order of 5% at takeoff thrust. Fuel flow is additionally corrected to a reference fuel lower heating value (LHV_{ref}=18580 BTU/lb). Corrected thrust and fuel flow are readily obtained from the engine performance data. The obtained T3 and p3 data were not corrected, except for the PW4000 engine datasets that included corrected values of T3.

Temperature is corrected as:

$$T_{corr} = \frac{T}{\theta^a}$$

The theta exponent *a* is, in theory, = 1. In practice, it varies with thrust and it is determined empirically. The exponent is a function of N1 (low pressure shaft speed). For the CFM56 engine variants, the value of the exponent decreased with increasing thrust from ~1 at idle to ~0.85 at takeoff. Using *a*=1 for all test points led to a maximum absolute difference of < 2K, which is much less than the observed variability between different engines of the same type. It is, therefore, a reasonable assumption for our analysis.

Pressure is corrected as:

$$p_{corr} = \frac{p}{\delta^b}$$

The delta exponent *b* =1.

The corrected p3, fuel flow, and thrust were interpolated as a function of corrected T3 using polynomial functions. The functions were then used to determine the reference p3, fuel flow, and thrust as a function of measured T3. For example, the T3-correlated thrust is then the thrust the engine would produce at the measured T3 at ISA sea level conditions.

The concentrations of raw NOx, CO, CO2 and SO2 measured downstream of the dryer were corrected to a wet basis. The “wet correction” factor *K* ranged from ~0.94 to ~0.99. The gaseous EIs of NOx and CO were determined from measured concentrations from two different analyzers (see section 4.4.6). In our analysis below, we use the mean values of the two CO and NOx measurements.

The nvPM mass and number EIs were calculated using the complete formulas, i.e. accounting for the CO and HC in the exhaust sample (SAE International, 2021). The EIs were then corrected for thermophoretic losses. The thermophoretic loss correction factor, independent of particle size(E. F. Durand et al., 2020), ranged from ~1.1 to ~1.3 (see section 8.2). No thermophoretic correction was applied to the CFM56-5C data, which has a mixed exhaust nozzle. The mean exhaust gas temperature does not significantly exceed the sample line temperature of 160°C in Section 1 of the sampling system and therefore, the thermophoretic loss is negligible.

More significant is the correction due to size-dependent particle losses in the sampling and measurement system. The ICAO Annex 16. Vol. II prescribes a system loss correction methodology taken over from the SAE ARP6481 (SAE International, 2019). This method takes the nvPM mass and number and system penetration parameters as inputs. It assumes a lognormal distribution at the engine exit plane with a geometric standard deviation of 1.8 and an effective density of 1 g/cm^3. This method has very high uncertainties at low nvPM mass concentrations (limit of detection and issues with sampling system background contamination due to shedding of particles from the cyclone). Here, we determined the system loss correction factors using measured particle size distributions with the SMPS. We used the measured size bins without any assumption of the size distribution shape. This method is described in detail in Durand et al., 2023. It uses the SMPS data and the system penetration model as input. The system penetration was calculated using the ARP6481 methodology. The main inputs are the geometry, temperatures, and flow rates in each segment of the sampling system. Additionally, for the losses in nvPMni, the counting efficiencies at 10 and 15 nm and the VPR penetration at 15, 30, 50 and 1000 nm are required. We used the average values of the counting efficiencies and VPR penetrations determined during the instrument calibration in 2019-2022, which were performed with an updated methodology. Since not all engine tests included the SMPS, the system loss correction factors were interpolated as a function of T3 (section 8.2). The mass-based system loss correction factors ranged from 1.1 to 1.5 and the number-based correction factors were in the range from 2 to 5.5.

Unlike for the gaseous EIs, no ambient corrections are prescribed for the nvPM EIs. Methods have been developed that correct for the effects of p3 and AFR for nvPM, but they may not be universally applicable for emissions certification of all engine types.(Ahrens et al., 2023) The ambient corrections for certified nvPM emission are foreseen to be solely in the competence of the engine manufacturers.

4.5.1. Calculation of LTO cycle emissions

The gaseous and nvPM EIs and fuel flow were interpolated as a function of T3 to determine average values for the regulatory LTO cycle and compared with the certified emissions in the ICAO EEDB. This databank is maintained by the EU Aviation Safety Agency (EASA) and is available online (ICAO, 2023). The EEDB contains emission indices and fuel flows for the four modes of the LTO cycle. The LTO cycle includes five operating phases with four thrust settings (% of rated thrust): 7% for taxi and ground idle in and out (22 min), 30% for approach (4 min), 85% for climb (2.2 min) and 100% for take-off (0.7 min). The cycle was developed in the early 1970s based on a survey of major US airports at the time and it reflected peak operations. The LTO cycle is not necessarily realistic, but it provides a constant frame of reference for investigating engine emissions performance.

The certified gaseous emissions and nvPM emissions were extracted from the EEDB. However, only the CFM56-5B and 7B engines were nvPM-certified. The other engine types were only certified for smoke number (SN), which is a measure of exhaust smoke visibility, and it correlates well with nvPM mass concentration. We extracted the certification SN and estimated nvPM mass and number emissions using the First Order Approximation (FOA) 4 method (ICAO, 2020) and the SCOPE11 method, which has additional steps for the estimation of EI nvPM number (Agarwal et al., 2019). In both methods, nvPM mass concentration at the engine exit plane is determined from an empirical correlation between SN and nvPM mass. In the next step, EI nvPM mass is calculated using assumed air-fuel ratios (AFR) for each LTO mode. The FOA4 method is derived from SCOPE11, and the EI nvPM mass calculations are identical. EI nvPM number is calculated from mass by assuming a lognormal particle size distribution (PSD) with a geometric standard deviation (GSD) of 1.8, average particle density of 1 g/cm^3 and a given geometric mean diameter (GMD). The FOA4 assumes GMD of 20 nm for taxi and approach and 40 nm for climb and take-off. The SCOPE11 method determines exit plane GMD from an empirical correlation with combustor exit nvPM mass concentration.

As mentioned above, in the emissions certification procedure, the engine thrust is set using the combustor inlet temperature T3, where the T3 values correspond to a given thrust at ISA sea level. In the engine tests at SR Technics, the engine operating conditions were set using the spool speeds (low pressure spool N1, high pressure spool N2) or engine pressure ratio (EPR). To compare the results with the ICAO EEDB, we determined correlations between T3 and fuel flow, thrust and p3 at SLS for each engine type. The emission indices were interpolated as a function of T3 and compared with the ICAO EEDB on a thrust scale using the T3-correlated thrust. The T3-correlated thrust is not thermodynamically sound for evaluating engine performance; it is a concept used for emissions certification to keep one of the measured combustor inlet parameters constant. Depending on ambient temperature, the T3-correlated thrust, may differ strongly from the actual thrust produced by the engine. For example, on a hot day, the T3-correlated thrust at N1 for take-off will exceed the 100% rated thrust at SLS. On a cold day, at the same N1, the T3-correlated thrust will be <<100% rated thrust at SLS.

5. Results

5.1. LTO gaseous emissions

5.1.1. CFM56-7B

The CFM56-7B was produced with two single annular combustor variants. The original single annular combustor (SAC) was replaced by a Tech Insertion (TI) combustor in 2007. The TI combustor has reduced NOx for compliance with the CAEP/8 standard.

The regulatory gaseous EIs are plotted as a function of T3 in Figure 6. For the NOx emissions in panel a), we differentiate between the two combustor types labeled as SAC and Tech Insertion. The data are color-mapped with ambient temperature. The red circles represent the average EIs for the LTO points of all thrust ratings determined from interpolations. The lower NOx emissions of the TI combustor are evident in our measurement data. The LTO emission indices of CO and HC in panels b) and c) are averages of both combustor variants. Figure 7 shows a comparison of the EIs for the LTO points with the ICAO EEDB data. Our results agree well with the certified data for NOx and CO. The measured HC emissions at LTO thrust above 7% exceeded the certification data. The same trends are reflected in the LTO total emissions (g/LTO cycle for a given thrust rating) shown in Figure 8. The CO emissions for the average of both combustors are within the certified results for the SAC and TI variants. The HC emissions were a factor of ~2 higher than the certification data. The NOx emissions agreed with the certified emissions within 5% for the SAC and 10% for the TI variants.

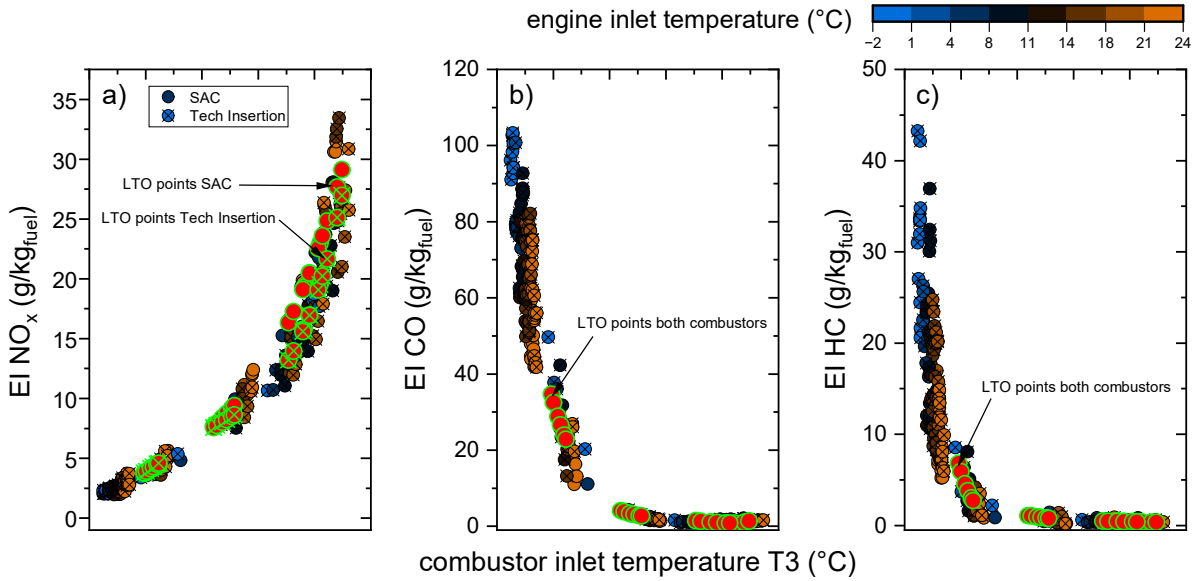

Figure 6 CFM56-7B - EI NOx (a), EI CO (b) and EI HC(c) as a function of T3.

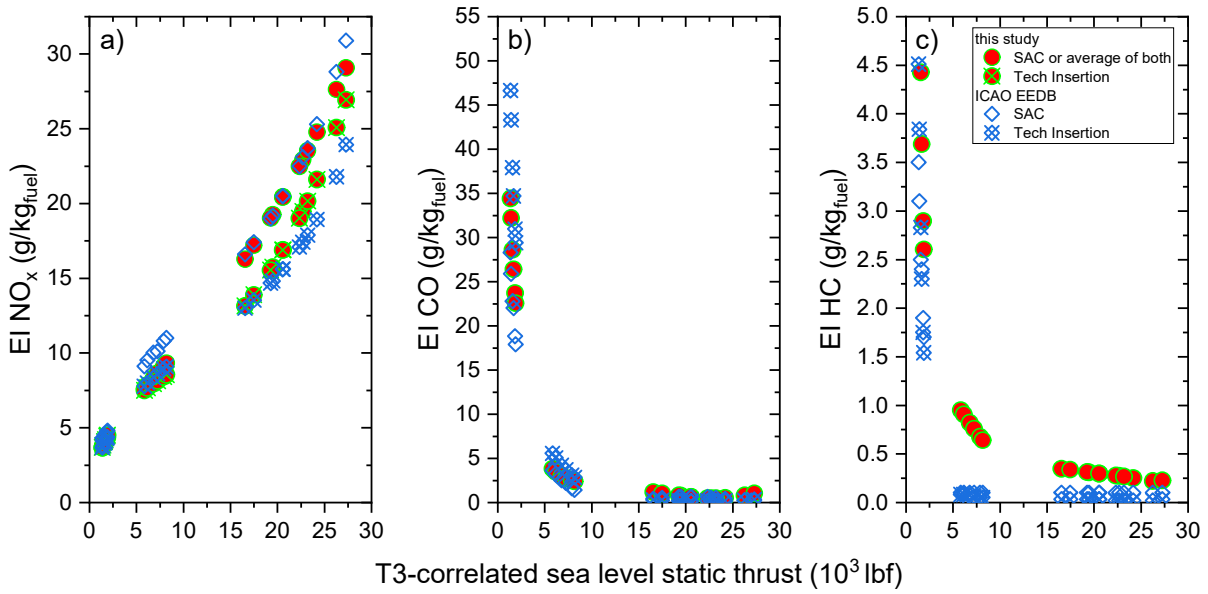

Figure 7 CFM56-7B - Comparison of measured gaseous emissions with the ICAO EEDB data: EI NOx (a), EI CO (b) and EI HC (c).

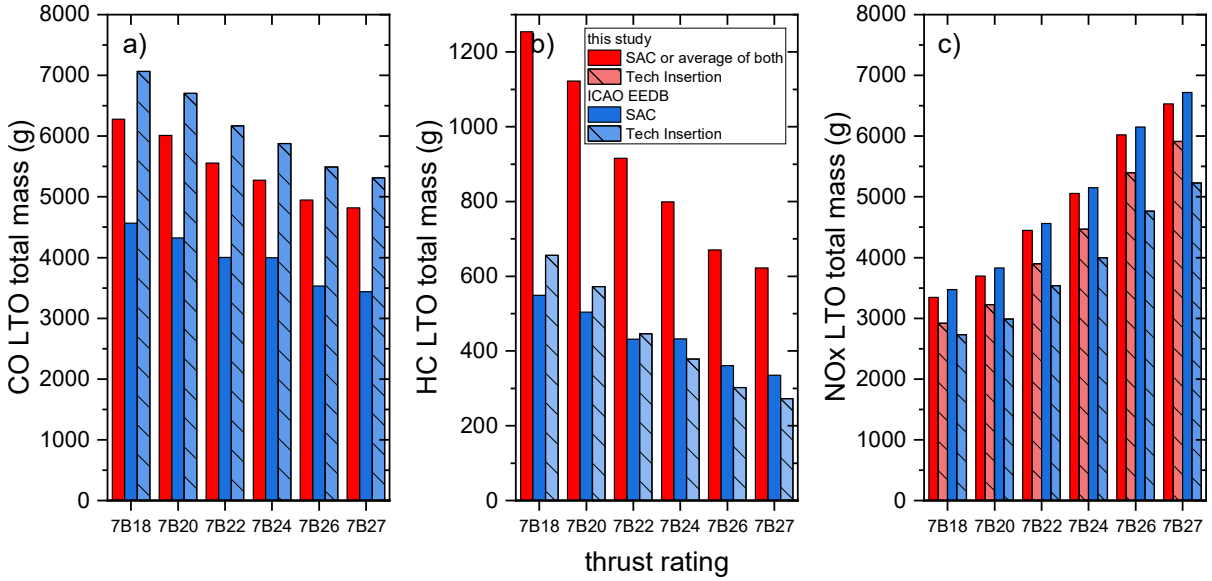

Figure 8 CFM56-7B - LTO total emissions of CO (a), HC (b) and NOx (c).

5.1.2. CFM56-5B

The CFM56-5B engine, like the -7B, received during its production run an updated combustor for lower NOx emissions and compliance with CAEP/8. We differentiate between the SAC and TI combustors for NOx.

The regulatory gaseous EIs are plotted as a function of T3 in Figure 9. The data are color-mapped with ambient temperature. The red circles represent the average EIs for the LTO points of all thrust ratings determined from interpolations. The lower NOx emissions of the TI combustor are evident in our measurement data. The LTO emission indices of CO and HC in panels b) and c) are averages of both combustor variants. Figure 10 shows a comparison of the EIs for the LTO points with the ICAO EEDB data. Our results agree well with the certified data, especially the trend for NOx for the two combustors is well visible. The CO emissions agree well with the EEDB at all power conditions. The HC emissions

agree well at 7% thrust. At 30% thrust, our data are in line with the certified results for the SAC variant but overestimate the TI. At high thrust, our results are higher than certification data.[3]

The LTO total emissions (g/LTO cycle for a given thrust rating) are shown in Figure 11. The overall agreement is excellent, especially for NOx (within 6% for all ratings). The CO emissions for the average of both combustors are within the certified results for the SAC and TI variants. The HCs are in line with the certification data for the SAC variant.

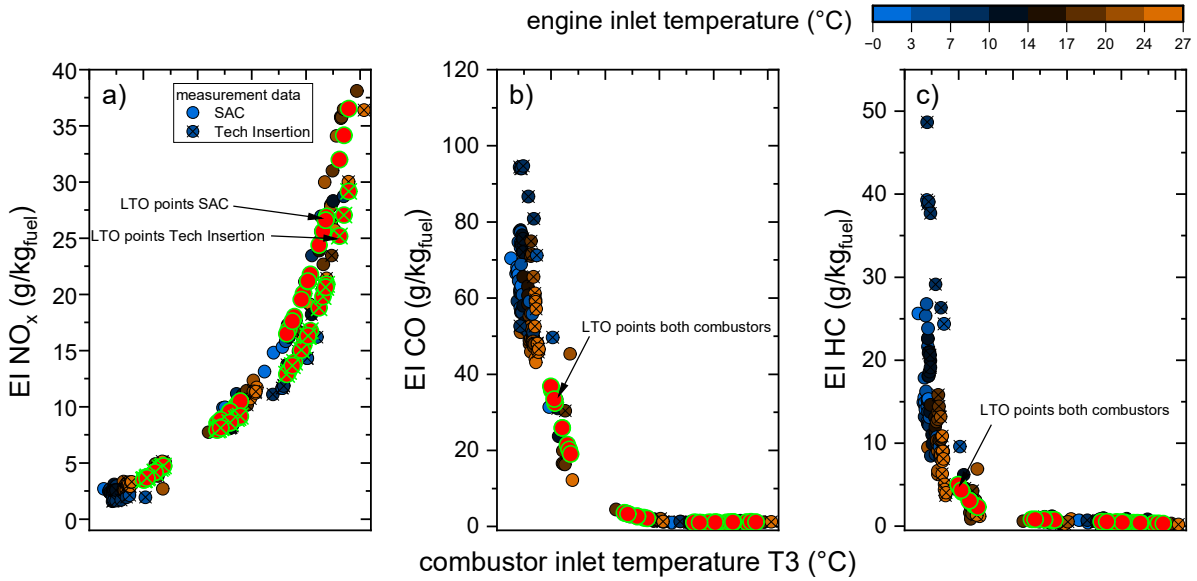

Figure 9 CFM56-5B – EI NOx (a), EI CO (b) and EI HC (c) as a function of T3.

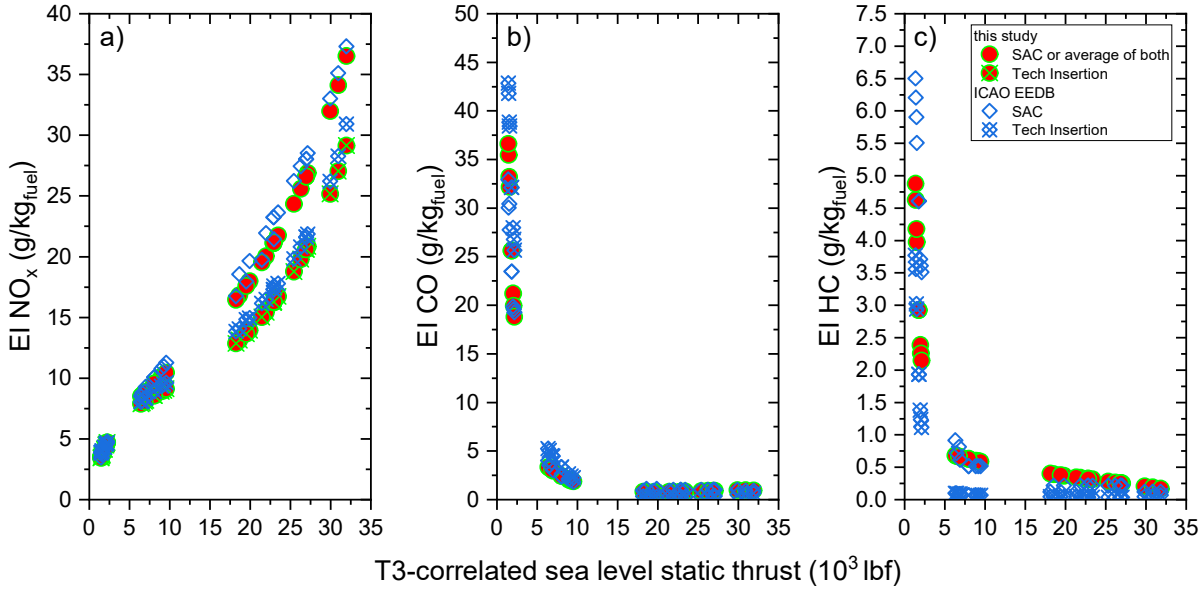

Figure 10 CFM56-5B - Comparison of measured gaseous emissions with the ICAO EEDB data: EI NOx (a), EI CO (b) and EI HC (c).

[3] There is a misalignment in the gaseous EIs in the ICAO EEDB data for the SAC variant for the 5B8 and 5B9 ratings. This is well visible in the NOx and CO emissions characteristics. The issue seems to be with the reported rated thrust for these variants in the EEDB. The rated thrust for 5B8 is 21300 lbf and 23000 lbf for the 5B9. The EIs in the EEDB seem to be reported for lower thrusts. The gaseous emissions would align with the rest of the data as a function of thrust for 5B8 rated at 20000 lbf and 5B9 at 21300 lbf. All the data should align perfectly as a function of thrust since the tests were done on a single engine. However, these adjustments would not bring the smoke numbers in alignment. We use the reported rated thrust in the EEDB in all calculations here.

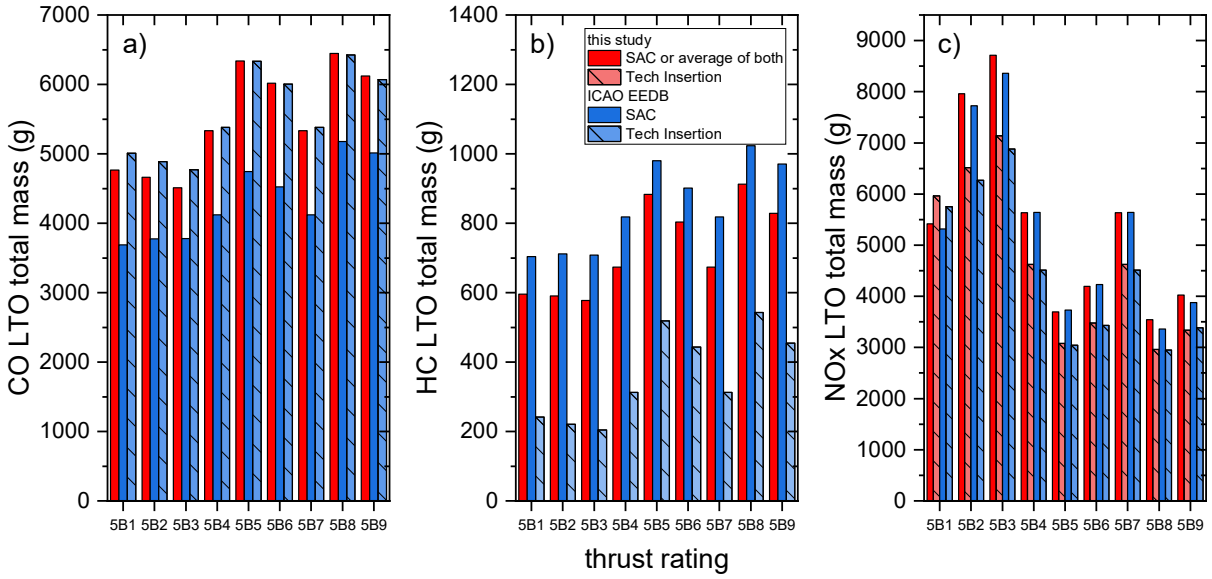

Figure 11 CFM56-5B - LTO total emissions of CO (a), HC (b) and NOx (c).

5.1.3. CFM56-5C

The CFM56-5C engine only had one combustor variant during its production run. The engine received an upgrade package "/P" in 2003. However, as the ICAO EEDB data indicate, the EIs used for the certification of this variant were obtained from the emissions data of the original version in 1991. This engine has a mixed flow nozzle and therefore higher scatter, and uncertainties are expected using a single point exhaust sampling probe.

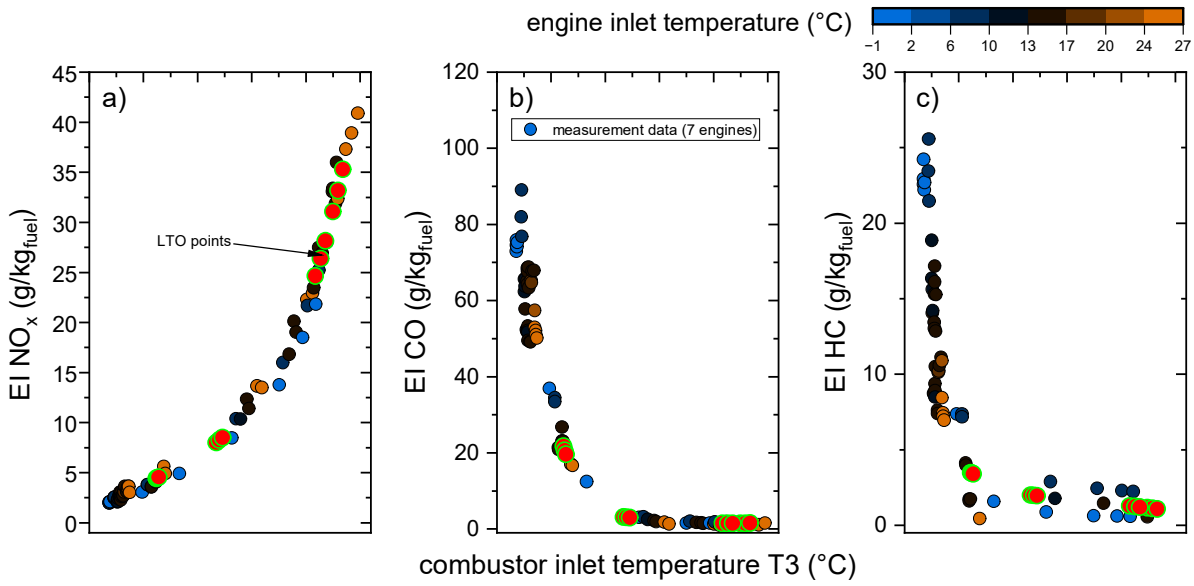

Figure 12 CFM56-5C – EI NOx (a), EI CO (b) and EI HC (c) as a function of T3.

The regulatory gaseous EIs are plotted as a function of T3 in Figure 12. The data are color mapped with ambient temperature. The red circles represent the average EIs for the LTO points of all thrust ratings determined from interpolations. Figure 13 shows a comparison of the EIs for the LTO points with the ICAO EEDB data. Our results agree well with the certified data for NOx and CO. The HC emissions measured were higher than certified emissions >7% thrust. The HC emissions have high spatial

variability at low thrust and in the mixed flow configuration, HCs may be present in the bypass, either originating from ambient air or from the de-oiler vent.

The LTO total emissions (g/LTO cycle for a given thrust rating) are shown in Figure 14. The overall agreement is excellent, especially for NOx, which was within the certification data for the two engine variants. The CO emissions were lower than certified. This can be due to the spatial variability at low thrust (sampling uncertainty). The total HCs are in line with the certification data thanks to the low measured EIs at 7%.

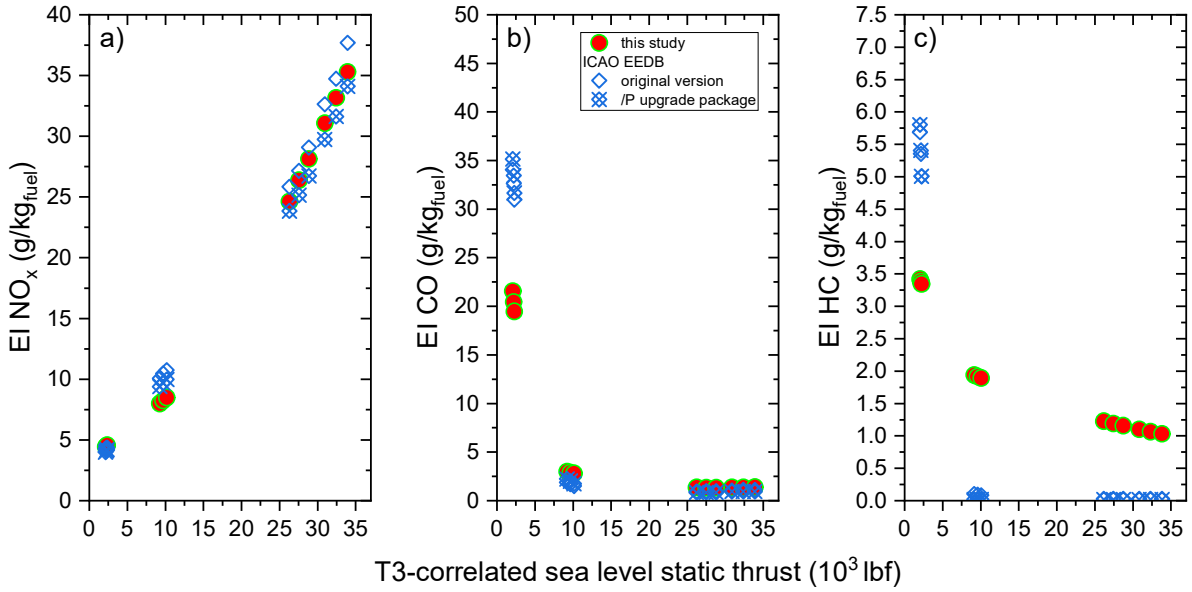

Figure 13 CFM56-5C - Comparison of measured gaseous emissions with the ICAO EEDB data: EI NOx (a), EI CO (b) and EI HC (c).

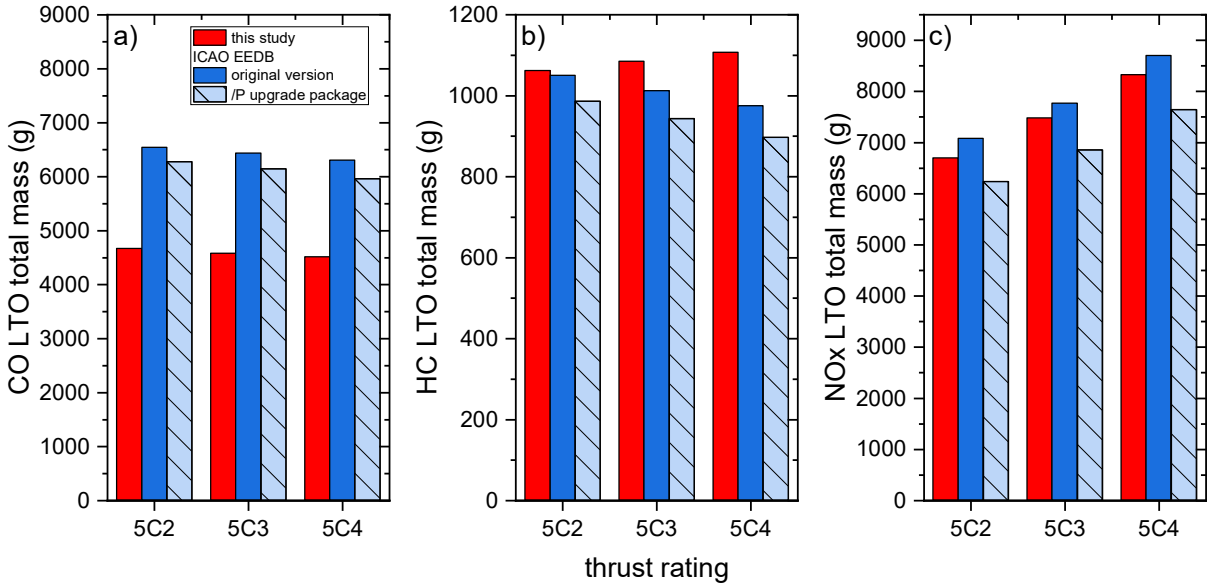

Figure 14 CFM56-5C - LTO total emissions of CO (a), HC (b) and NOx (c).

5.1.4. PW4000-94

The ICAO EEDB lists two main combustor variants for the PW4000-94 engine, Reduced smoke (introduced in 1987) and Phase III (introduced in 1993). The Phase III combustor variants PW4060 and PW4062 were recertified in 2012 and complied with the CAEP/6 NOx standard (labeled as “Phase III

new" in the plots below). The PW4062 engine, the highest-rated version, is still in production as the F139 engine for the KC-46 Pegasus multirole tanker.

The regulatory gaseous EIs are plotted as a function of T3 in Figure 15. The data are color-mapped with ambient temperature. The red circles represent the average EIs for the LTO points of all thrust ratings determined from interpolations. Figure 16 shows a comparison of the EIs for the LTO points with the ICAO EEDB data. Our results agree well with the certified data for CO and the measured NOx EIs are, surprisingly, up to 30% lower than the certification data. The HC emissions measured at LTO thrust >7% exceeded the certified emissions.

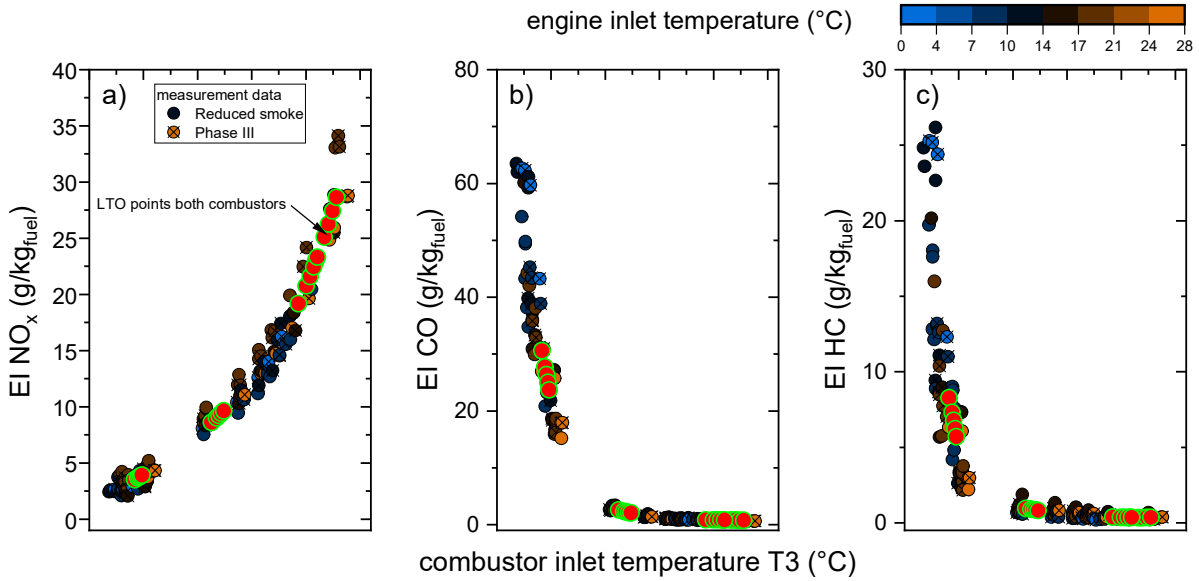

Figure 15 PW4000-94 – EI Nox (a), EI CO (b) and EI HC (c) as a function of T3.

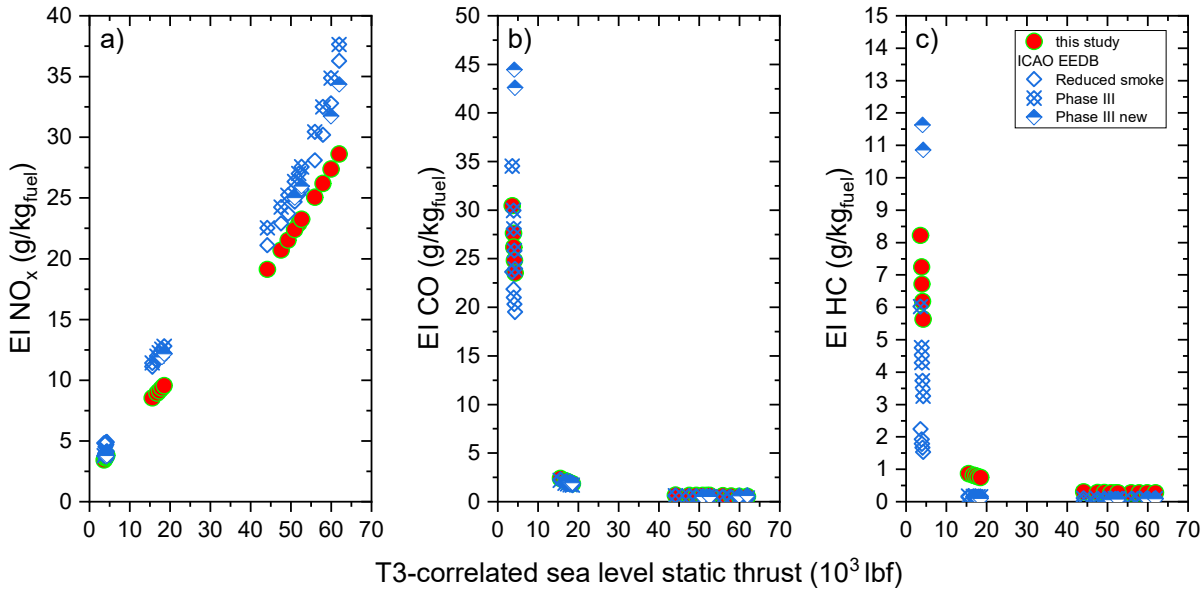

Figure 16 PW4000-94 – Comparison of measured gaseous emissions with the ICAO EEDB data: EI Nox (a), EI CO (b) and EI HC (c).

The LTO total emissions (g/LTO cycle for a given thrust rating) are shown in Figure 17. The overall agreement is excellent for CO and Nox, whereas the HC emissions were on average above the certified emissions of the Reduced smoke and Phase III combustors, but they were lower than the certified

emissions of the updated Phase III variant. It is unknown which Phase III combustor variants were used on the engines tested.

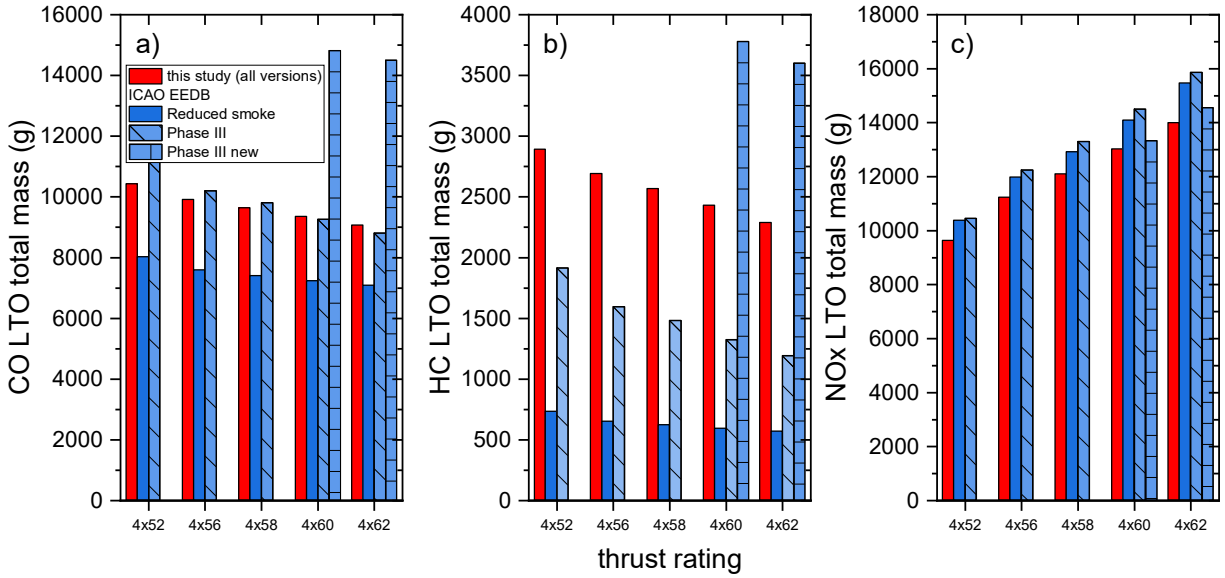

Figure 17 PW4000-94 - LTO total emissions of CO (a), HC (b) and NOx (c).

5.1.5. PW4000-100

The PW4000-100 engine was equipped with two main combustor types: Floatwall and Talon II. Talon (Technology for Advanced Low NOx) combustors are advanced Rich-Quench-Lean (RQL) combustors for, as the name suggests, low NOx (McKinney et al., 2007). In an RQL combustor, there is a tradeoff between smoke (nvPM mass) and NOx. With Talon II, the smoke number (see section 5.2 below) was close to the certification limit. This issue was rectified with the Talon IIB combustor, which, however, had higher NOx. Talon IIB was the last iteration of this combustor for the PW4000-100 that was introduced in 2008 with the uprated PW4170 (Advantage 70) variant, offering a 2k lbf thrust bump over the original PW4168 variant.

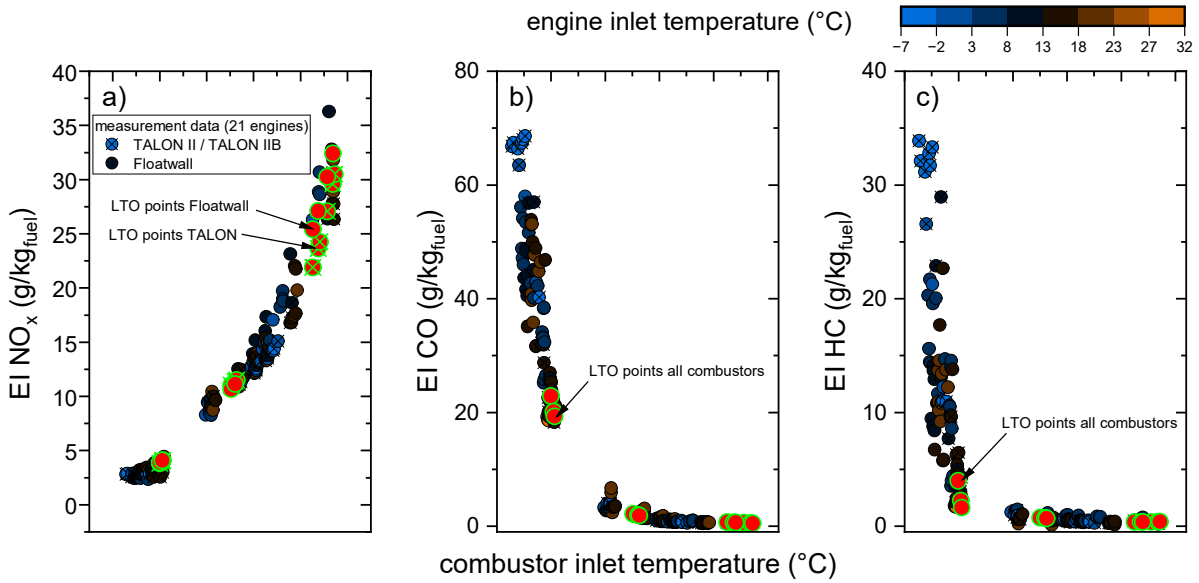

Figure 18 PW4000-100 - EI NOx (a), EI CO (b) and EI HC (c) as a function of T3.

The regulatory gaseous emissions are plotted as a function of T3 in Figure 18. The data are color-mapped with ambient temperature. The red circles represent the average EIs for the LTO points of all thrust ratings determined from interpolations. We differentiate between the Floatwall and Talon II/IIB combustors for NOx. Figure 19 shows a comparison of the EIs for the LTO points with the ICAO EEDB data. Our results agree well with the certified data for CO. In the NOx emissions, the differences between the Floatwall and Talon II combustors are noticeable, although the differences are not as significant as in the certification data. Our measurement data for the Floatwall combustor, like the results for the PW4000-94, underreport the certified emissions. On the other hand, the measured HC emissions at LTO points >7% thrust were higher than certification data.

The LTO total emissions (g/LTO cycle for a given thrust rating) are shown in Figure 20. The overall agreement is excellent for CO and NOx, whereas the HC emissions were on average above the certified emissions of the Talon II/IIB variants, but they are in line with the certification data of the Floatwall combustor.

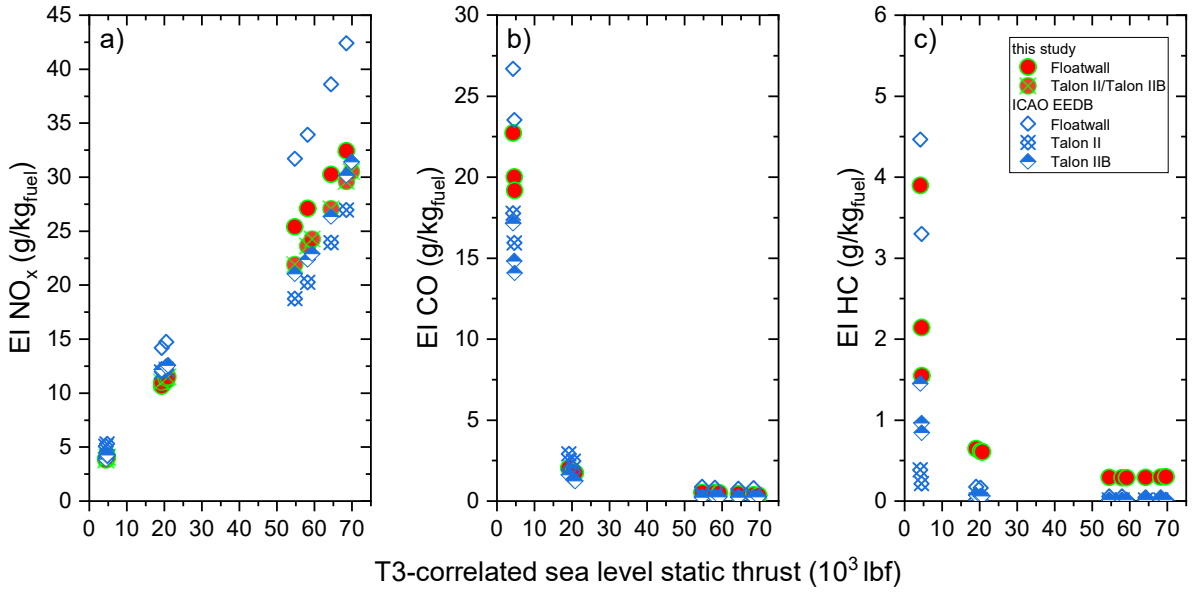

Figure 19 PW4000-100 - Comparison of measured gaseous emissions with the ICAO EEDB data: EI NOx (a), EI CO (b) and EI HC (c).

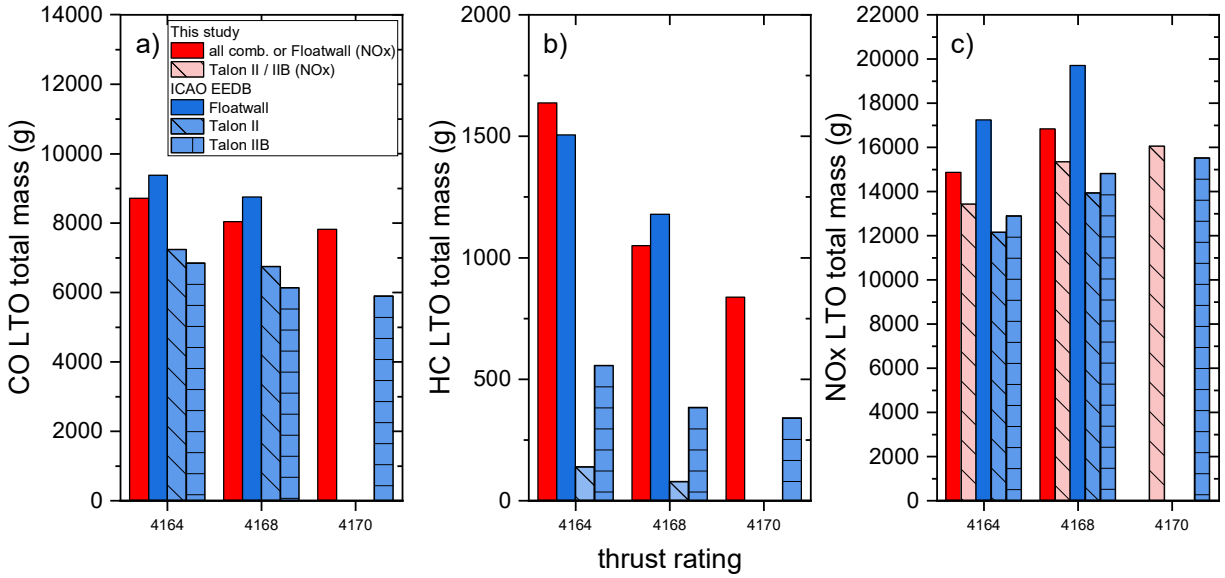

Figure 20 PW4000-100 - LTO total emissions of CO (a), HC (b) and NOx (c).

5.1.6. Primary NO2/NOx

NOx are emitted in the form of NO and NO2 and the fraction emitted as NO2 is particularly interesting for local air quality modeling. Figure 21 shows the ratio of the primary NO2 to NOx on the volume fraction basis (ppm/ppm) for the combined dataset of all engines tested. The fraction of NO2 was highest at low thrust and decreased to <0.1 above 20% thrust. The magenta-colored diamonds represent interpolated values at 5%, 7%, 10%, 30%, 85% and 100% thrust. The trend and magnitude are in line with literature values. Underwood (2007) reported mean NO2 fractions over LTO cycle modes ranging from 0.045 (range 0.01-0.08) at take-off to 0.375 (range 0.25-0.5) at idle.

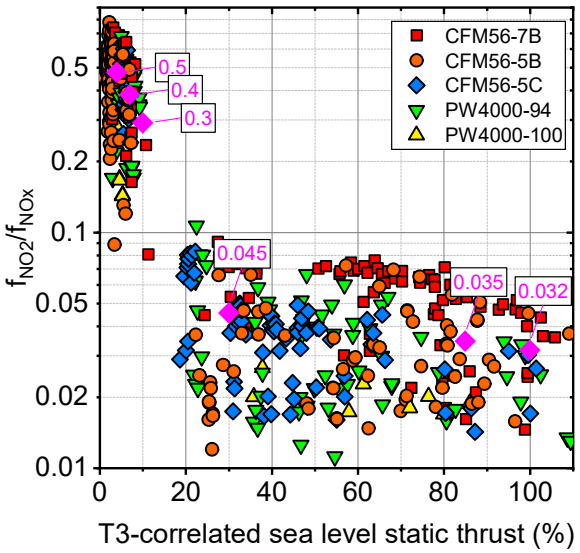

Figure 21 fraction of NOx emitted as NO2 plotted as a function of % thrust (max. rated).

5.1.1. NOx as a function of engine maintenance workscope (CFM56-7B)

While the average NOx emissions for a given engine type agreed with certification data, the question remains whether there is any measurable effect of the engine workscope on NOx. In the engine performance data of the CFM56-7B, the group of engines receiving performance restoration or overhaul had a greater EGT margin and lower specific fuel consumption (SFC) than engines receiving a less extensive repair, as shown in Figure 22.

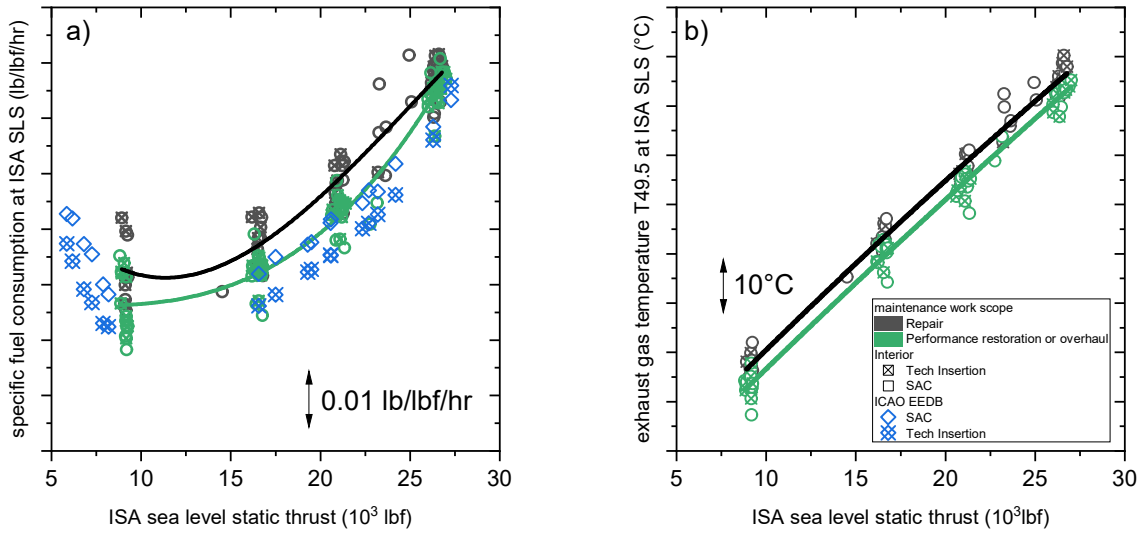

Figure 22 Effect of engine workscope on performance of CFM56-7B engines: specific fuel consumption (a) and exhaust gas temperature (b) as a function of thrust.

Proprietary work done by OEMs[4] has confirmed an increase in NOx by 2-3% because of engine deterioration due to accumulation of flight cycles. This potential difference is lower than the measurement uncertainty of EI NOx in our study. Figure 23 shows the CFM56-7B engines classified by combustor type and workscope. No significant differences could be determined in the NOx emissions as a function of workscope.

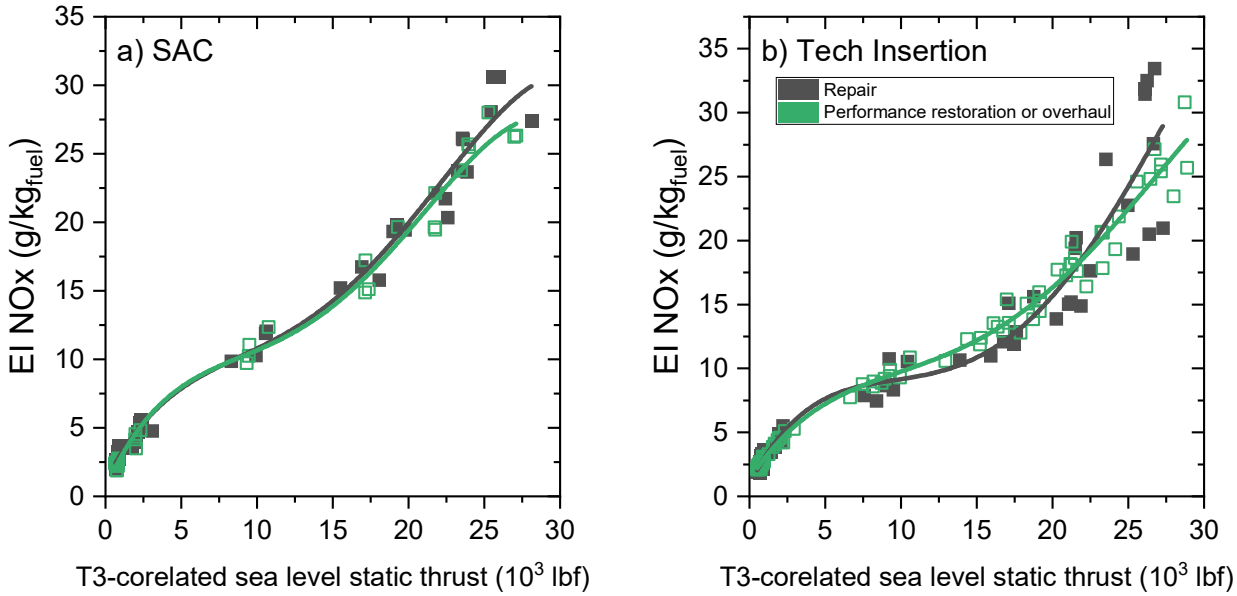

Figure 23 EI NOx for the CFM56-7B with the original combustor (a) and Tech Insertion combustor (b) as a function of thrust. The data are color coded with engine workscope.

5.1.2. Summary of gaseous LTO emissions

For all five engine types tested, we found an excellent agreement between the mean NOx emissions measured and those reported in the ICAO EEDB (panel a in Figure 24 and Figure 25). EI NOx for all LTO points was within 25% of the certification data and so were the LTO total emissions.

No significant differences could be determined in the NOx emissions as a function of workscope for the CFM56-7B engines (most comprehensive dataset in this study). To avoid random engine-to-engine variability in such an analysis, a single engine should be tested at various stages in its lifecycle and before and after an overhaul.

The measured CO emissions were also in good agreement, except for the CFM56-5C engine, where EEDB data were higher than reported here. CO is dominant at low thrust, which typically has a more heterogeneous spatial distribution of pollutants at the engine exit plane. The single-point measurements of the mixed-flow nozzle of the CFM56-5C may differ significantly from a representative multi-point average sample. The same issue can be seen for HC emissions. The HC emissions had a high scatter, and the certified EI HC were, on average, 25% lower than our measurement data. In terms of LTO total, the certified HC emissions were, on average, 40% lower than our results. For some engine types, like the PW4000-94, the difference was up to 100%. For all engine types, we observed non-zero HC emissions at high thrust, which were higher than certified emissions. These HC emissions could be a result of lower combustion efficiency or possibly also due to the sampling system background (contamination).

[4]Proprietary work done by engine manufacturers and reported to the ICAO's Committee on Aviation Environmental Protection (CAEP).

The HC and CO emissions, as it is common for gas turbine engines, peak at minimum idle, which for the engine types tested is below 7% rated thrust. The 7% thrust point may significantly underestimate the real-world emissions from taxiing aircraft, especially at low ambient temperatures. The minimum idle in test cell measurements is not representative of real-world operations because no air is extracted from the compressors for cabin ventilation and de-icing (bleed air) and there are no accessories driven by the engine. These additional loads and air extraction increase the fuel flow and reduce the AFR, which leads to a reduction of HC and CO emissions. In the SR Technics test cell, auxiliary loads can be simulated. With the simulated load on, the HC and CO emissions decreased but were higher than at 7% thrust (limited data; now shown).

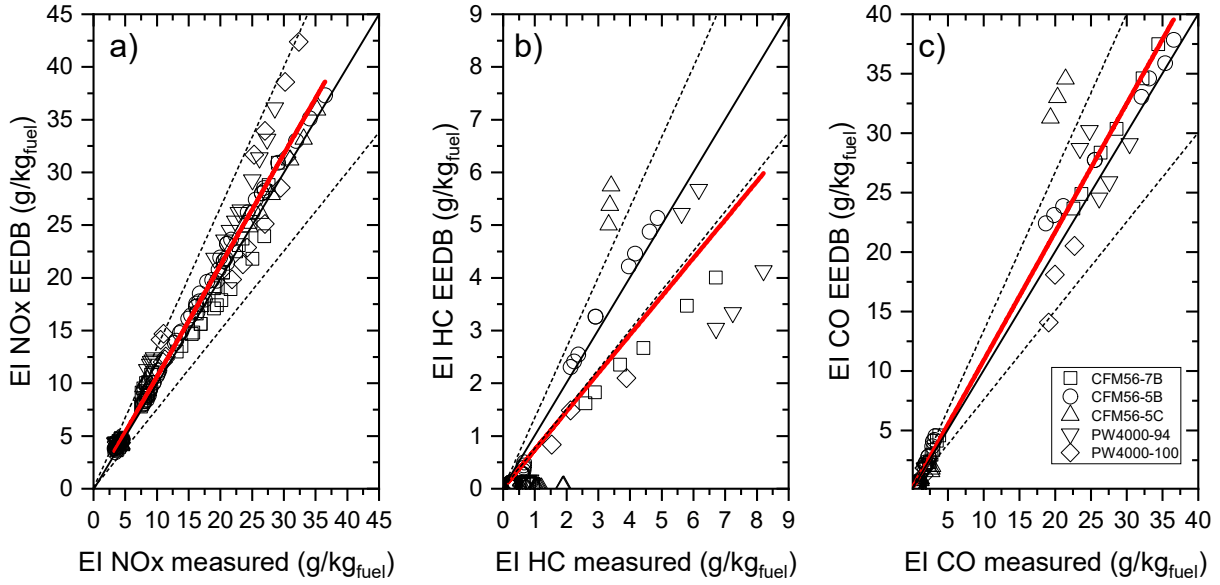

Figure 24 Parity plots of EI NOx (a), EI HC (b) and EI CO (c). The dashed lines represent +/-25% from the 1:1 line. The red lines are linear regressions without a forced intersect ($y_0 \neq 0$).

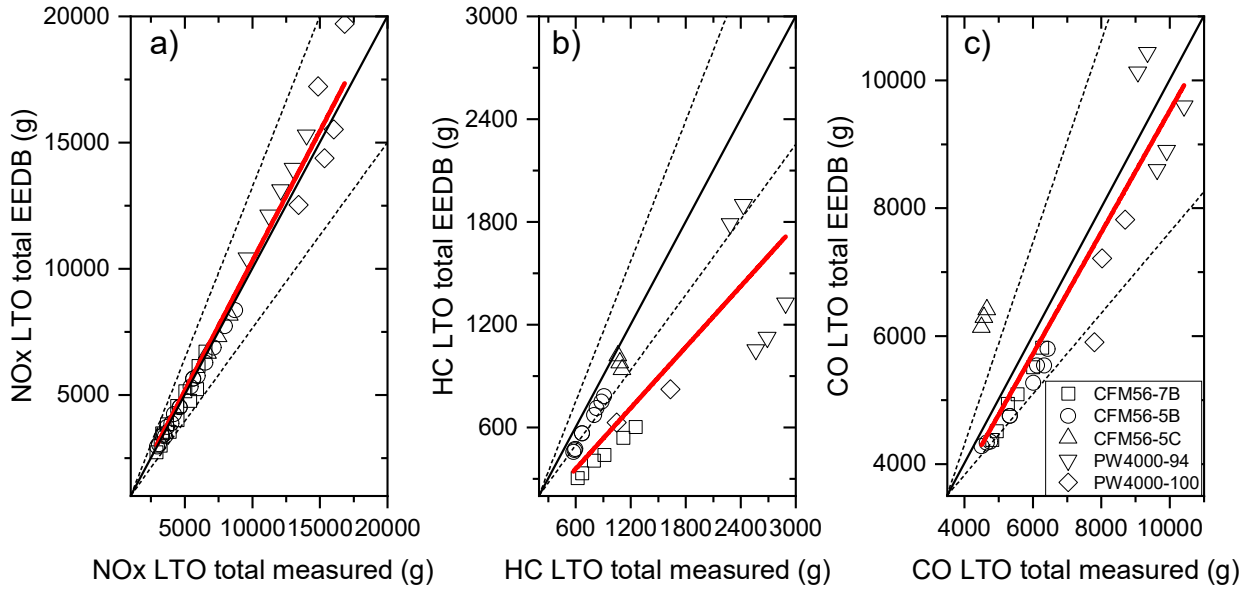

Figure 25 Parity plots of the LTO total NOx (a), HC (b) and CO (c). The dashed lines represent +/-25% from the 1:1 line. The red lines are linear regressions without a forced intersect ($y_0 \neq 0$).

5.2. Smoke number

Figure 26 shows SN as a function of thrust for the CFM56-7B (a), CFM56-5B (b), PW4000-94 (c) and PW4000-100 (d) collected during a subset of engine tests from 2017 to 2021. SN was measured also for two CFM56-5C engines with a mixed-flow nozzle but no direct comparison with the ICAO EEDB is possible because the certified SN were measured in the engine core flow, and the results are not shown here.

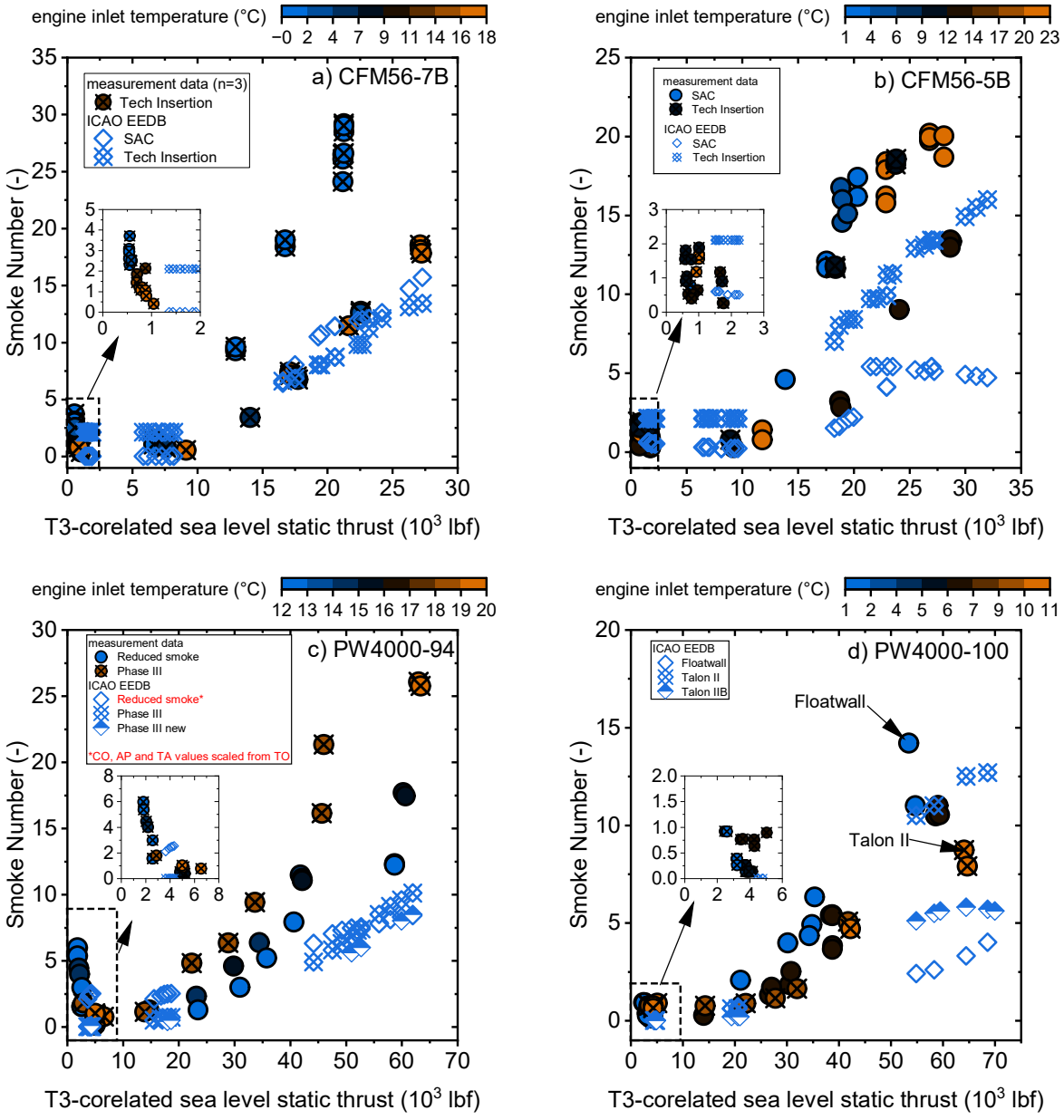

Figure 26 Smoke numbers as a function of thrust for the CFM56-7B (a), CFM56-5B (b), PW4000-94 (c) and PW4000-100 (d).

For the CFM56-7B engine (panel a), the certified SN of the two combustor types is very similar at high thrust, within the measurement uncertainty of SN measurement (system-to-system reproducibility of +/- 3 SN). At 7% and 30% thrust, the two combustors have a distinct offset which does not seem real, and it was not reproduced in our measurements. Two engines were in line with the certification data, whereas one engine produced SN of 30, a factor of 3 higher than the certification value at the given thrust. Interesting is the ambient temperature effect of SN measured at ground idle (inset of panel a),

which seems to be well measurable with SN. The SN at ground idle varied from 0.25 close to standard day (~18°C) to 4 on a cold day (~0°C).

For the CFM56-5B engine (panel b), the certification data show very distinct trends between the original and Tech Insertion combustors[5]. However, this trend was not reproduced in our measurements. The engines with SAC combustors produced maximum SN of 20, a factor of 4 higher than the certified value for this thrust. The one tested engine with the TI combustor produced SN in line with the SAC engines tested.

The PW4000-94 engines tested (panel c) produced maximum SN significantly higher than certified for all combustor variants. The certification data of all three combustor types are very similar, with a maximum value of 10 at the highest rated thrust. The Reduced smoke combustor data in the EEDB only include the SN for take-off and SN for the lower thrust levels were scaled using the recommended scaling factors (ICAO, 2020). At maximum thrust, we measured SN from 12 to up to 27. Note that SN is not corrected for ambient temperature effects and at a given T3-correlated thrust, the combustor inlet pressure decreases with increasing ambient temperature. High pressure tends to worsen the smoke emissions. The maximum SN found here would be likely even higher, had the engine with SN = 27 been operated at lower ambient temperatures. At ground idle, SN had a distinct correlation with ambient temperature, as shown in the inset.

The PW4000-100 engines have three combustor variants (panel d), where the original Floatwall combustor had the lowest certified SN. The low NOx combustors, thanks to the tradeoff between smoke and NOx in RQL combustors, had significantly higher SN. So much so that the Talon II combustor had only a 6.5% margin to the ICAO regulatory limit. The redesigned Talon IIB had improved smoke with slightly worse NOx, as discussed in the gaseous emissions above. The trends in the certified emissions were not observed in our data. The Floatwall combustor produced the highest SN, up to a factor of 3 higher than certified value. On the other hand, the one tested Talon II engine was lower than the certification data, between the certified values for Talon II and IIB.

Overall, in the limited SN datasets, the maximum SN measured for each engine type was higher than the certification data and the results varied markedly between engines of the same type. Using certified SN for estimating nvPM emissions may grossly underestimate the nvPM mass emissions of in-service engines.

[5] Similar to the certified gaseous emissions of the CFM56-5B, there is a misalignment in the SN of the SAC variant for the 5B8 and 5B9 ratings. The data for all ratings were collected on the same engine and should produce a smooth curve. The issue seems to be with the reported rated thrust.

5.3. LTO non-volatile PM emissions

5.3.1. CFM56-7B

The emission indices of nvPM mass and number for CFM56-7B engines are shown as a function of T3 in Figure 27. The data are color mapped with engine inlet temperature. The nvPM mass and number emissions varied greatly, by up to an order of magnitude at a given T3 and similar ambient temperature at high thrust. At ground idle (<7% F_{oo}), the EIs increased with decreasing ambient temperature. This effect is well visible for both nvPM mass and number. For example, the EI nvPM number ranged from 6e14 at the warmest condition to 6e15 at the coldest condition. The nvPM emissions of the two combustors were in the same range and we did not distinguish between them in our analysis. The red circles represent the average EIs for the LTO points of all thrust ratings determined from interpolations.

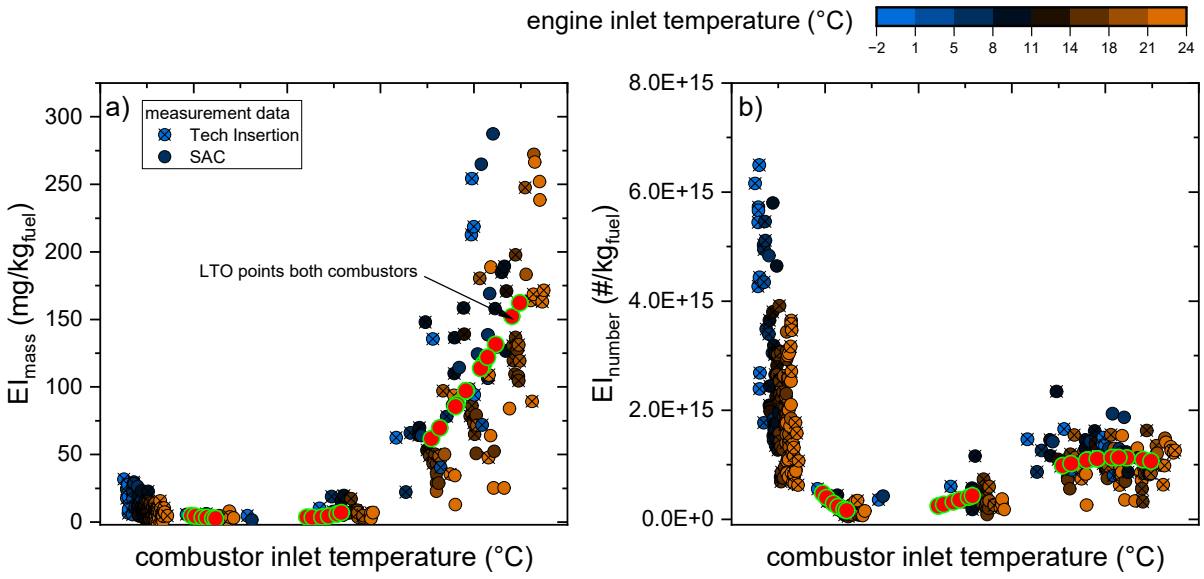

Figure 27 CFM56-7B – EI nvPM mass (a) and EI nvPM number (b) as a function of T3.

The average nvPM EIs as a function of thrust are compared with nvPM certification data and estimates obtained from SN using the FOA4 and SCOPE 11 method in Figure 28. The two combustor variants of CFM56-7B were certified for SN and only the TI version was additionally certified for nvPM[6]. The maximum nvPM mass EI was a factor of 2 higher than certification data. We note that the nvPM EIs (and SN) in the ICAO emissions databank are not corrected for ambient conditions. The nvPM certification data were collected at ambient temperatures between 22 and 38°C, considerably higher than our study. With increasing ambient temperature, the nvPM emissions at a given T3 decrease, mainly because of a lower combustor inlet pressure. The nvPM number EIs agreed with the nvPM certification data across all LTO points. The maximum nvPM number EIs were lower than certified. With increasing mass emissions, particle number tends to decrease due to increased soot coagulation in the combustor. Therefore, an engine that has excessive nvPM mass emissions, may have lower nvPM number emissions. The estimates obtained from smoke number agreed reasonably with the nvPM mass certification data at high thrust and underpredicted the average EIs from this study. For nvPM number EIs, we observed considerable differences between the predictions obtained with SCOPE11 and FOA4. The only difference between the two methods is the assumed GMD for converting nvPM mass to nvPM number (see section 4.5). FOA4 underpredicted the average EIs by ~70%, whereas SCOPE11 estimates were up to 50% higher. At 7% thrust, the differences increased to up to an order of magnitude.

[6] A closer look at the ICAO EEDB data reveals that the nvPM certification data for the CFM56-7B engine were obtained using the same engine used for the nvPM certification of CFM56-5B.

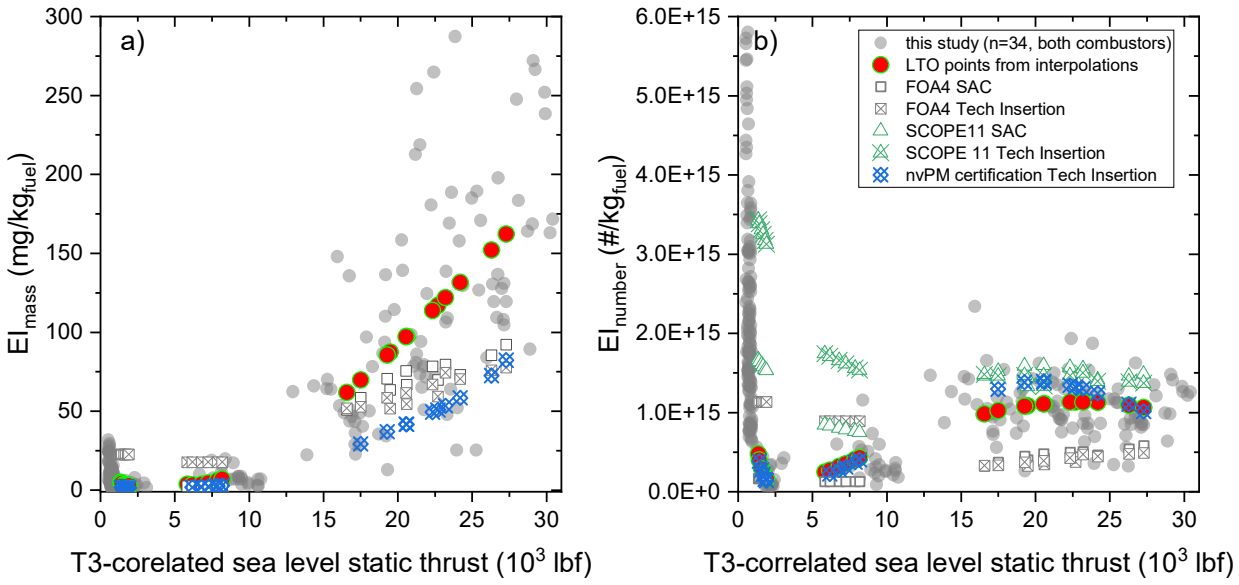

Figure 28 CFM56-7B – Average EI nvPM mass (a) and EI nvPM number (b) as a function of thrust compared with certification data and estimates from smoke number.

Figure 29 shows a comparison of the LTO total emissions for nvPM mass and number for all certified ratings. Compared to the nvPM certification data, the nvPM mass was more than a factor of 2 higher. However, the nvPM number agreed closely with the certification data. The smoke-number based predictions using FOA4 underestimated our results by up to 40% at the highest rating, with smaller differences seen for the lowest ratings. The massive differences seen between the EIs predicted from SN can be seen in the LTO nvPM number emissions. The SCOPE11 total number overestimated our results by up to a factor of 3.

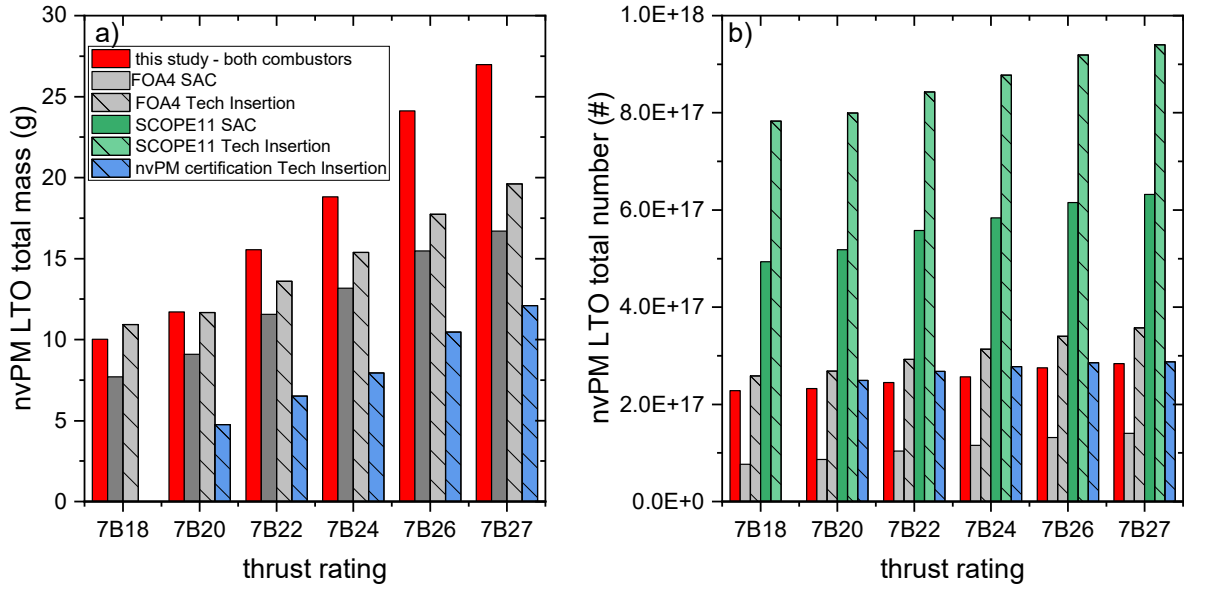

Figure 29 CMF56-7B – nvPM LTO total mass (a) and nvPM LTO total number (b) for all certified thrust ratings.

5.3.2. CFM56-5B

The emission indices of nvPM mass and number for CFM56-5B engines are shown as a function of T3 in Figure 30. The data are color mapped with engine inlet temperature. The nvPM mass and number emissions varied greatly, by up to a factor of 5 at a given T3 and similar ambient temperature at high thrust. At ground idle (<7% F_{oo}), like for the CFM56-7B, the EIs increased with decreasing ambient temperature. This effect is well visible for both nvPM mass and number. For example, the EI nvPM number ranged from 3e14 at the warmest condition to 5e15 at the coldest condition. The nvPM emissions of the two combustors were in the same range and we did not distinguish between them in our analysis. The red circles represent the average EIs for the LTO points of all thrust ratings determined from interpolations.

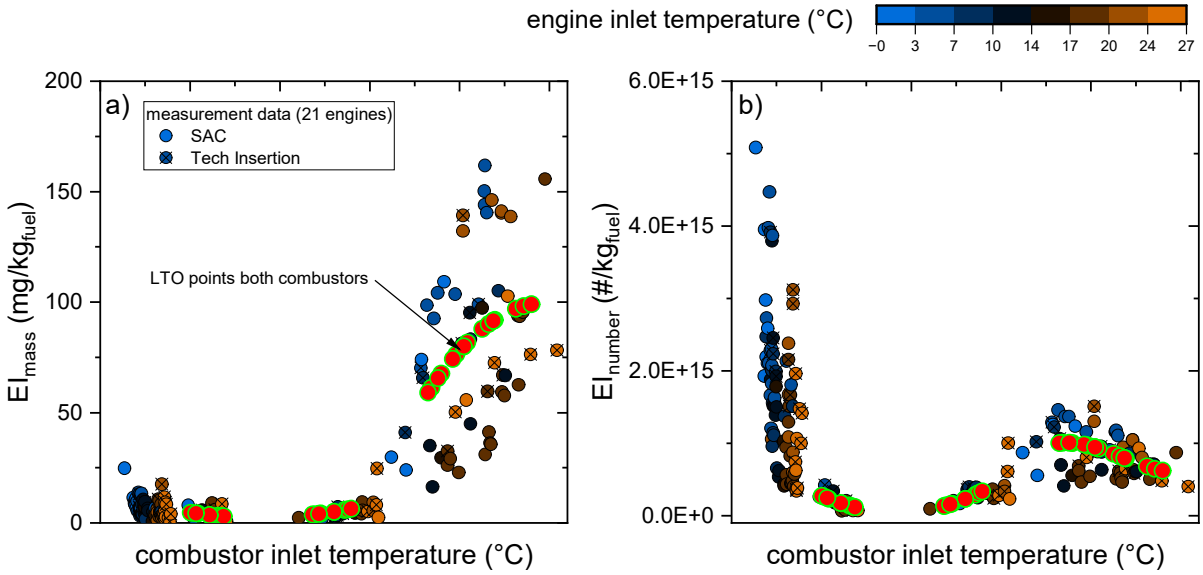

Figure 30 CFM56-5B – EI nvPM mass (a) and EI nvPM number (b) as a function of T3.

The average nvPM EIs as a function of thrust are compared with nvPM certification data and estimates obtained from SN using the FOA4 and SCOPE 11 method in Figure 31. The two combustor variants of CFM56-5B were certified for SN. The TI version was additionally certified for nvPM. The maximum nvPM mass EI agreed with the nvPM certification data of the Tech Insertion combustor. Based on the SN data, the nvPM mass EIs of the SAC version should be approximately 50% lower than TI. Some results at climb or take-off thrust overlap with these lower predicted EIs. The nvPM number EIs agreed with the nvPM certification data at 7% rated thrust and were lower than certification data at all other LTO points. Similar to the CFM56-7B engine, FOA4 underestimated the nvPM number EIs at high thrust, while SCOPE11 estimates were above our average EIs. At idle, the SCOPE11 EIs were up to a factor of 30 higher than certification nvPM data and our results.

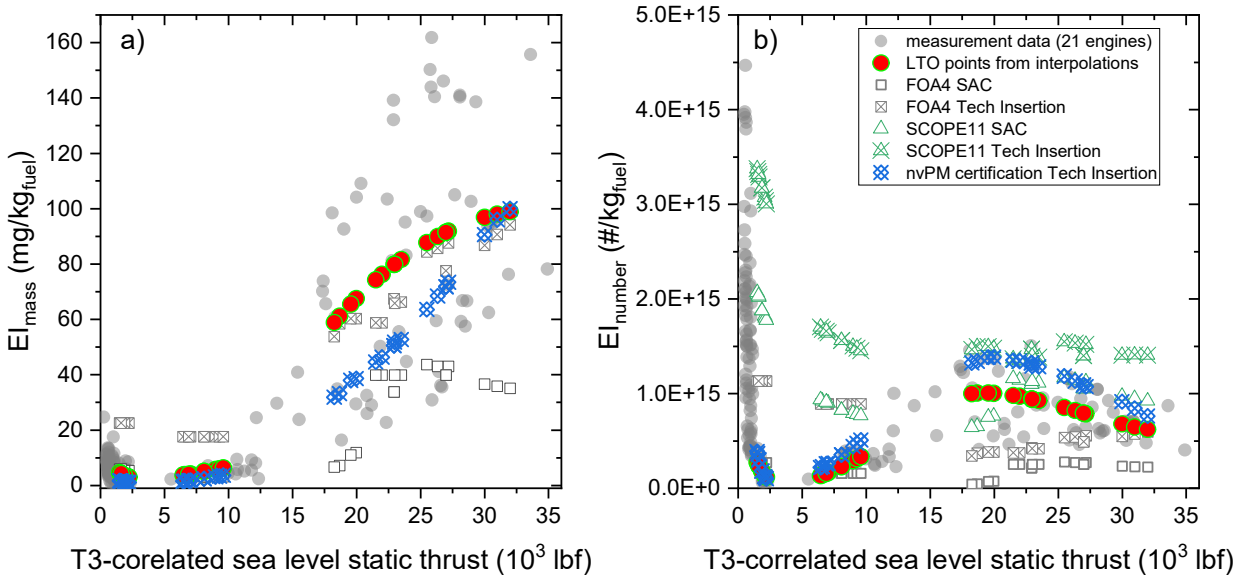

Figure 31 CFM56-5B – Average EI nvPM mass (a) and EI nvPM number (b) as a function of thrust compared with certification data and estimates from smoke number.

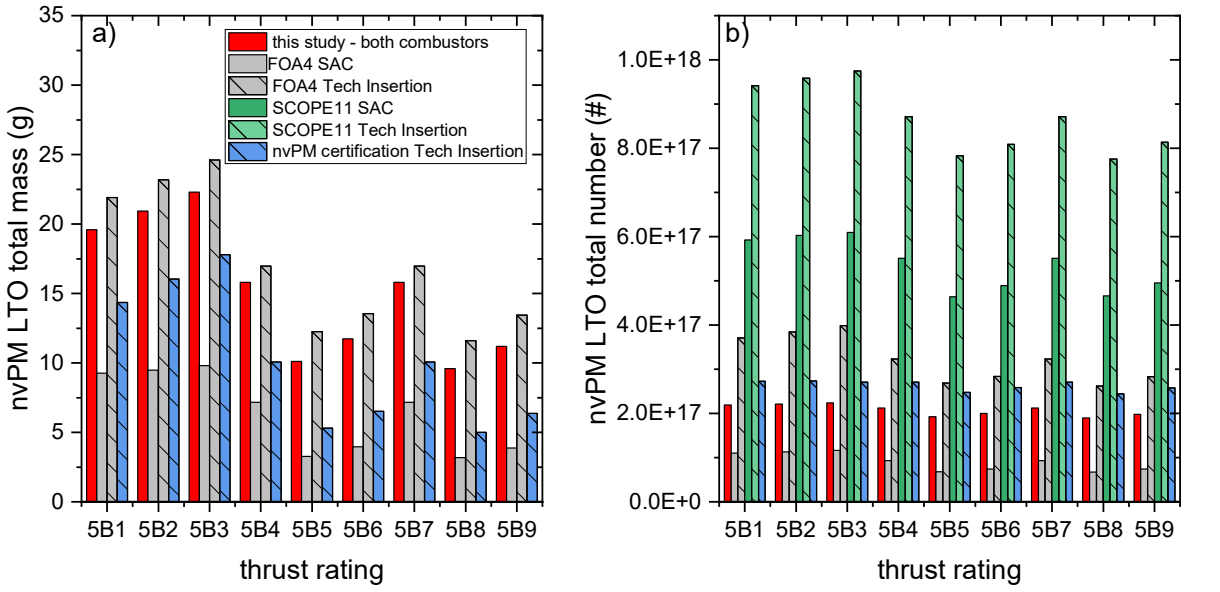

Figure 32 CMF56-5B – nvPM LTO total mass (a) and nvPM LTO total number (b) for all certified thrust ratings.

Figure 32 shows a comparison of the LTO total emissions for nvPM mass and number for all certified ratings. Compared to the nvPM certification data, our results for nvPM mass were higher for all ratings by ~30-80%. The nvPM number was lower than nvPM certification data for all ratings, within ~30%. The smoke-number based predictions varied significantly between combustors due to their different SN emission characteristics. Our results were within the range predicted using FOA4 for the two combustor types for all ratings. On the other hand, SCOPE11 overestimated the number emissions by a factor of ~3-5 at all ratings.

5.3.3. CFM56-5C

The emission indices of nvPM mass and number for CFM56-5C engines are shown as a function of T3 in Figure 33. The data are color mapped with engine inlet temperature. The nvPM mass emissions and number varied greatly, by up to a factor of 5 at a given T3 at high thrust. At ground idle (<7% F_{oo}), the EIs increased with decreasing ambient temperature, as seen for the other CFM56 variants. For example, the EI nvPM number ranged from 4e14 at the warmest condition to 5.2e15 at the coldest condition. The red circles represent the average EIs for the LTO points of all thrust ratings determined from interpolations.

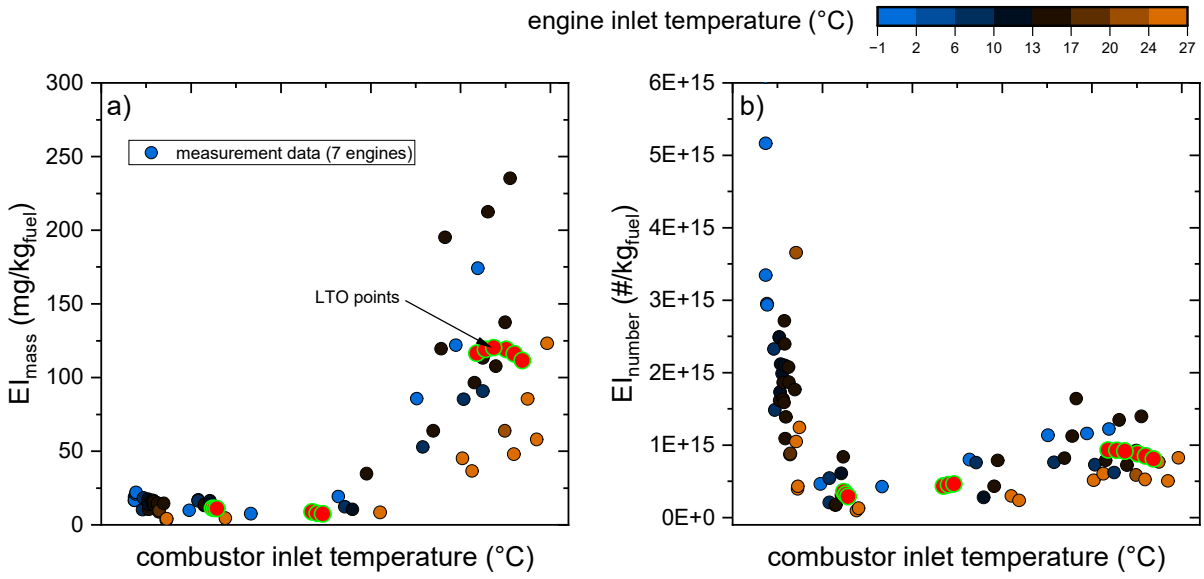

Figure 33 CFM56-5C – EI nvPM mass (a) and EI nvPM number (b) as a function of T3.

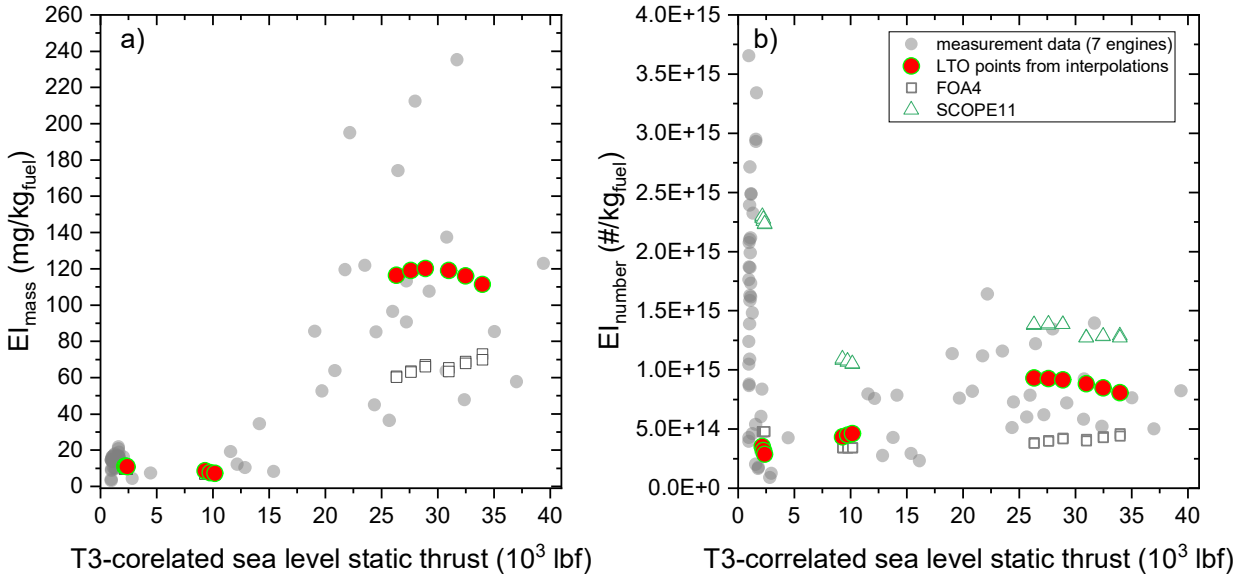

Figure 34 CFM56-5C – Average EI nvPM mass (a) and EI nvPM number (b) as a function of thrust compared with estimates from smoke number.

The average nvPM EIs as a function of thrust are compared with estimates obtained from SN using the FOA4 and SCOPE11 method in Figure 34. The engine was not nvPM certified since it was out of production before the introduction of the nvPM standard. At high thrust, the maximum EI nvPM mass was a factor of ~2 higher than FOA4 estimates. The nvPM number EIs were between the predictions from FOA4 and SCOPE11. The FOA4 underestimated the maximum nvPM number EI by ~60%. Conversely, SCOPE11 was 40% higher than this study. The relative differences increased at the 7% thrust with SCOPE11 overpredicting the measurement data by up to a factor of 10 while the FOA4 prediction was only 40% higher.

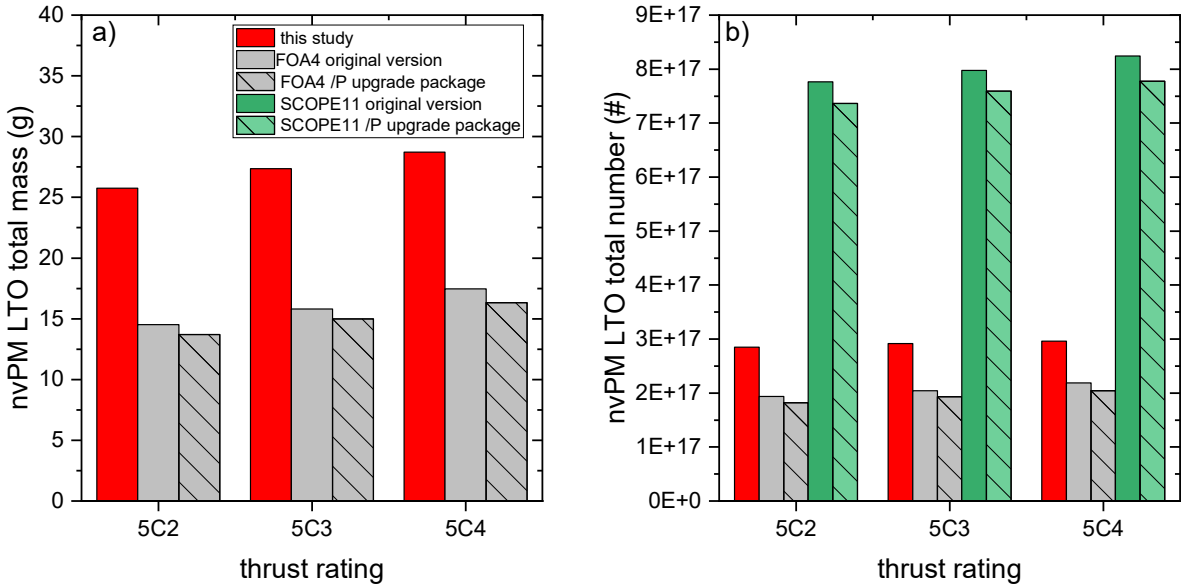

Figure 35 CMF56-5C – nvPM LTO total mass (a) and nvPM LTO total number (b) for all certified thrust ratings.

Figure 35 shows a comparison of the LTO total emissions for nvPM mass and number for all certified ratings. The nvPM mass found in this study was ~70% higher than the SN-based predictions using FOA4. For nvPM number, the FOA4 underestimated our results by ~30% whereas the SCOPE11 predicted emissions by a factor of ~3 higher.

5.3.4. PW4000-94

The emission indices of nvPM mass and number for PW4000-94 engines are shown as a function of T3 in Figure 36. The data are color mapped with engine inlet temperature. The nvPM mass emissions and number varied greatly, by up to a factor of 4 at a given T3 at high thrust. At ground idle (<7% F_{oo}), the EIs increased with decreasing ambient temperature, however, the trends are not as pronounced as for the CFM56 engines, and the results varied greatly between different engines at a similar ambient temperature (a factor of ~4 for nvPM number). The red circles represent the average EIs for the LTO points of all thrust ratings determined from interpolations.

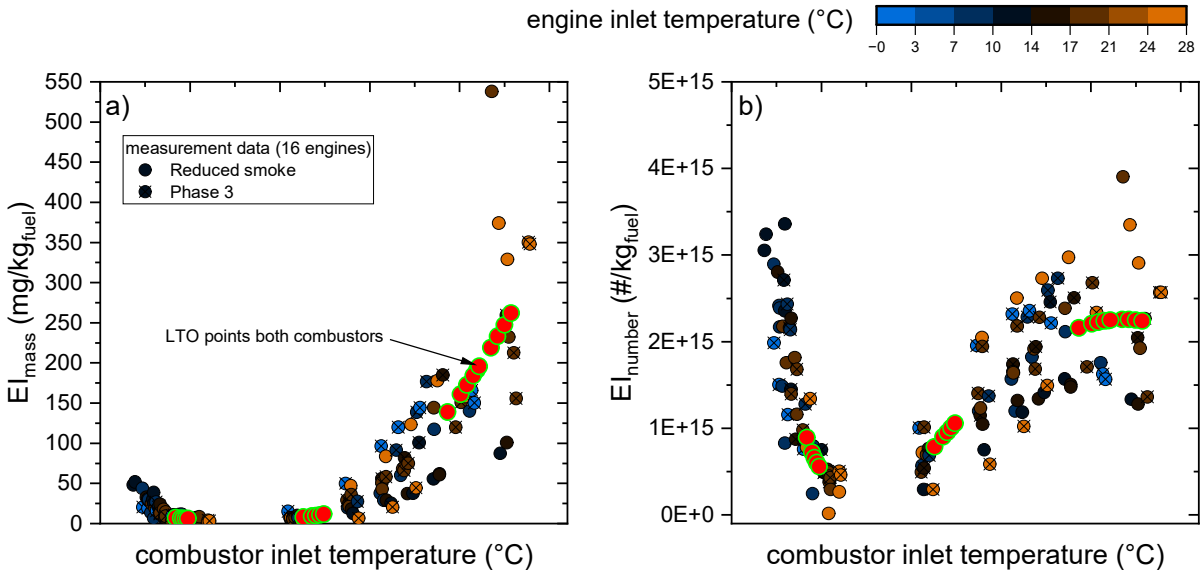

Figure 36 PW4000-94 – EI nvPM mass (a) and EI nvPM number (b) as a function of T3.

The average nvPM EIs as a function of thrust are compared with estimates obtained from SN using the FOA4 and SCOPE11 method in Figure 37. The engine was not nvPM certified since it was out of production before the introduction of the nvPM standard[7]. At high thrust, the maximum average EI nvPM mass was a factor of ~5 higher than FOA4 estimates. The maximum average nvPM number EIs at high thrust were noticeably higher than the predictions using both FOA4 and SCOPE11, by up to a factor of 7 for the FOA4. The fact that the SCOPE11 underestimated measurement data is linked to the very low smoke numbers reported in the EEDB for this engine (Figure 26). At idle (7% of rated thrust), the SCOPE 11 overestimated the experimental results by a factor of 3-7.

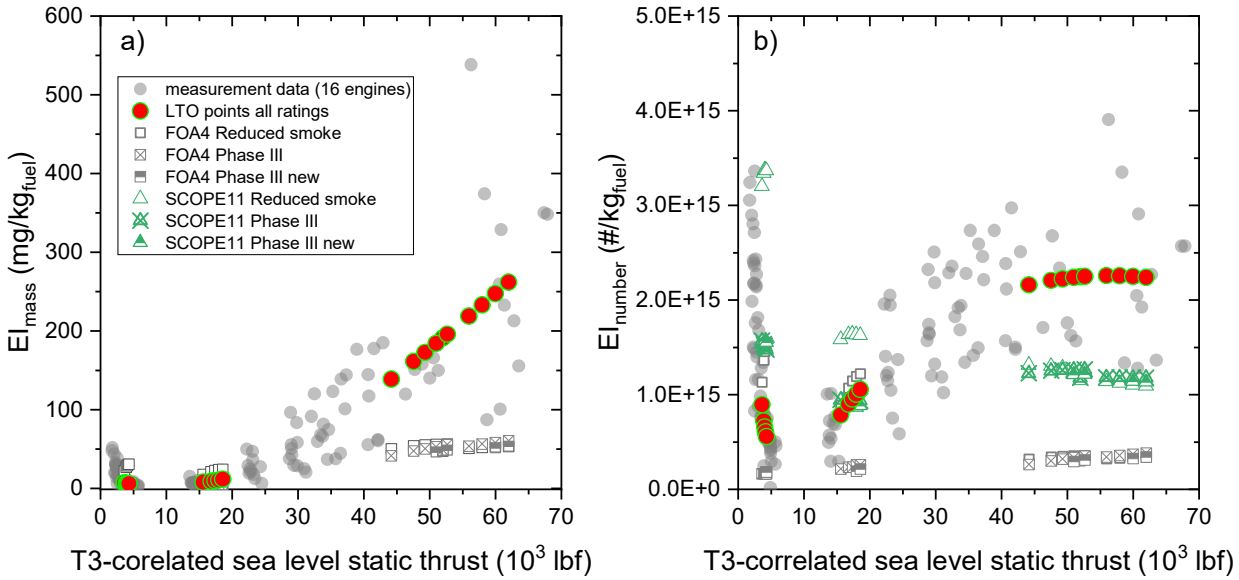

Figure 37 PW4000-94 – Average EI nvPM mass (a) and EI nvPM number (b) as a function of thrust compared with estimates from smoke number.

[7] As of 2023, the PW4062-3 variant is still in production for military applications, designated as the F139 engine by the U.S. Air Force.

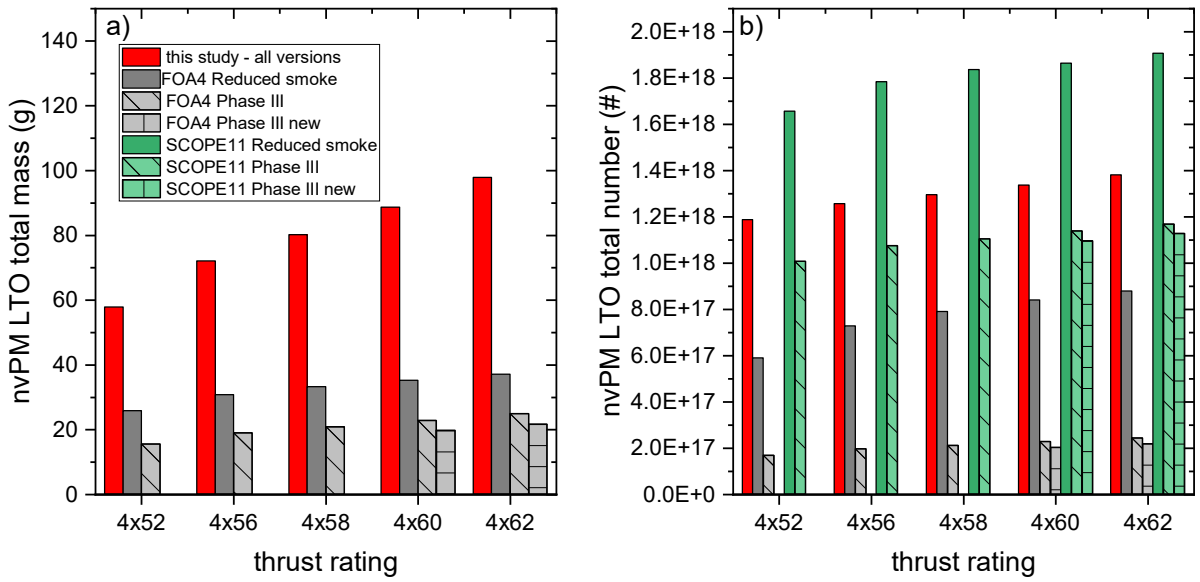

Figure 38 PW4000-94 – nvPM LTO total mass (a) and nvPM LTO total number (b) for all certified thrust ratings.

Figure 38 shows a comparison of the LTO total emissions for nvPM mass and number for all certified ratings. The nvPM mass emissions of the in-service engines were on average up to a factor of ~5 higher than predicted using certification SN. For nvPM number, the FOA4 underestimated the experimental results by up to a factor of ~6, while the SCOPE11 predictions were much closer to the experimental results. The predictions for the Phase III combustor were within 15% of the experimental results. This "lucky" coincidence is due to the low certification SN values.

5.3.5. PW4000-100

The emission indices of nvPM mass and number for PW4000-100 engines are shown as a function of T3 in Figure 39. The data are color mapped with engine inlet temperature. The nvPM mass emissions and number varied greatly, by up to a factor of 7 at high thrust. At idle, the nvPM emissions varied with ambient temperature. However, unlike for the CFM56 engines, the trend is less evident, likely due to greater differences between combustor types. The engine-to-engine and combustor type effects seem to be dominant. For example, the EI nvPM number with the Talon II combustor on a winter day was up to an order of magnitude lower than the EI nvPM number with the Floatwall combustor on a warm day. The red circles represent the average EIs for the LTO points of all thrust ratings and engine variants determined from interpolations.

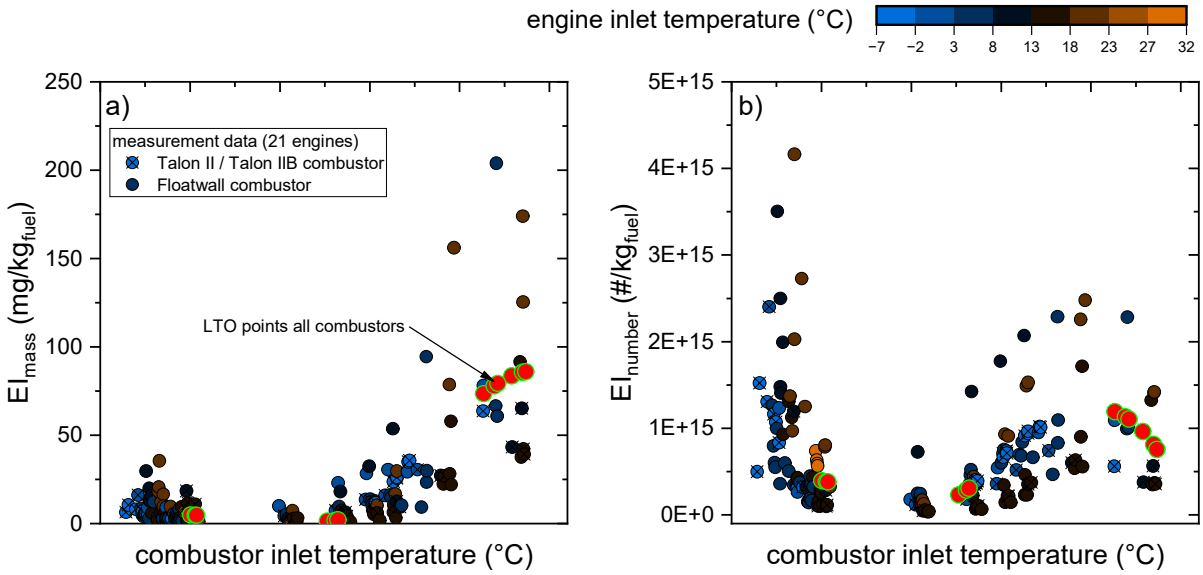

Figure 39 PW4000-100 EI nvPM mass (a) and EI nvPM number (b) as a function of T3.

The average nvPM EIs as a function of thrust are compared with estimates obtained from SN using the FOA4 and SCOPE11 methods in Figure 40. This engine type was not nvPM certified since it was out of production before the introduction of the nvPM standard. At high thrust, the interpolated maximum EI nvPM mass agreed within 15% with the EIs predicted from certification SN for the Talon II combustor and it was a factor of ~3 higher than the prediction for the Floatwall combustor. For nvPM number, the interpolated EIs at 85% and 100% thrust were within the range predicted using SCOPE11 for all three combustor variants. The FOA4-based predictions, as seen for all engines above, underestimated the average nvPM EIs at high thrust. The largest differences, by over an order of magnitude, can be seen at the 85% rated thrust (55-60k lbf) of the Floatwall variant. At 7% thrust, the SCOPE 11 overestimated the experimental results by a factor of ~4.

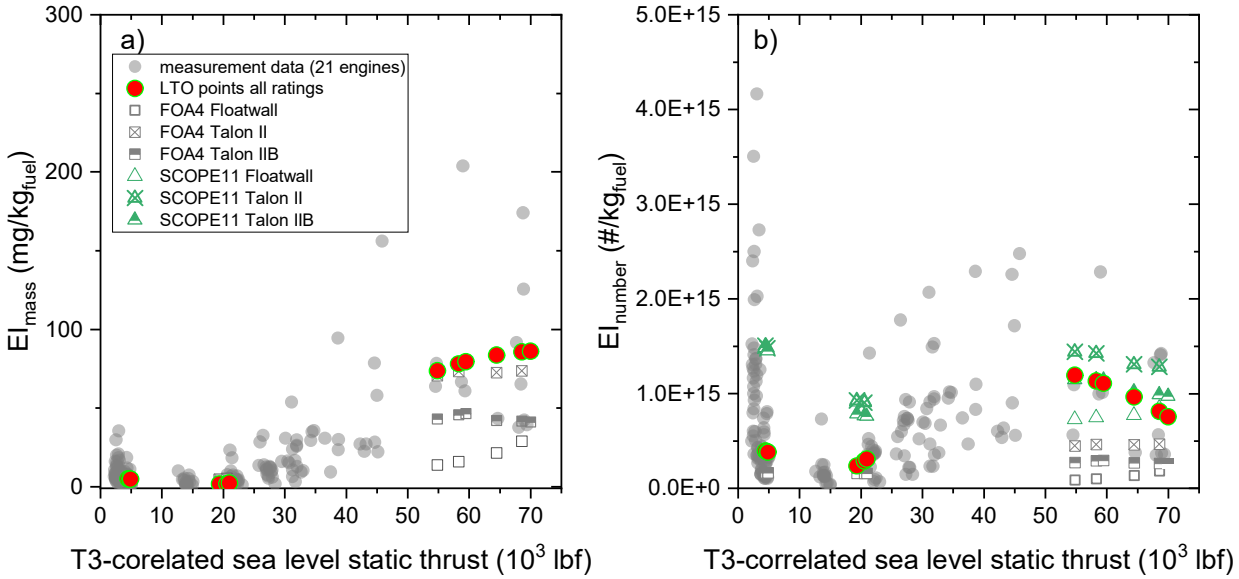

Figure 40 PW4000-100 – Average EI nvPM mass (a) and EI nvPM number (b) as a function of thrust compared with estimates from smoke number.

Figure 41 compares the LTO total emissions for nvPM mass and number for all certified ratings. For the nvPM, the predicted emissions from certified SN for the Floatwall variant severely underestimated

the mean emissions performance of the engines tested. For the common 4168 rating, the experimental results are a factor of 4 higher than predicted Floatwall emissions. On the other hand, the Talon II certification data are closer to the experimental results, within 15%. For nvPM number, the FOA4 prediction for the Floatwall variant was a factor of ~5 lower than the experimental results. The Talon II/IIB, although slightly higher, significantly underreported the experimental results. The SCOPE11 predictions, on the other hand, overestimated the experimental data by up to a factor of ~2.

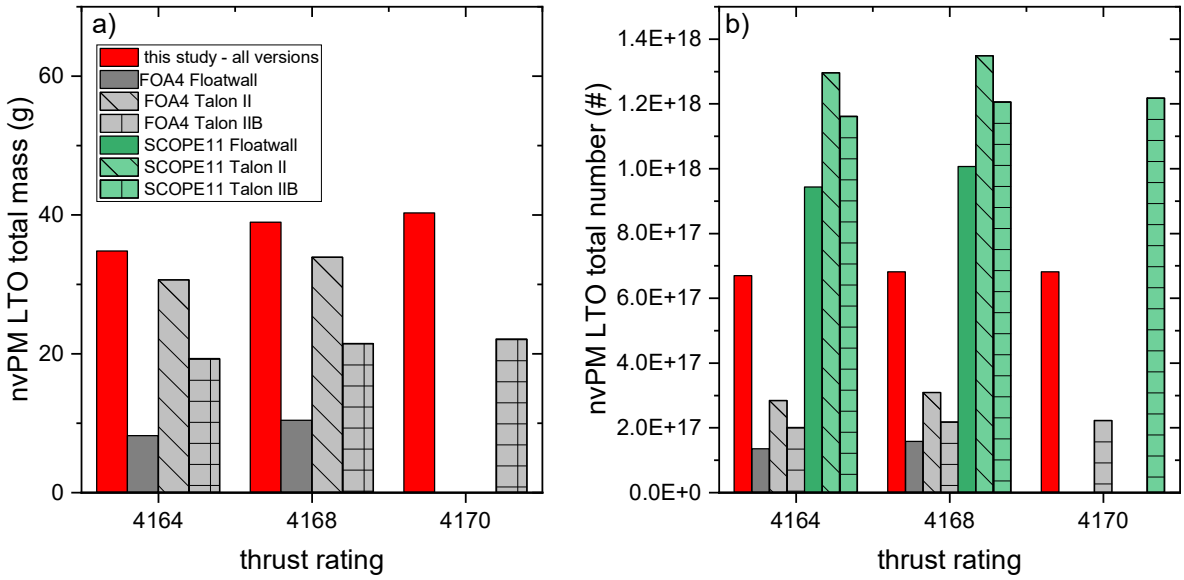

Figure 41 PW4000-100 – nvPM LTO total mass (a) and nvPM LTO total number (b) for all certified thrust ratings.

5.3.6. Summary of nvPM LTO emissions

In contrast to the gaseous emissions, the nvPM emissions varied greatly for each engine type, and the certified emissions; especially, the predictions from certified smoke numbers provided a rather poor approximation of the observations in this study.

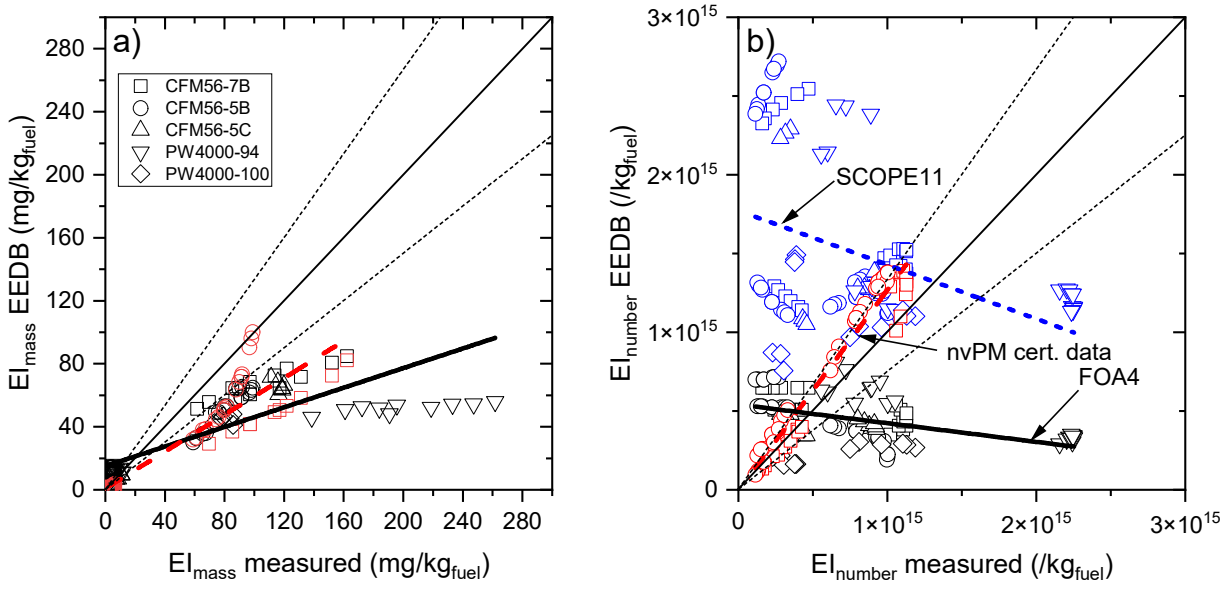

Figure 42 Parity plots of EI nvPM mass (a) and EI nvPM number (b). The thin dashed lines represent +/- 25% from the 1:1 line.

Figure 42 compares the nvPM number and mass EIs determined for all LTO points of all engine types in this study, with our results on the x-axis and the ICAO EEDB data on the y-axis. For engines with more than one combustor variant, the EEDB-based data are averages of all tested combustor variants. The certification nvPM data (CFM56-5B and -7B engines only) correlated best with the experimental data (R^2 =0.84 for nvPM mass and 0.96 for nvPM number). This is not surprising since the measurements were done using the same sampling and measurement standard (except for the exhaust sampling probe) and the same nominal set of nvPM instruments. The certification nvPM mass emissions underpredicted the experimental results (dashed red line in panel a, slope 0.58), while the the nvPM number EIs were, on average, higher (dashed red line in panel b, slope 1.28). The overall nvPM number EI agreement was very good, considering the measurement uncertainties and emissions variability.

The use of nvPM certification data is a significant step forward from the SN-based predictions. The mass-based EIs determined using FOA4 had a good correlation (R^2 =0.68) with our data, however, they overall underpredicted the experimental results (solid black line in panel a, slope 0.31). The predicted nvPM number EIs had a negative and poor correlation with experimental results (R^2=0.18 for FOA4 and 0.13 for SCOPE11). Note that the only difference in SCOPE11 and FOA4 conversion of nvPM mass EI to nvPM number is in the GMD. FOA4 assumes fixed GMDs for a given LTO mode (20 nm at 7% and 30% thrust and 40 nm at 85% and 100% thrust) while SCOPE11 predicts GMD from an empirical correlation with nvPM mass concentration (the GMDs in the SCOPE11 are not derived from measured size distributions but from estimates using the regulatory system loss correction method (SAE International, 2019). The SCOPE11 method tends to predict much smaller GMDs than those assumed by FOA4, which results in up to an order of magnitude higher predicted EI nvPM number.

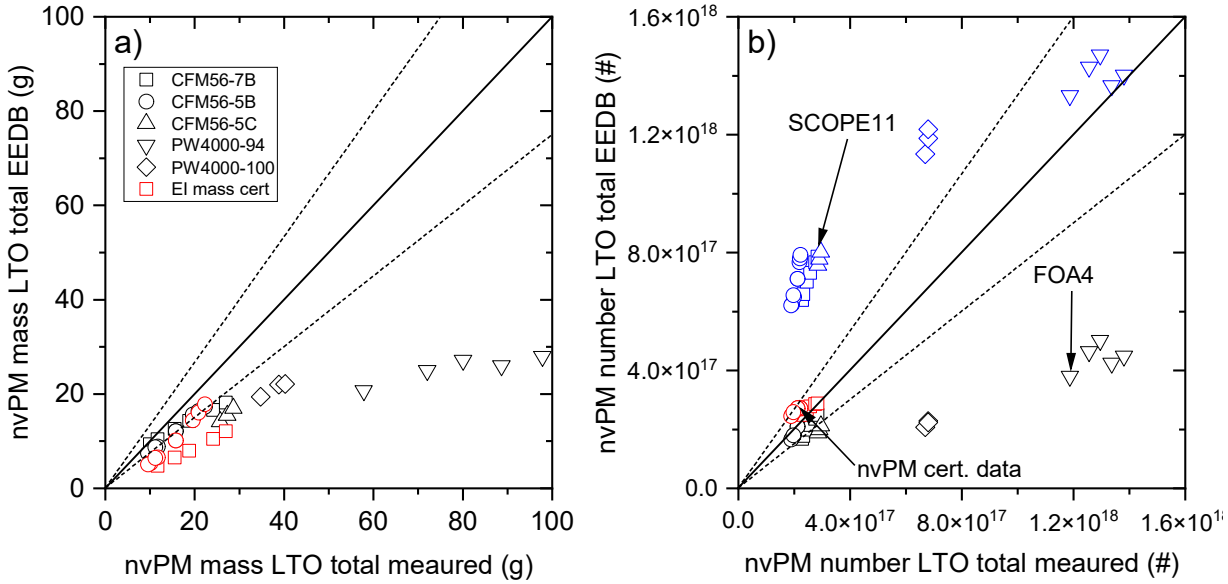

Figure 43 Parity plots of nvPM mass LTO total (a) and nvPM number LTO total (b). The dashed lines represent +/-25% from the 1:1 line.

Figure 43 compares the EEBD-based and measured LTO total nvPM mass and number emissions. For engines with more than one combustor variant, the EEDB-based data are averages of all tested combustor variants. As seen for the individual engine types, the certification data, both certified nvPM emissions and SN-based approximations, underestimated the experimental results. For the PW4000-94, the difference was more than a factor of ~4. For EI number, the nvPM certification data of the CFM56-5B and -7B engines were within 25% of this study. The FOA4 method underestimated the experimental results, whereas SCOPE11 tends to overestimate. The predictions for the PW4000-94 engine were within 25% of the experimental results. This is a coincidence due to the very low certified SN for this engine type, in stark contrast with the SN determined in this study.

The higher variability of nvPM emissions than gaseous emissions is to be expected. First, one must not forget that the nvPM emissions are a result of an extremely small combustion inefficiency (combustion efficiency at high thrust for all engine types tested >99.9%), and on a mass basis, the concentrations measured are several order magnitudes lower than gaseous emissions (e.g. typical EI NOx at take-off ~30000 mg/kg whereas nvPM mass is on the order of ~100 mg/kg). Thus, the slightest degradation can result in a relatively high increase in nvPM mass (or smoke).

The measurement uncertainty is inherently higher due to the less homogeneous spatial distribution of particles in the exhaust compared to gases. Although the sampling locations were determined to get good carbon balance based on CO2 (air-fuel ratio check), the point-by-point measured concentration of CO2 is not necessarily correlated with nvPM mass and number. Previous studies at SR Technics[8] found up to a factor of ~2 differences in nvPM mass at different angular positions at the same exhaust nozzle radius at high thrust. At idle, the difference between the maximum nvPM mass (or number) and the minimum measured at the same radius was up to a factor of 5.

Additional sources of uncertainty are ambient conditions and fuel composition. Fuel composition is thought to have a minor effect here, especially at high thrust, where the fuel composition effects are negligible (Brem et al., 2015; Durdina et al., 2021). The ambient conditions, as shown above and in greater detail in section 5.5 below, may have a significant impact on nvPM emissions, especially at ground idle. There is currently no standardized correction for ambient conditions (e.g., based on P3 and AFR) that would fit all engine types. In the future, ambient corrections for nvPM will be likely performed using proprietary empirical equations determined by the engine manufacturers.

However, the relatively large datasets for each engine type, unmatched by any other previous studies, are thought to provide a reasonable estimate of the average emissions performance of a given engine type. The results suggest higher nvPM mass emissions of in-service engines than estimated from certification data of newly manufactured engines. For the nvPM number, SN-based approximations may lead to severe underestimation or overestimation, depending on the method. Except for the PW4000-94 engine, the measured EI nvPM number was between predictions calculated with FOA4 and SCOPE11.

For the engine types tested, the nvPM number EIs peaked at ground idle, <7% thrust. Ground (or minimum) idle is not covered by the emissions certification. The engines tested here did not have any auxiliary loads (no accessories) and no bleed air (cabin ventilation) was extracted. Thus, the ground idle may not represent real-world operations. Nevertheless, the real-world ground idle nvPM emissions of engines with similar characteristics as those tested are likely underestimated with the 7% LTO point, especially in cold condition, as shown in section 5.6 below.

5.4. Engine workscope effect on nvPM emissions – CFM56-7B engines

We conducted emission measurements during engine tests after maintenance on the engines at SR Technics. At SR Technics, engines undergo one of three maintenance procedures (work-scopes) – repair (RE), engine performance improvement (EP), and complete engine overhaul (OV), as mentioned above.

Under the RE procedure, major parts of the engines undergo visual inspections; where necessary, damaged parts are repaired or overhauled. EP procedures have more parts overhauled and/or repaired during maintenance. Engines undergoing EP may have major deterioration, limiting the performance of the engine or too low EGT margin. Similar to engines undergoing EP maintenance, overhauled engines

[8] Particulate Matter and Gas Phase Emission Measurement of Aircraft Engine Exhaust. Final project report. https://www.bazl.admin.ch/dam/bazl/fr/dokumente/Politik/Umwelt/PM%20Measurement%20of%20Aircraft%20Engines_Swiss%20Research%20Public%20Results_2012-2015.pdf.download.pdf/PM%20Measurement%20of%20Aircraft%20Engines_Swiss%20Research%20Public%20Results_2012-2015.pdf
.

have all or most modules overhauled or repaired. Engines with life limited parts (LLPs) at their end of life and/or with high operating hours may undergo overhaul.

In figures and discussions below, the different power settings are classified as follows: thrusts less than 15% of maximum rated thrust (F_{oo}) were classified as idle; between 15% and 45% F_{oo} were grouped as approach (App); between 70% and 90% F_{oo} were grouped as climb out (C/O); thrusts greater than 90% F_{oo} as take-off (T/O); others (between 45 % and 70% F_{oo}) as non-LTO.

As engines age, engine deterioration may lead to increased fuel consumption and lowering of the EGT margin (Chen & Sun, 2018; Zaporozhets & Synylo, 2017). Increased fuel consumption may in-turn lead to increase in emissions. As presented above, CFM56-7B engines with different work-scopes tested after maintenance at SR Technics indicate that overhauled engines had slightly lower fuel consumption and EGT than engines with other maintenance profiles (Figure 22), especially at high power settings, though not statistically significant ($p<0.05$).

Research indicates that engine maintenance may restore an engine's emission performance (Chen & Sun, 2018). Emissions measurements alongside engine maintenance tests post-maintenance consistently indicate higher improvements in overhauled CFM56-7B engines compared to other maintenance profiles. Figure 44 presents violin plots in figure of EIs of nvPM mass and number at the engine exit, i.e., corrected for thermophoretic and system losses. The bar in the middle of the violin plots indicate the statistical distribution of the data in each bar. OV'd engines generally had lower nvPM emissions in mass and number around each thrust range compared to the EP'd and RE'd engines. The difference between OV'd engines and others is most pronounced at highest thrusts (Figure 45 and Figure 46).

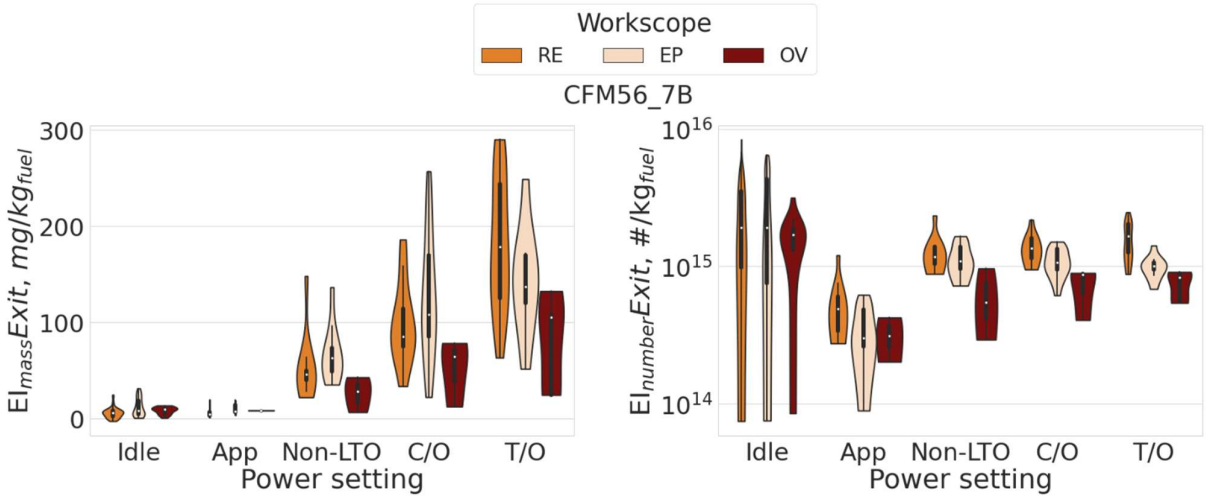

Figure 44. Violin plots presenting the distribution (center bar) and spread in nvPM emissions (EI_{mass} (left) and EI_{number} (right). Datasets are color-mapped by the type of maintenance work conducted on the engines before emission measurements.

Two-way ANOVA tests on the mean EI_{mass} at the engine exit indicate significant differences between engine emissions considering the interaction between the work-scope and the power setting. Emissions at the different power settings irrespective of the work-scope were significantly different as well as between the different maintenance work-scopes, irrespective of the power setting ($p<0.05$). Table 3 presents the t-test results for EI_{mass} at different power settings comparing engines with different maintenance work-scopes, indicating that, where significant, overhaul generally led to lower emission except at the lower power settings (idle and approach)

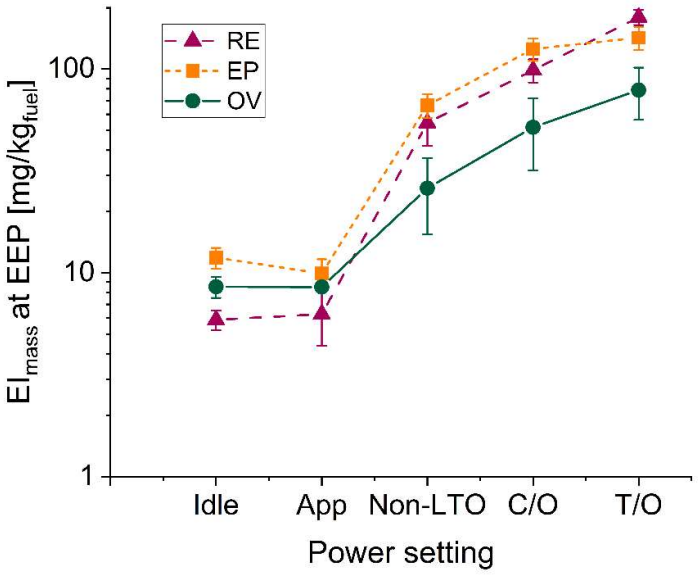

Figure 45. Mean EI_{mass} at each power setting, colored by the maintenance work on the tested engine; error bars are standard error around the mean.

Table 2 Mean EI_{mass} at a power setting for engines treated with different work-scopes

	RE	EP	OV
Idle	5.87	11.86	8.55
App	6.27	9.92	8.52
C/O	98.8	125.4	51.8
Non-LTO	54.5	66.5	26.0
T/O	179.9	142.7	79.0

Table 3. T-Test comparing means of EI_{mass} at different power settings and engines with different maintenance work-scopes

Power	Category 1	Category 2	t-statistic	p-value	Reject H_0
Idle	EP	OV	1.92	0.06	FALSE
Idle	EP	RE	3.88	0.00	TRUE
Idle	OV	RE	2.22	0.04	TRUE
App	EP	OV	0.81	0.44	FALSE
App	EP	RE	1.43	0.17	FALSE
App	OV	RE	1.19	0.27	FALSE
Non-LTO	EP	OV	2.94	0.03	TRUE
Non-LTO	EP	RE	0.79	0.44	FALSE
Non-LTO	OV	RE	-1.75	0.12	FALSE
C/O	EP	OV	2.88	0.03	TRUE
C/O	EP	RE	1.30	0.21	FALSE
C/O	OV	RE	-1.97	0.12	FALSE
T/O	EP	OV	2.17	0.06	FALSE
T/O	EP	RE	-1.54	0.14	FALSE
T/O	OV	RE	-3.70	0.01	TRUE

For EI_{number} at the engine exit, ANOVA test indicates that there was no significant difference in the mean between the data groups considering the interaction between the work-scope and the power setting ($p<0.05$). There were significant differences between the means of the different power setting, but not the means of the different work-scopes. T-tests comparing the work-scope means at each power setting (Figure 46, and Table 5) show that highest differences in number emissions were at the highest power settings with overhaul resulting in significantly lower emissions than other work-scopes ($p<0.05$).

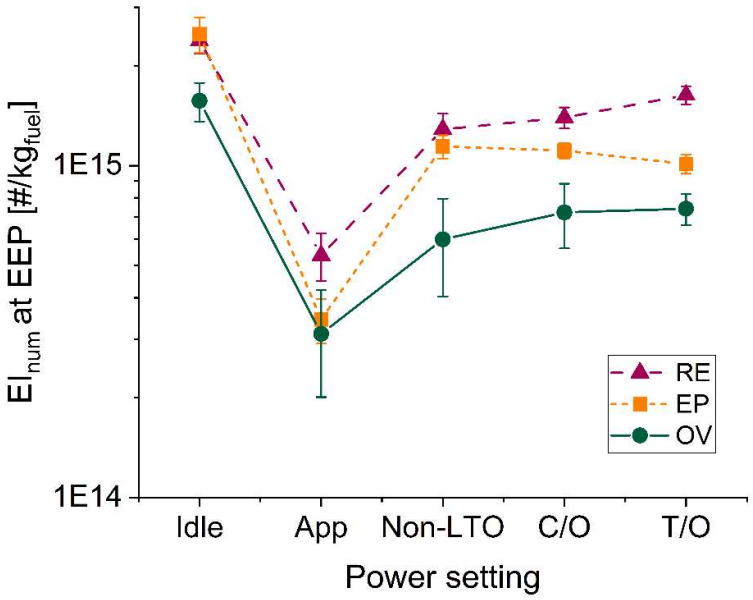

Figure 46. Mean EI_{num} at each power setting, colored by the maintenance work on the tested engine; error bars are standard error around the mean.

Table 4 Mean EI_{num} at a power setting for engines treated with different work-scopes

	RE	EP	OV
Idle	2.38E+15	2.49E+15	1.57E+15
App	5.37E+14	3.44E+14	3.11E+14
Non-LTO	1.29E+15	1.14E+15	5.99E+14
C/O	1.40E+15	1.11E+15	7.23E+14
T/O	1.63E+15	1.01E+15	7.42E+14

Table 5 T-Test comparing means of EI_{numer} at different power settings and engines with different maintenance work-scopes

Power	Category 1	Category 2	t-statistic	p-value	Reject H_0
Idle	EP	OV	2.50	0.02	TRUE
Idle	EP	RE	0.30	0.76	FALSE
Idle	OV	RE	-2.78	0.01	TRUE
App	EP	OV	0.27	0.82	FALSE
App	EP	RE	-1.88	0.08	FALSE
App	OV	RE	-1.60	0.22	FALSE
Non-LTO	EP	OV	2.52	0.09	FALSE
Non-LTO	EP	RE	-0.83	0.42	FALSE
Non-LTO	OV	RE	-2.81	0.04	TRUE
C/O	EP	OV	2.28	0.12	FALSE
C/O	EP	RE	-2.42	0.03	TRUE
C/O	OV	RE	-3.56	0.03	TRUE
T/O	EP	OV	2.59	0.03	TRUE
T/O	EP	RE	-5.15	0.00	TRUE
T/O	OV	RE	-6.93	0.00	TRUE

In summary, our observations indicate that engines that have been recently overhauled may have lower nvPM emissions compared to repaired engines. The differences in emissions due to work-scope are most pronounced at higher power settings than at idle. Overhauled engines had significantly lower number emissions than at idle than other work-scope, which is beneficial for local airport air quality.

5.5. Statistical analysis of ambient conditions effects – CFM56-7B engines

Ambient conditions can influence certain engine parameters, with consequences on engine emissions (Turgut, 2016). For instance, increase in ambient temperature has been shown to lead to increase in engine combustor inlet temperature, T3, (Turgut, 2016). The effect of ambient conditions especially engine inlet air temperature (TT2) and relative humidity (RELHUMI) is also observed to be strongest at low power than at high power settings (Turgut, 2016). In our CFM56-7B case study, we observed higher Spearman's rank correlation between TT2 and T3 at low power (T3 < 300°C, correlation = 0.68), indication a strong relationship between these parameters. At high power, however, this correlation was lower (0.3). For RELHUMI, this correlation with T3 was much lower (-0.27 at low power and -0.07 at high power), indicating a weaker influence of RELHUMI on T3. For both TT2 and RELHUMI, the effect of ambient conditions falls off at higher thrusts.

Colder temperatures have also been associated with higher emissions, especially at idle conditions. The effects of ambient conditions on gaseous emissions have been well investigated. The effect on nvPM emissions is however still under investigation. Taking nvPM emissions measured on CFM56-7B engines at SR Technics, we investigate the relationship between ambient conditions and nvPM emissions. Here, we assess the effect of TT2 and RELHUMI at low and high power settings separately.

Figure 47 presents EIs of nvPM mass and number as a function of T3, colored by the TT2. One can also observe that EIs under warmer ambient temperatures were generally lower than at colder temperatures especially for mass emissions for each cluster of thrusts and at low power. The relationship with TT2 is not as pronounced for number emissions. The relationship between TT2 and nvPM emissions is not purely linear especially at higher power and for number emissions. At low power Pearson's correlations (indicator of linear relationship) were -0.54 with mass and -0.34 with number emissions. At high power, the correlations were much lower, -0.13 for mass and -0.08 for number emissions.

Figure 48 presents nvPM EIs as a function of T3, colored by ambient RELHUMI during the measurements. Visually, there is very little trend with RH compared to TT2. There is some correlation between TT2 and RH. However, the influence of RH and nvPM emissions may not be linear, as expressed in poor Pearson's correlations at both low (0.05 for mass and 0.03 for number) and high (0.15 for mass and 0.17 for number) power settings.

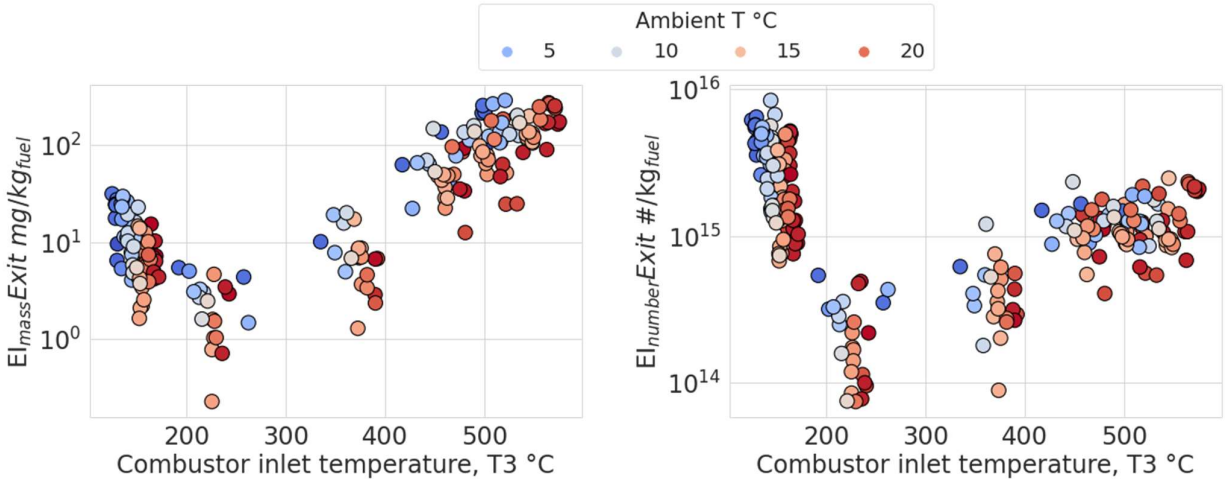

Figure 47 EI_{mass} (left) and EI_{number} (right) as a function of combustor inlet temperatures and color-mapped by ambient temperature in °C during emission measurements.

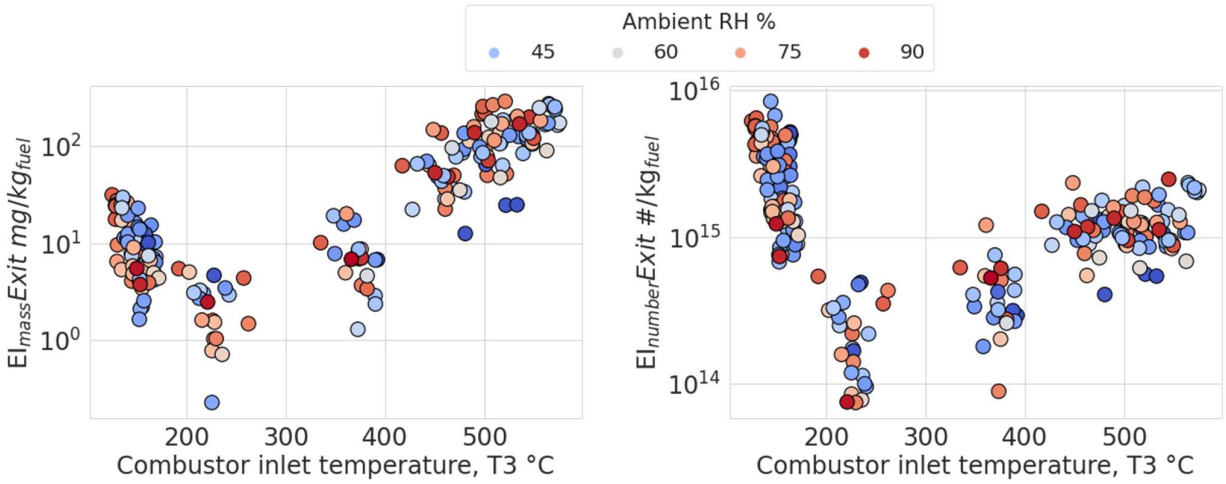

Figure 48. EI_{mass} (left) and EI_{number} (right) as a function of combustor inlet temperatures and color-mapped by relative humidity of the engine inlet air during emission measurements.

We used simple linear least square models to assess the significance of the relationship between ambient RELHUMI and TT2, and nvPM EIs. For this analysis, we split the available data into low power (T3 ≤ 300°C) and high power (T3 > 300 °C). Different combinations of T3, combustor inlet pressure (p3), TT2 and RELHUMI were assessed in their predictability of EI_{mass} and EI_{number}. This investigation presents a simple assessment of the effects of ambient conditions on nvPM emissions using linear regression on the natural log of EIs. Below, we present the best models.

EI_{mass}

The most successful model at low power for EI_{mass} was "*$ln(EI_{mass}) = T3 + TT2:RELHUMI$*", where TT2:RELHUMI accounts for the interaction between TT2 and RELHUMI, addressing the question of correlations between them. At high power, the most successful model was "*$ln(EI_{mass}) = T3 + TT2$*". Other combinations (Table 6, best models are in bold (red for low power; blue for high power)) led to lower quality models with penalties for over fitting in the model Akaike Information Criterion (AIC) and the Bayesian Information Criterion (BIC), which describe the quality of the model using the number of variables in the model; the lower the AIC and BIC (BIC penalizes more than AIC if more regressors are used), the better the model (Hossein Bonakdari & Mohammad Zeynoddin, 2022; V.A. Profillidis & G.N. Botzoris, 2019). In the high power case, "*$ln(EI_{mass}) = T3 + TT2 + T3:TT2$", had the lowest AIC, but the additional variable T3:TT2 did not improve the model (p=0.126 on ANOVA test, significance at 0.05).*

Table 6

	LOW POWER				HIGH POWER			
FORMULA	**Model Rsq**	**Model Rsq-adj**	**AIC**	**BIC**	**Model Rsq**	**Model Rsq-adj**	**AIC**	**BIC**
$LN(EI_{MASS}) = T3 + TT2 + T3:TT2$	0.562	0.55	204.7	215.6	0.833	0.828	172.9	183.7
$ln(EI_{mass}) = T3 + TT2:T3$	0.562	0.554	202.7	210	0.822	0.818	178.1	186
$LN(EI_{MASS}) = T3 + TT2$	0.561	0.553	202.9	211	**0.829**	**0.826**	**173.3**	**181.4**
$LN(EI_{MASS}) = T3 + TT2:RELHUMI$	**0.614**	**0.607**	**188.2**	**196.7**	0.77	0.765	205.9	213.9
$ln(EI_{mass}) = T3 + P3 + TT2:RELHUMI$	0.614	0.603	190.4	201.3	0.789	0.783	198.2	208.9
$ln(EI_{mass}) = T3 + RELHUMI + TT2:RELHUMI$	0.615	0.605	190.0	200.9	0.822	0.817	179.8	190.6
$ln(EI_{mass}) = T3 + TT2 + TT2:RELHUMI$	0.619	0.609	188.8	199.7	0.829	0.824	175.3	186.1

Model output: Low power (T3 ≤ 300 °C)

a. Model parameters: COEF = variable coefficients, std err = standard error, T = T statistic, PR(>T) = P-value of T > 0.05

	COEF	STD ERR	T	PR>|T|
INTERCEPT	5.2382	0.278	18.864	0.000

T3	-0.0179	0.002	-10.253	0.000
TT2:RELHUMI	-0.0006	0.000	-4.758	0.000

b. Anova table: F= F statistic, PR(>F) = P-value of F > 0.05; here, both regressors are significant in the model.

	F	**PR(>F)**
T3	152.001	0.0
TT2:RELHUMI	22.637	0.0

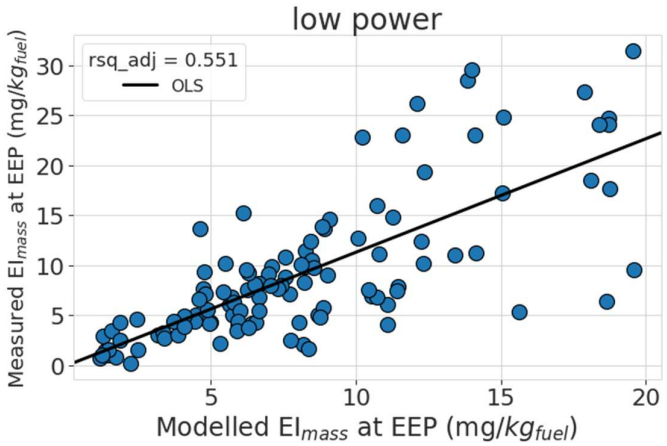

Figure 49 Measured EI$_{mass}$ as a function of modelled EI$_{mass}$ at low power, assessing the performance of the model, "*ln(EI$_{mass}$) = T3 + TT2:RELHUMI*"

Model output: High power (T3 > 300 °C)

a. Model parameters: COEF = variable coefficients, std err = standard error, T = T statistic, PR(>T) = P-value of T > 0.05

	COEF	**STD ERR**	**T**	**PR>|T|**
INTERCEPT	-3.7291	0.380	-9.808	0.000
T3	0.0182	0.001	22.434	0.000
TT2	-0.0646	0.008	-8.456	0.000

b. Anova table: F= F statistic, PR(>F) = P-value of F > 0.05; here both regressors are significant in the model

	F	**PR(>F)**
T3	442.484	0.0
TT2	71.508	0.0

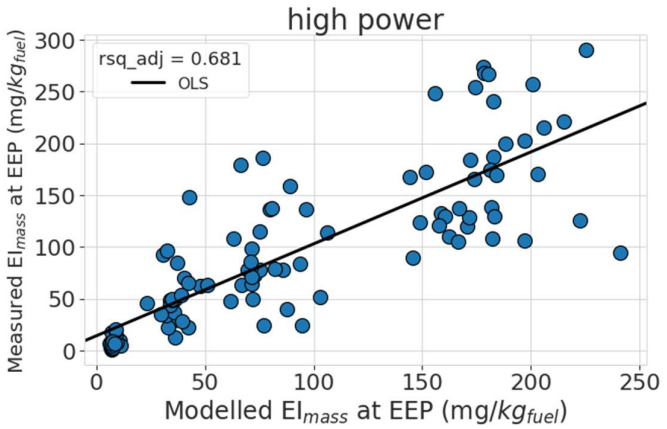

Figure 50. Measured EI$_{mass}$ as a function of modelled EI$_{mass}$ at high power, assessing the performance of the model, *ln(EI$_{mass}$) = T3 + TT2*

EI_{number}

The EI_{number} case required more complex regressors than EI_{mass}. Of the considered models, "*$ln(EI_{number})$ = T3 + T3:P3 + TT2 + TT2:RELHUMI*" was the best model at low power. At high power, "*$ln(EI_{number})$ = T3 + P3 + TT2*" was the best fit. Table 7 presents some of the models considered and parameters for identifying the best, including model R-squared values, BIC and AIC. At high power, the ANOVA test on the model parameters indicate the relevance of p3 in the model should be further investigated.

Table 7

	LOW POWER				HIGH POWER			
FORMULA	**Model Rsq**	**Model Rsq-adj**	**AIC**	**BIC**	**Model Rsq**	**Model Rsq-adj**	**AIC**	**BIC**
$LN(EI_{NUMBER})$ = T3 + TT2 + RELHUMI + TT2:RELHUMI	0.779	0.772	225.3	239	0.541	0.524	131.9	145.5
$LN(EI_{NUMBER})$ = T3 + TT2 + TT2:RELHUMI	0.774	0.768	226.8	238.4	0.527	0.514	133.3	144.2
$LN(EI_{NUMBER}R)$ = T3 + RELHUMI + RELHUMI:TT2	0.763	0.757	233.1	244.7	0.541	0.528	129.9	140.9
$LN(EI_{NUMBER})$ = T3 + P3 + RELHUMI + RELHUMI:TT2	0.771	0.764	230	244.5	0.629	0.616	107.6	121.3
$LN(EI_{NUMBER})$ = T3 + P3 + TT2 + TT2:RELHUMI	0.808	0.802	206.6	221	0.658	0.645	98.34	112
$LN(EI_{NUMBER})$ = T3 + T3:P3 + TT2 + TT2:RELHUMI	**0.814**	**0.808**	**202.7**	**217.2**	0.638	0.625	104.7	118.4
$LN(EI_{NUMBER})$ = T3 + P3 + TT2	0.789	0.784	217.5	229.1	**0.658**	**0.649**	**96.38**	**107.3**

Model output: low power (T3 ≤ 300 °C)

a. Model parameters: COEF = variable coefficients, std err = standard error, T = T statistic, PR(>T) = P-value of T > 0.05;

	COEF	STD ERR	T	P>|T|
INTERCEPT	44.3564	0.832	53.315	0.000
T3	-0.0784	0.009	-8.658	0.000
T3:P3	5.683e-08	1.08e-08	5.267	0.000
TT2	0.0810	0.013	6.337	0.000
TT2:RELHUMI	-0.0006	0.000	-3.705	0.000

b. Anova table: F= F statistic, PR(>F) = P-value of F > 0.05; here all regressors are significant for the model. T3:P3 may require further investigation of its significance.

	F	PR(>F)
T3	516.644	0.000
T3:P3	4.606	0.034
TT2	28.179	0.000
TT2:RELHUMI	13.727	0.000

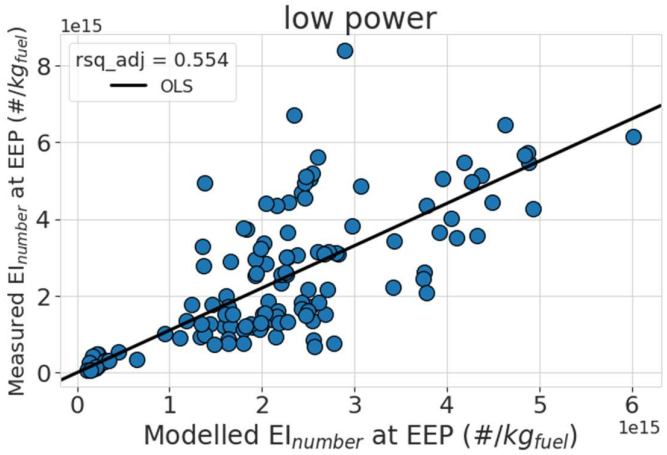

Figure 51 Measured EI_{number} as a function of modelled EI_{number} assessing the performance of the chosen model at low power; model: *$ln(EI_{number}) = T3 + T3:P3 + TT2 + TT2:RELHUMI$*

Model output: high power (T3 > 300 °C)

a. Model parameters: COEF = variable coefficients, std err = standard error, T = T statistic, PR(>T) = P-value of T > 0.05

	COEF	STD ERR	T	P>|T|
INTERCEPT	25.3289	0.975	25.989	0.000
T3	0.0375	0.005	7.998	0.000
P3	-3.651e-06	5.58e-07	-6.549	0.000
TT2	-0.1022	0.013	-7.924	0.000

b. Anova table: F= F statistic, PR(>F) = P-value of F > 0.05; here the relevance of p3 in the model is questionable and requires further investigation

	F	PR(>F)
T3	145.232	0.000
P3	3.494	0.064
TT2	62.797	0.000

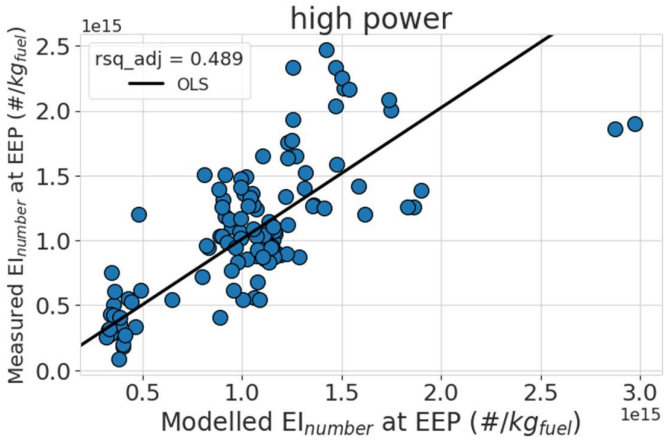

Figure 52 Measured EI_{number} as a function of modelled EI_{number} assessing the performance of the chosen model at high power; model: *$ln(EI_{number}) = T3 + P3 + TT2$*

In summary, the assessment here indicates the significance of the effect of ambient conditions on nvPM number and mass emissions. Both relative humidity and temperature significantly influenced emissions of mass and number at low power. At high power however, the more effective models required accounting for temperature effects only; relative humidity did not provide additional necessary improvements to the models. This indicates that the effect of relative humidity falls off at high power. While T3 was sufficient in the models for EI_{mass}, the better models for EI_{number} required the combustor inlet pressure, p3.

5.6. nvPM emissions at sub-7% thrust – CFM56-7B engines

As presented above, relative humidity and temperature significantly influence nvPM emissions at low power. Here, we focus on an assessment of the effect of ambient conditions on nvPM emissions at sub-7% of maximum rated thrust (idle) for CFM56-7B engines.

We split the low power data into ground idle (GI) and approach idle (AI). GI was classified as thrust settings below 5% of the engine's maximum rated thrust (F_{oo}) and AI, thrust between 5% and 8% F_{oo} (Figure 53). Average GI thrust was 2.83 ± 0.3 %F_{oo}. For power settings below GI, the combustor inlet temperature (T3) ranged from 120 °C to 180 °C. Our results indicate very strong linear correlations between TT2 and T3 (0.97) at GI, which is very similar to that observed by Turgut (2016) also for CFM56-7B engines (0.957) at GI. We observed moderate inverse correlation between RELHUMI and T3 (-0.51). AI thrust was 6.83 ± 0.3 %F_{oo}. TT2 was also strongly correlated with T3 (0.98; 0.973 in Turgut, 2016, while correlation with RELHUMI was much lower (-0.35).

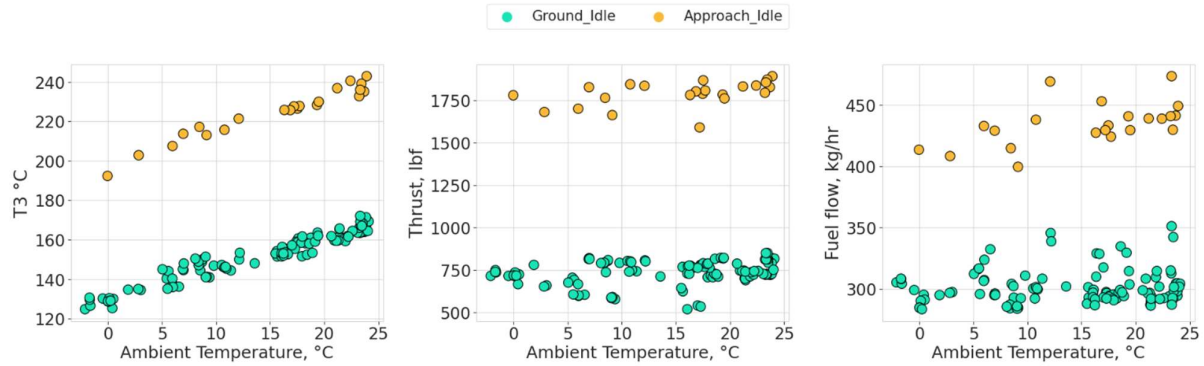

Figure 53. Showing combustor in-let temperature (T3, left), thrust corrected for test cell conditions (middle) and fuel flow (right) as a function of ambient temperature. Each plot is color-mapped by the idle groups (ground and approach idle)

Emission indices of nvPM mass (EI_{mass}) and nvPM number (EI_{number}) at GI were generally higher than emissions at AI (Figure 54). Figure 54 also indicates that for a given thrust, emissions are higher at lower ambient temperature than at higher ambient temperature (see also Figure 55). This decrease in EIs with increase ambient temperature may be due to the increase in combustion efficiency as combustor temperature (T3) increases with increase in ambient temperature. At GI, EI_{mass} was moderately inversely correlated with TT2 (-0.58); EI_{number} was moderately inversely correlated with TT2 (-0.45). At AI, EIs were slightly less correlated with TT2 compared to at GI (-0.57 for EI_{mass} and -0.38 for EI_{number}); analysis of the AI emissions is limited by the availability of very few data.

In summary, due to often long idle time at airports, GI emissions may significantly negatively impact to airport local air quality. Under colder ambient temperatures, the atmospheric boundary layer is generally stable with low atmospheric mixing and dilution. As a result, higher emissions at lower ambient temperatures during GI may lead to even higher implications on airport air quality. Research on ambient temperature effect on sub-7% idle emissions has shown similar findings with aviation gaseous emissions and volatile organic compounds (VOCs), where sub-7% emissions were significantly higher at lower ambient temperatures (*Measurement of Gaseous HAP Emissions from Idling Aircraft as a Function of Engine and Ambient Conditions*, 2012). Ground support equipment presently used at most airports in developed countries could contribute to limiting this implication by minimizing the time in GI, especially in colder periods of the year. One should note that our emission measurements at GI were without load on the engine; additional load may bring the thrust settings towards AI with lower emissions than at GI.

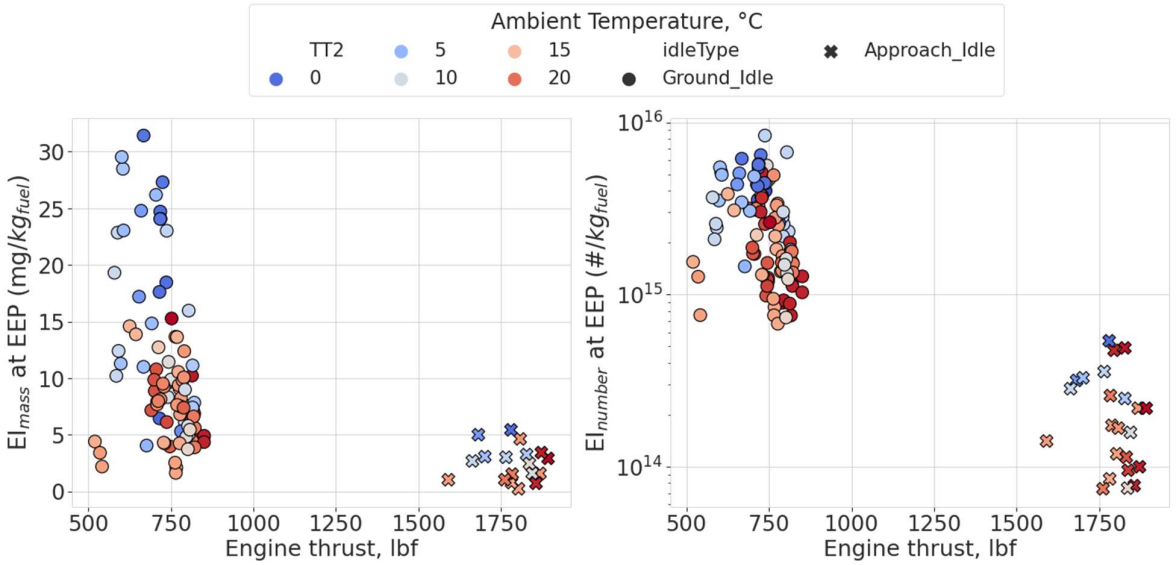

Figure 54. Emission indices of nvPM mass emission (left) and number (right) as a function of engine thrust corrected for test cell conditions. Data are color-mapped by ambient temperature and styled by idle type.

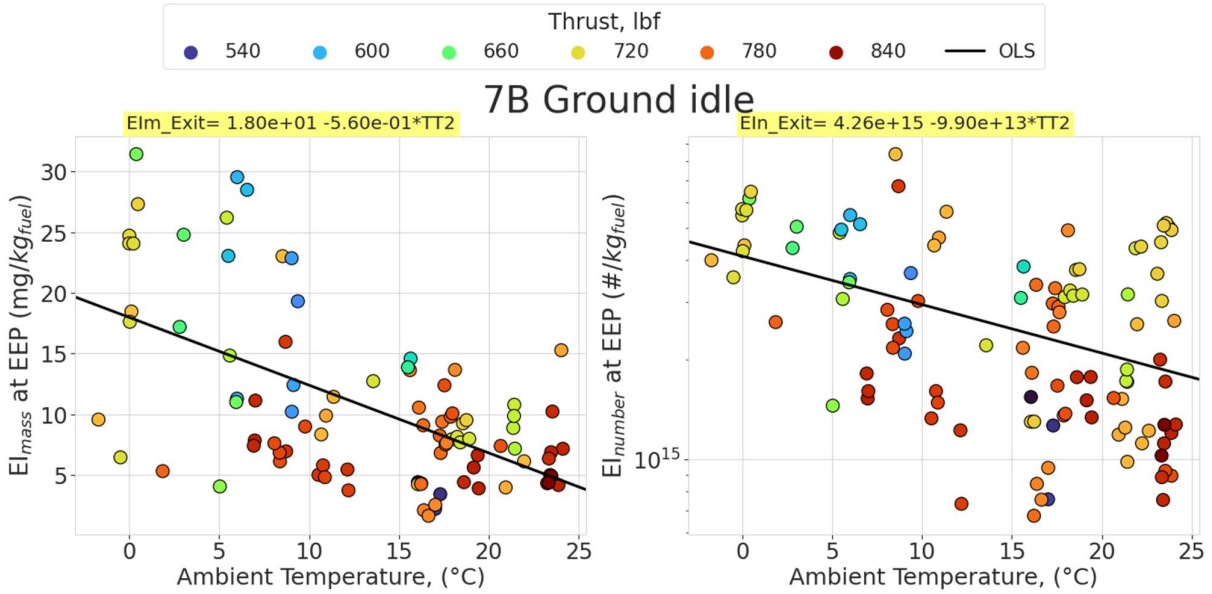

Figure 55. Emissions indices of nvPM mass (left) and number (right) at engine exit plane (EEP) as a function of ambient temperature in °C at ground idle; data points are color-mapped by the thrusts in lbf.

6. Conclusions

Variability of emissions and comparison with ICAO certification data

This study identifies significant variability in gaseous emissions, smoke number, and nvPM across different turbofan engines. When comparing these results to the ICAO certification data, our results for NOx and CO emissions were generally in good agreement, with LTO cycle NOx emissions agreeing within 25% and CO emissions aligning with certified results for different combustor variants. However, HC emissions at LTO thrust levels above 7%, while generally low, they were found to be higher than certified values for all five engine types investigated.

The smoke number and nvPM emissions showed more significant variances than gaseous emissions. The nvPM mass emissions and smoke number were generally higher than the ICAO certified values for all engine types tested. Notably, the LTO total nvPM mass emissions estimated from certification smoke number underpredicted the empirical data based on average emission characteristics of a given engine type by up to a factor of 4. For each engine type, we found “super-emitters”, with nvPM mass emissions more than twice the group average. The nvPM number emissions agreed more closely with the nvPM certification data, but the agreement with SN-based estimates was poor with differences of up to an order of magnitude in both directions depending on the predictive method used.

Impact of engine maintenance/overhaul on nvPM emissions

Maintenance workscopes, including repair and overhaul, were found to significantly impact nvPM emissions. Overhauls led to substantial reductions in nvPM emissions for CFM56-7B engines, highlighting the importance of regular maintenance for optimal engine performance and reduced emissions.

Effect of ambient conditions on nvPM emissions

Ambient conditions, particularly temperature and relative humidity, have measurable effects on nvPM emissions, especially at low thrust levels. At ground idle, which represents thrust settings below 7% of the engine's maximum rated thrust, the emission indices for both nvPM mass and number were found to increase with decreasing ambient temperature by up to an order of magnitude. This observation indicates that environmental factors play a crucial role in determining emission levels at lower thrust settings relevant for local air pollution, highlighting the need for further research to understand and mitigate these effects.

Call to action for future research

To reduce uncertainties in aviation emission inventories, future research should focus on:

- Enhancing predictive models for emissions across various operating conditions and engine types
- Investigating the long-term impact of engine maintenance practices on emission characteristics
- Exploring the influence of ambient conditions on emissions in more detail
- Improving data collection and analysis methods, including the adjustment of certification data for ambient conditions

This report underscores the complexities in understanding aviation emissions and the importance of continuous research to support effective environmental policies and technological advancements in aviation.

7. References

Ackert, S. (2015). *Managing Technical Aspects of Leased Assets*. Engine Maintenance Management, Madrid, Spain.

Agarwal, A., Speth, R. L., Fritz, T. M., Jacob, S. D., Rindlisbacher, T., Iovinelli, R., Owen, B., Miake-Lye, R. C., Sabnis, J. S., & Barrett, S. R. H. (2019). SCOPE11 Method for Estimating Aircraft Black Carbon Mass and Particle Number Emissions. *Environmental Science & Technology*, *53*(3), 1364–1373. https://doi.org/10.1021/acs.est.8b04060

Ahrens, D., Méry, Y., Guénard, A., & Miake-Lye, R. C. (2023). A New Approach to Estimate Particulate Matter Emissions From Ground Certification Data: The nvPM Mission Emissions Estimation Methodology. *Journal of Engineering for Gas Turbines and Power*, *145*(3), 031019. https://doi.org/10.1115/1.4055477

Brem, B. T., Durdina, L., Setyan, A., Kuo, Y. Y., Bahk, Y. K., Buha, J., & Wang, J. (2016). *Particulate Matter and Gas Phase Emission Measurement of Aircraft Engine Exhaust, Final Report (04/2012 – 11/2015)*. https://www.bazl.admin.ch/dam/bazl/fr/dokumente/Politik/Umwelt/PM%20Measurement%20of%20Aircraft%20Engines_Swiss%20Research%20Public%20Results_2012-2015.pdf.download.pdf/PM%20Measurement%20of%20Aircraft%20Engines_Swiss%20Research%20Public%20Results_2012-2015.pdf

Brem, B. T., Durdina, L., Siegerist, F., Beyerle, P., Bruderer, K., Rindlisbacher, T., Rocci-Denis, S., Andac, M. G., Zelina, J., Penanhoat, O., & Wang, J. (2015). Effects of Fuel Aromatic Content on Nonvolatile Particulate Emissions of an In-Production Aircraft Gas Turbine. *Environmental Science & Technology*, *49*(22), 13149–13157. https://doi.org/10.1021/acs.est.5b04167

Chen, D., & Sun, J. (2018). Fuel and emission reduction assessment for civil aircraft engine fleet on-wing washing. *Transportation Research Part D: Transport and Environment*, *65*, 324–331. https://doi.org/10.1016/j.trd.2018.05.013

Durand, E., Durdina, L., Smallwood, G., Johnson, M., Spirig, C., Edebeli, J., Roth, M., Brem, B., Sevcenco, Y., & Crayford, A. (2023). Correction for particle loss in a regulatory aviation nvPM emissions system using measured particle size. *Journal of Aerosol Science*, *169*, 106140. https://doi.org/10.1016/j.jaerosci.2023.106140

Durand, E. F., Crayford, A. P., & Johnson, M. (2020). Experimental validation of thermophoretic and bend nanoparticle loss for a regulatory prescribed aircraft nvPM sampling system. *Aerosol Science and Technology*, *0*(0), 1–15. https://doi.org/10.1080/02786826.2020.1756212

Durdina, L., Brem, B. T., Elser, M., Schönenberger, D., Siegerist, F., & Anet, J. G. (2021). Reduction of Nonvolatile Particulate Matter Emissions of a Commercial Turbofan Engine at the Ground Level from the Use of a Sustainable Aviation Fuel Blend. *Environmental Science & Technology*, *55*(21), 14576–14585. https://doi.org/10.1021/acs.est.1c04744

Durdina, L., Brem, B. T., Setyan, A., Siegerist, F., Rindlisbacher, T., & Wang, J. (2017). Assessment of Particle Pollution from Jetliners: From Smoke Visibility to Nanoparticle Counting. *Environmental Science & Technology*, *51*(6), 3534–3541. https://doi.org/10.1021/acs.est.6b05801

Hossein Bonakdari & Mohammad Zeynoddin. (2022). Chapter 5—Goodness-of-fit & precision criteria. In Hossein Bonakdari & Mohammad Zeynoddin (Eds.), *Stochastic Modeling* (pp. 187–264). Elsevier. https://doi.org/10.1016/B978-0-323-91748-3.00003-3

ICAO. (2017). *Annex 16—Environmental Protection Volume 2—Aircraft Engine Emissions*. https://store.icao.int/annex-16-environmental-protection-volume-2-aircraft-engine-emissions.html

ICAO. (2020). *Doc 9889, Airport Air Quality Manual*. https://www.icao.int/publications/documents/9889_cons_en.pdf

ICAO. (2023). *ICAO Aircraft Engine Emissions Databank* (Version v29B) [dataset]. https://www.easa.europa.eu/en/domains/environment/icao-aircraft-engine-emissions-databank

Kurzke, J., & Halliwell, I. (2018). *Propulsion and Power*. Springer International Publishing. https://doi.org/10.1007/978-3-319-75979-1

Lobo, P., Durdina, L., Smallwood, G. J., Rindlisbacher, T., Siegerist, F., Black, E. A., Yu, Z., Mensah, A. A., Hagen, D. E., Miake-Lye, R. C., Thomson, K. A., Brem, B. T., Corbin, J. C., Abegglen, M., Sierau, B., Whitefield, P. D., & Wang, J. (2015). Measurement of Aircraft Engine Non-Volatile PM Emissions: Results of the Aviation-Particle Regulatory Instrumentation Demonstration Experiment (A-PRIDE) 4 Campaign. *Aerosol Science and Technology*, *49*(7), 472–484. https://doi.org/10.1080/02786826.2015.1047012

McKinney, R., Cheung, A., Sowa, W., & Sepulveda, D. (2007, January 8). The Pratt & Whitney TALON X Low Emissions Combustor: Revolutionary Results with Evolutionary Technology. *45th AIAA Aerospace Sciences Meeting and Exhibit*. 45th AIAA Aerospace Sciences Meeting and Exhibit, Reno, Nevada. https://doi.org/10.2514/6.2007-386

Measurement of Gaseous HAP Emissions from Idling Aircraft as a Function of Engine and Ambient Conditions. (2012). Transportation Research Board. https://doi.org/10.17226/13655

SAE International. (2019). *ARP 6481- Procedure for the Calculation of Sampling Line Penetration Functions and Line Loss Correction Factors*. https://doi.org/10.4271/ARP6481

SAE International. (2021). *ARP 6320A - Procedure for the Continuous Sampling and Measurement of Non-Volatile Particulate Matter Emissions from Aircraft Turbine Engines*. https://doi.org/10.4271/ARP6320

Turgut, E. T. (2016). Effects of Ambient Air Temperature on Gaseous Emissions of Turbofan Engines. *Journal of Propulsion and Power*, *32*(3), 713–725. https://doi.org/10.2514/1.B35916

Underwood, B. Y. (2007). *Revised Emissions Methodology for Heathrow. AEA Report for the Department for Transport.* (AEAT/ENV/R/2193).

V.A. Profillidis & G.N. Botzoris. (2019). Chapter 6—Trend Projection and Time Series Methods. In V.A. Profillidis & G.N. Botzoris (Eds.), *Modeling of Transport Demand* (pp. 225–270). Elsevier. https://doi.org/10.1016/B978-0-12-811513-8.00006-6

Valenta, T. (2010). *Jet Engines – from JT8D to Trent 1000*.

Zaporozhets, O., & Synylo, K. (2017). Improvements on aircraft engine emission and emission inventory asesessment inside the airport area. *Energy*, *140*, 1350–1357. https://doi.org/10.1016/j.energy.2017.07.178

8. Appendix

8.1. Carbon balance

Figure 56 shows the exhaust air-fuel ratios (AFR) as a function of T3-correlated thrust. The exhaust AFR was calculated from the measured gaseous emissions according to the ICAO Annex 16 Vol. II. The red curves represent modeled AFR from engine performance models calibrated to performance data (no model was created for the CFM56-5B engine). The blue diamonds represent the assumed AFRs used in the ICAO FOA4 method for the conversion of mass concentration determined from a correlation with SN to EI nvPM mass.

The agreement between the modeled and measured AFR was the best for the CFM56-7B engine across all thrust settings. Given the same combustor design in the CFM56-5B engine, we expect very similar AFR values as a function of % thrust. For both the -7B and -5B engines, the FOA4-assumed AFR represented well the measured values at 7% and 30%. At 85% and 100% rated thrust, the FOA4 values agreed well only for the highest ratings. Given the AFR dependence on thrust, the FOA4 values should be scaled with % rated thrust for the highest rating.

For the CFM56-5C engine, the measured AFRs were significantly lower than modeled values across all power conditions. This is an unfortunate consequence of single point sampling probe at the exit of a mixed exhaust nozzle. The mixer efficiency is <<100%, i.e., the bypass and core flow are not well mixed at the engine exit plane. While the AFR check failed, it does not necessarily mean that the emissions determined are not representative. The model for this engine has also higher uncertainties than the other engines due to limited data used for the calibration. Nevertheless, the modeled AFRs are plausible, considering bypass ratios of ~6 at take-off and around ~8-9 at idle.

The measured AFRs of the PW4000 engine variants were overall higher than for the CFM56-7B and -5B engines with a tendency to overestimate the model values at idle and at take-off thrust. We performed exhaust traversing experiments for both engine types at idle in vertical direction and 12 o'clock position and found minimum variations in AFR. However, due to the larger exhaust nozzle area compared to the CFM56, higher variability is expected, as also demonstrated by the higher variability in the measured AFR at medium to high thrust.

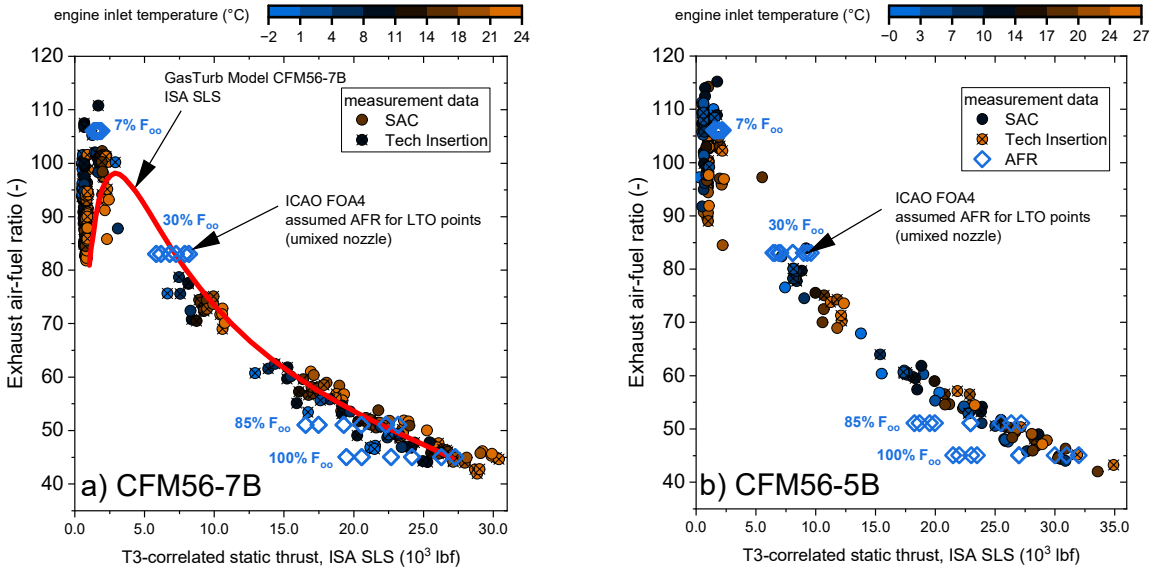

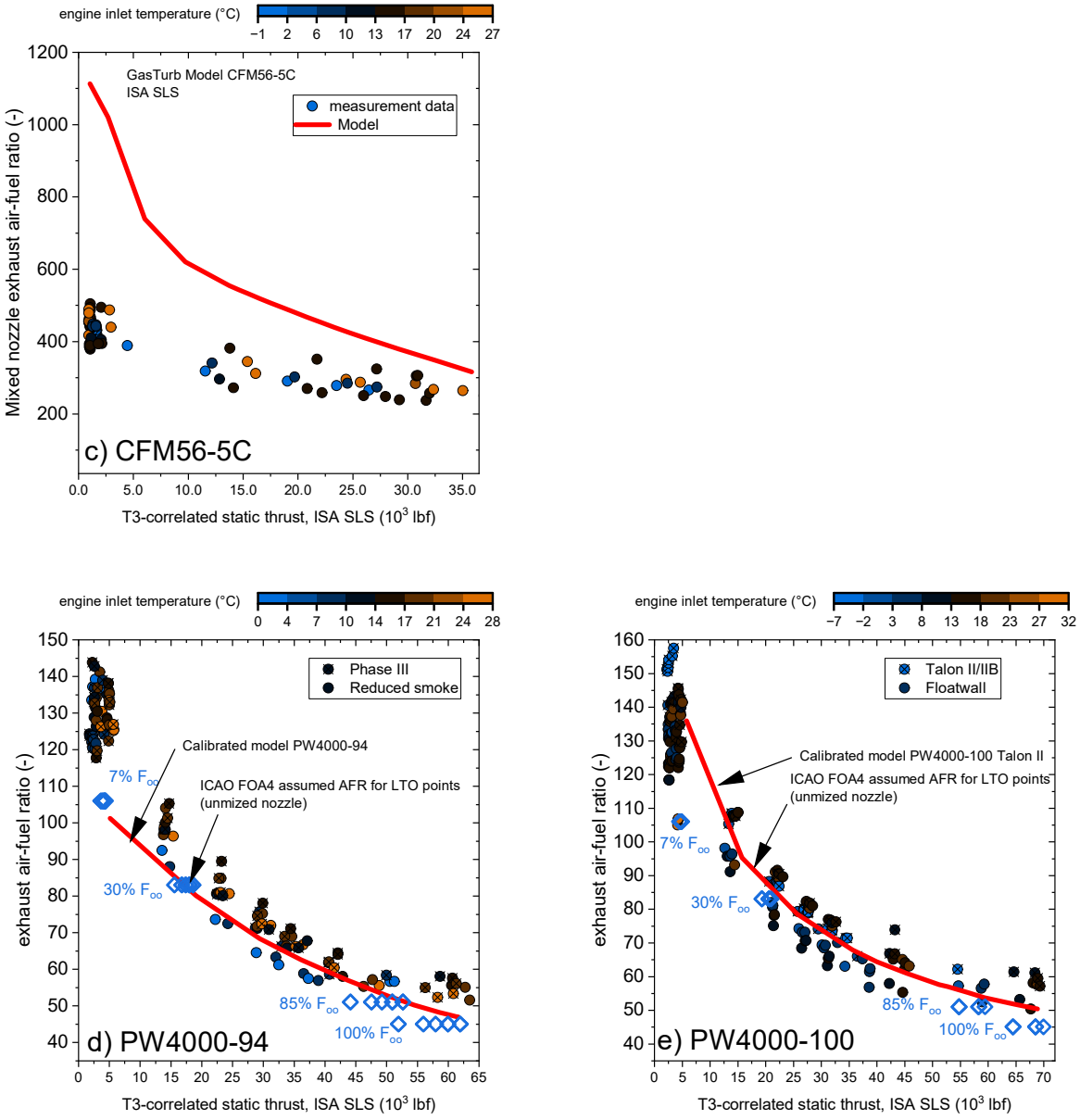

Figure 56 Exhaust air-fuel ratios and modeled engine exhaust nozzle air-fuel ratios (AFR5 or AFR8) at ISA SLS. No modeled AFR is available for the CFM56-5B engine.

8.2. nvPM loss correction factors

Figure 57 to Figure 61 show the exhaust gas temperature, thermophoretic loss correction factor k_{thermo} and mass- and number-based system loss correction factors $k_{S,Lmass}$ and $k_{SL,num}$ for the five engine types. The thermophoretic loss and system loss correction without PSD measurement were calculated using the standard methodology (SAE International, 2019, 2021). The system loss correction factors utilizing PSD measurement and used in this study were calculated using SMPS size bins and were interpolated as a function of T3 for each engine type. The PSD-based methodology is explained in detail in Durand et al., (2023).

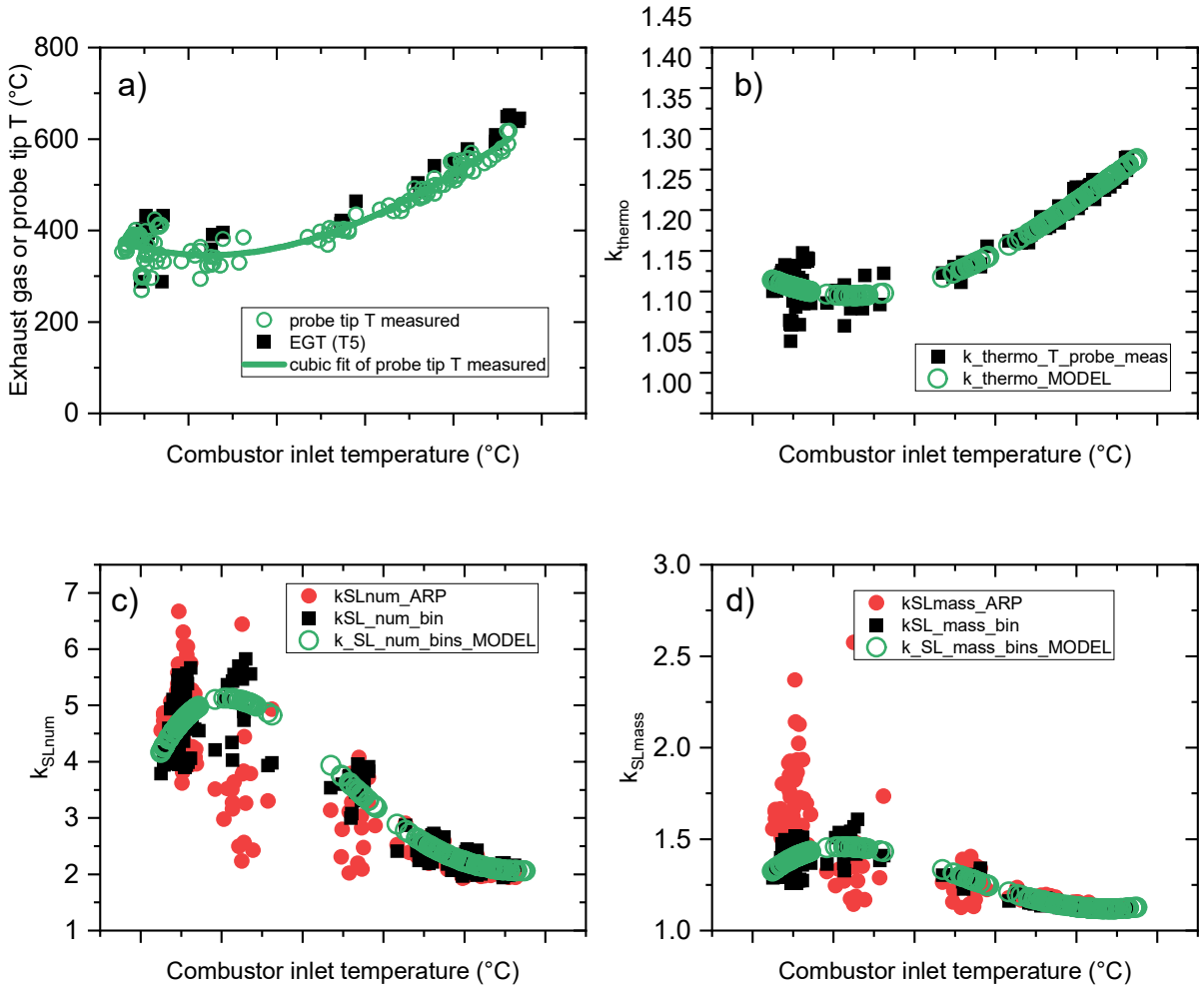

Figure 57 CFM56-7B: exhaust gas temperature (a), thermophoretic loss correction factor (b), number-based system loss correction factor (c), and mass-based system loss correction factor (d).

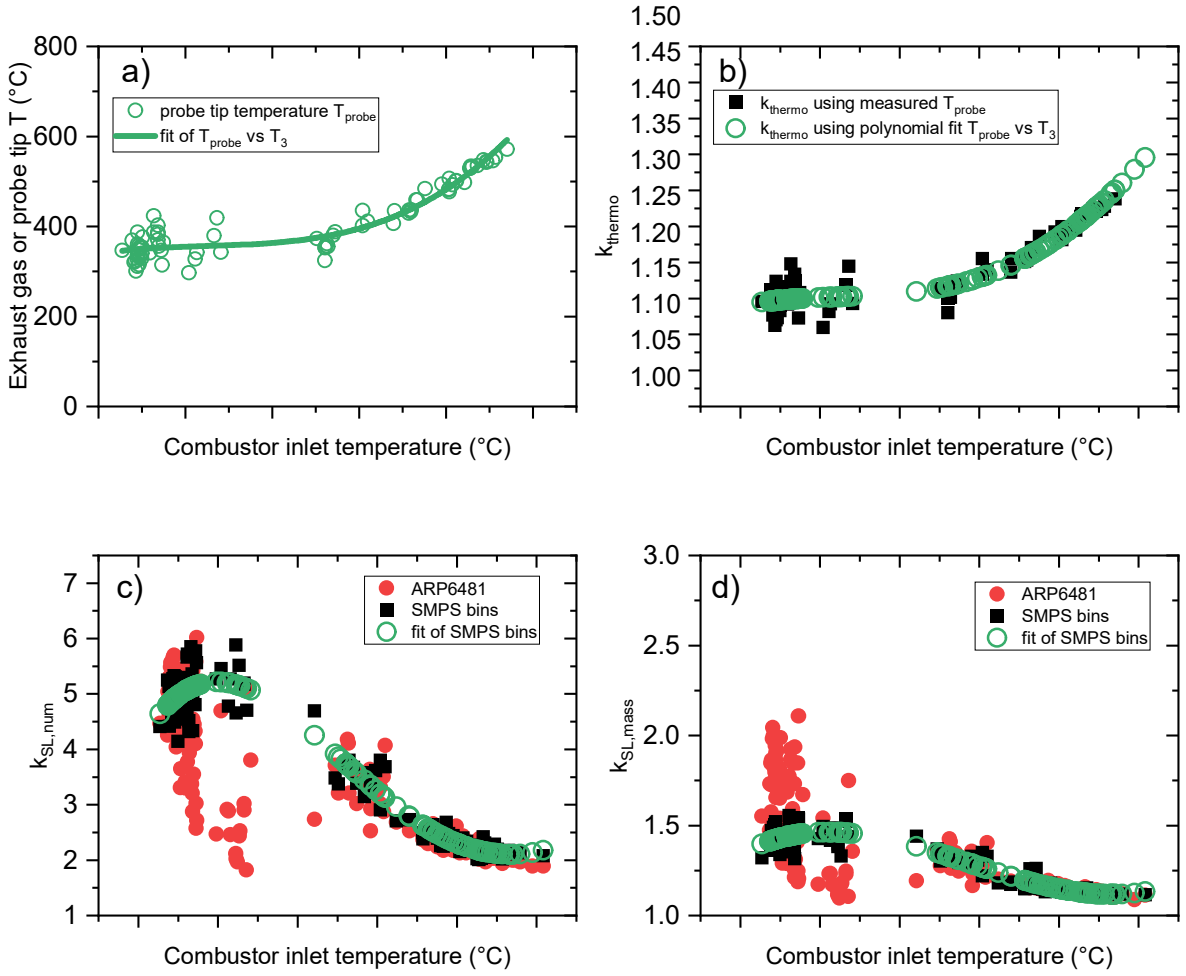

Figure 58 CFM56-5B: exhaust gas temperature (a), thermophoretic loss correction factor (b), number-based system loss correction factor (c), and mass-based system loss correction factor (d).

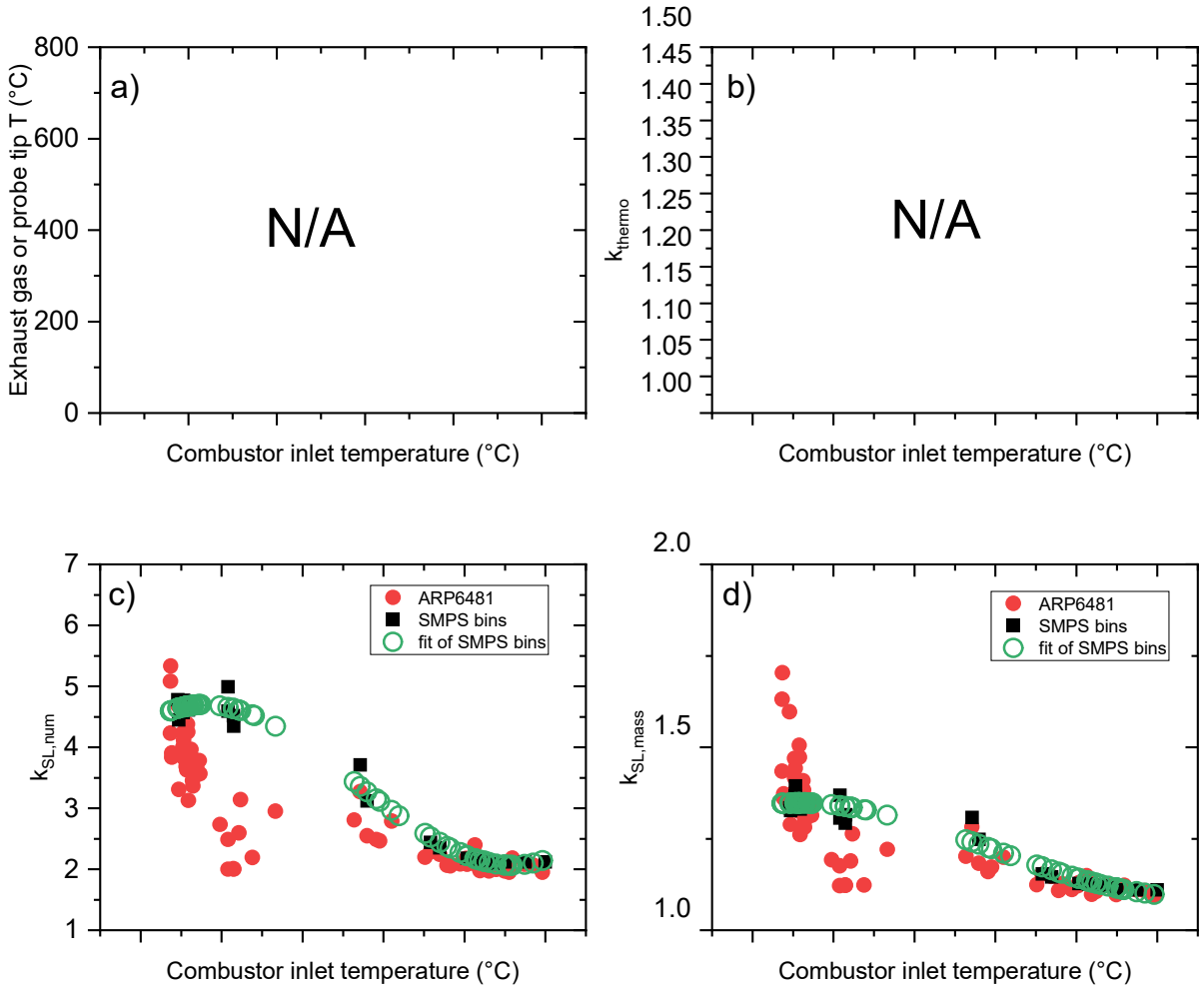

Figure 59 CFM56-5C: exhaust gas temperature (a), thermophoretic loss correction factor (b), number-based system loss correction factor (c), and mass-based system loss correction factor (d).

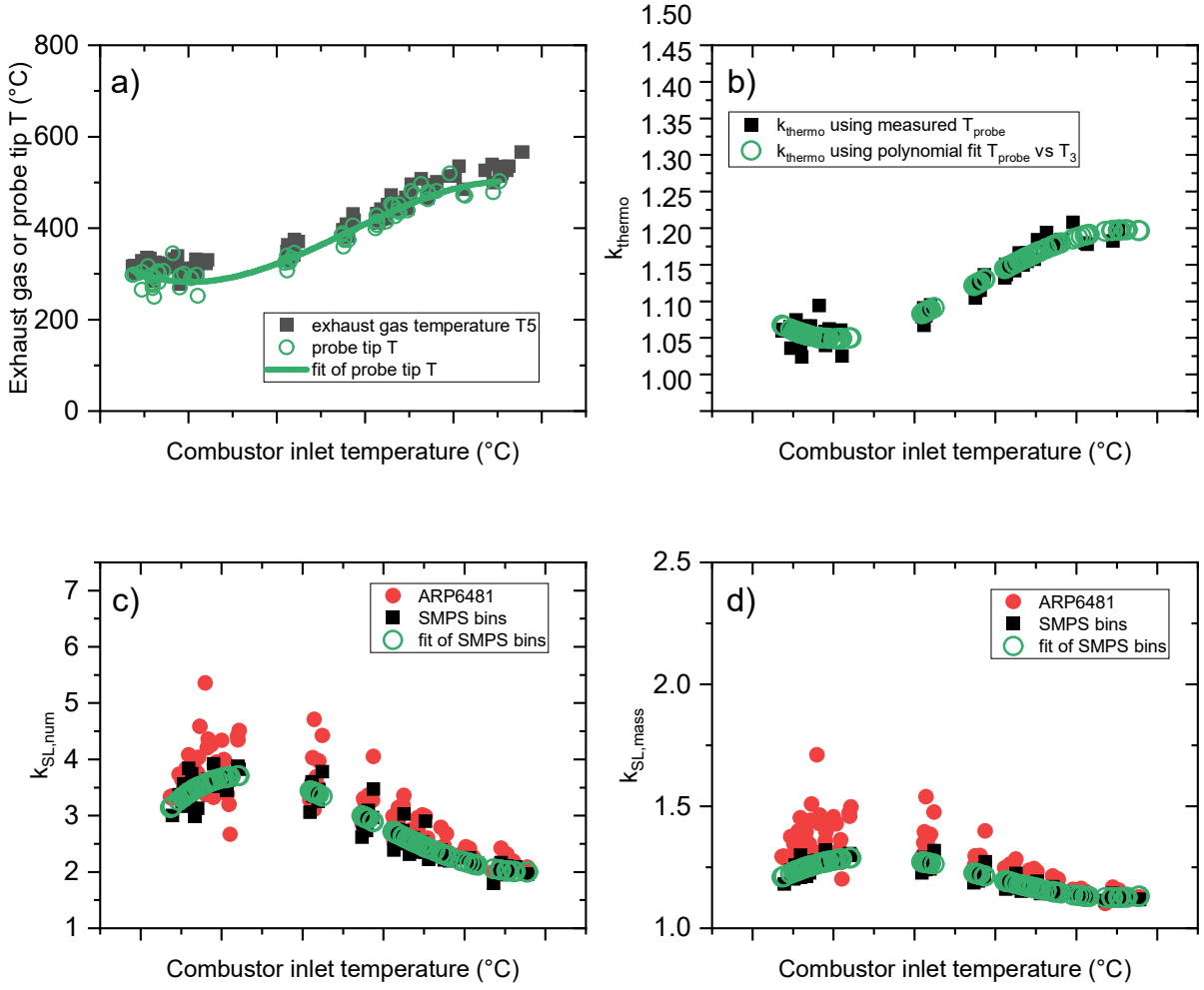

Figure 60 PW4000-94: exhaust gas temperature (a), thermophoretic loss correction factor (b), number-based system loss correction factor (c), and mass-based system loss correction factor (d).

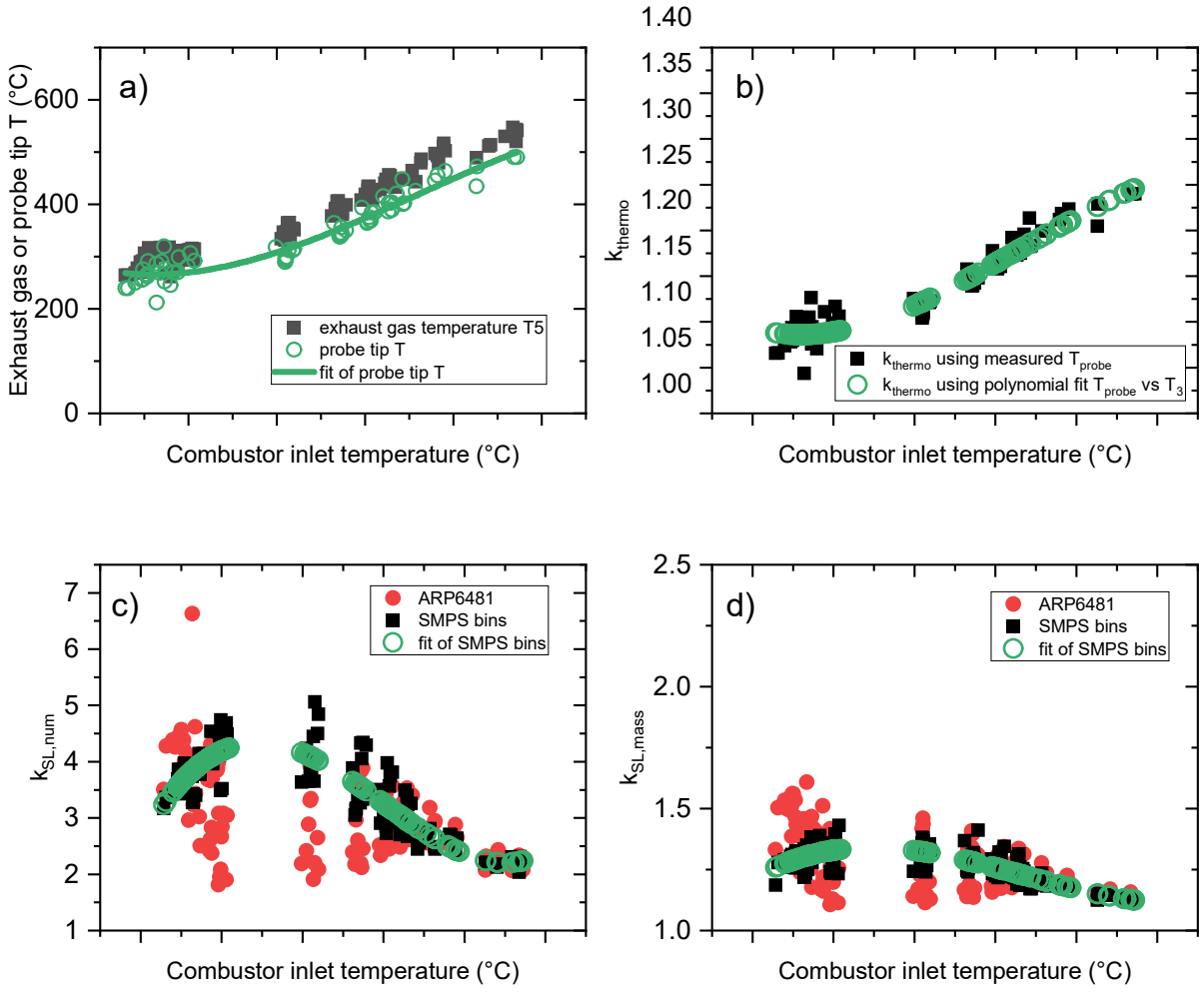

Figure 61 PW4000-100: exhaust gas temperature (a), thermophoretic loss correction factor (b), number-based system loss correction factor (c), and mass-based system loss correction factor (d).